8-2014

High Density EMI Filter Design in High Power Three-Phase Motor Drive Systems

Jing Xue
University of Tennessee - Knoxville, jxue3@vols.utk.edu

To the Graduate Council:

I am submitting herewith a dissertation written by Jing Xue entitled "High Density EMI Filter Design in High Power Three-Phase Motor Drive Systems." I have examined the final electronic copy of this dissertation for form and content and recommend that it be accepted in partial fulfillment of the requirements for the degree of Doctor of Philosophy, with a major in Electrical Engineering.

Fred Wang, Major Professor

We have read this dissertation and recommend its acceptance:

Leon Tolbert, Daniel Costinett, Judy Day

Accepted for the Council:

Carolyn R. Hodges

Vice Provost and Dean of the Graduate School

(Original signatures are on file with official student records.)

High Density EMI Filter Design in High Power Three-Phase Motor Drive Systems

A Dissertation Presented for the

Doctor of Philosophy

Degree

The University of Tennessee, Knoxville

Jing Xue

August 2014

Acknowledgements

This dissertation is accomplished under the advisory of my supervisor Dr. Fred Wang. I wish to show my most gratitude to him. His wisdom and his creative thinking has been my source of inspiration throughout this work. Beyond technical guidance, his professional attitude benefits me so much during my entire Ph. D. years. I truly appreciate it for all his patience and his time for mentoring me from the very beginning of my graduate years, both technically and mentally. I want to thank him for all his supports to my engineering career.

I would also like to express my sincere gratitude to my committee member Dr. Leon Tolbert. His classes and his seminars on technical writing give me very good training as a researcher and engineer. Also I would thank him for his guidance on this dissertation. I want to thank my committee member Dr. Daniel Costinett for all his suggestions and comments on this dissertation. I enjoy our discussion and feel glad to be able learn from him. Also I would like to show my appreciation to Dr. Judy Day for accepting my invitation to be my Ph. D. committee member. Her active spirit and meticulous attitude always help me improve this dissertation.

I would like to thank the Boeing Company for their financial support through my Ph. D. study. I would also show my gratitude to National Science Foundation (NSF) and the Department of Energy (DOE) for supporting our Center for Ultra-Wide-Area Resilient Electric Energy and Transmission Networks (CURENT).

I want to thank people from Virginia Tech for the cooperation and support during the Boeing project we have been working on. They are Dr. Dushan Boroyevich, Dr. Rolando Burgos, Dr. Paolo Mattavelli, Dr. Xuning Zhang, Mr. Igor Cvetkovic and Dr. Zhiyu Shen.

Mr. Robert Martin has been working with me ever since I have started my graduate study. I would thank him for all his supports in the lab and his funny stories. I would also like to thank Dr. Wenjie Chen and Dr. Xu Yang for all those valuable discussions.

My internship experience in Rockwell Automation gives me an important training as an engineer in industry. I would like to show my truly gratitude to the people there for giving me a warm welcome in such a cold spring. They are Dr. Richard Lukaszewski, Dr. Ranga Tallam, Dr. Lixiang Wei, Dr. Jiangang Hu, Dr. Zhendong Zhang, Mrs. Yali Tang, Mr. James Campbell, Mr. Doyle Busse and Mr. Xuechao Wang.

I would like to thank my colleagues in the University of Tennessee for all their helps and supports. It is a proud and cherished experience as a vol. I cannot list all my colleagues, but I would show my special thanks to Dr. Shengnan Li, Dr. Ming Li, Dr. Faete Filho, Dr. Mithat Can Kisacikoglu, Dr. Zhuxian Xu, Dr. Dong Jiang, Dr. Bailu Xiao, Dr. Fan Xu, Mrs. Lakshmi GopiReddy, Miss Liu Yang, Miss Jing Wang, Miss Yutian Cui, Mrs. Xiaojie Shi, Mrs. Yang Xue, Mr. Zhiqiang Wang, Mr. Ben Guo, Mr. Weimin Zhang, Mr. Yiwei Ma, Mr. Zheyu Zhang, Mr. Yalong Li, Mr. Bo Liu, Mr. Edward Jones, Mr. Bradford Trento, and Dr. Haifeng Lu.

I would like to thank the administrative staff members. Special thanks to Ms. Dana Bryson and Ms. Judy Evans for their kind help and supports during my Ph. D. years.

This dissertation made use of Engineering Research Center Shared Facilities supported by the Engineering Research Center Program of the National Science Foundation and DOE under NSF Award Number EEC-1041877 and the CURENT Industry Partnership Program.

My parents have always given me the opportunity to live well, and grow. I don't know even in my mother tone how to describe my gratitude feeling to them, Mr. Jianke Xue and Mrs. Jingxiu Nie. Papa and Mama, this achievement is dedicated to you.

I would also show my sincere appreciation to my parents-in-law, Mr. Jian Jiang and Mrs. Jianrong Chen, for all the support and encouragement.

I guess a Ph. D. dissertation is not the best place for a love declaration, but I have to make mine. Thank you Lu Jiang, for supporting me every day, for making life full of sunshine, for understanding me, for being such a great wife. Without your love and encouragement, this work cannot be possible.

Abstract

High density EMI filter is important in the application of more-electric-aircraft (MEA). In this work, the author is focusing on several major aspects of EMI filter design that would influence the power density.

In Chapter 1, the feature of EMI study and conventional design methods are reviewed.

The interaction between the common-mode (CM) and differential-mode (DM) noise is one key factor introducing unnecessary weight to EMI filter design. In Chapter 2, the author explains the origin of the mixed-mode (MM) noise on the output side of three-phase motor drives. Experimental results have verified the existence of the MM noise in three-phase motor drives and its impact on power density. In Chapter 3, the noise mode transformation (NMT) in three-phase motor drives due to system impedance unbalance is discussed. Simulation and experimental results show that the NMT will cause EMI filter overdesign if not considered during the design stage.

In Chapter 4 the author discusses the possibility of adding a CM inductor at the motor front and chassis end to reduce CM EMI filter weight. Experimental results show that the motor-end filter is effective in attenuating low frequency noise and has the benefit of being light weight comparing with the traditional three-phase CM choke.

Cooling of the filter is of great importance in high power systems. In Chapter 5, a practical liquid-cooling design procedure for EMI filters in high power motor drives has been discussed. Potting and thermal modeling are analyzed. Thermal test results verify the effectiveness of the procedure. In Chapter 6, the author models the impedance impact of potting material and cooling

cases on both CM and DM inductors. Experimental results match well with the developed models.

In Chapter 7, a comprehensive design procedure for high density EMI filter in high power motor drives has been proposed, based on the knowledge of previous chapters. As the verification of the procedure, a high density EMI filter is designed and tested in a 100 kW three-phase motor drive system for MEA application.

Conclusion and future work are summarized in Chapter 8.

Table of Contents

List of Figures

Chapter 1 Introduction

This dissertation focuses on the high density EMI filter design for the high power three-phase motor drive systems in aircraft applications. An overview of the more-electric-aircraft (MEA) concept and challenges is provided below. This is followed by a review of the design of the EMI filter in three-phase motor drive systems. Based on the knowledge from literatures, the approach for carrying out the researches is introduced. The specific problems to be addressed in this work are collected thereafter and the scope of the dissertation is explained.

1.1 Motivation and Background

The concept of more-electric-aircraft (MEA) is proposed in the mid 1980's [1-10]. Comparing with the other two types of power supplies in the secondary power system of aircraft, namely the hydraulics and pneumatics, electric power has the benefits of better power control, more fuel efficiency, fewer maintenance tasks and costs, as well as less audible noise. As a result, many of the tasks controlled by pneumatic and hydraulic systems previously, for example the air-conditioning, flight control and ice protection systems, are in the trend of being driven in the format of electric power. Among different formats of electric power supplies, the three-phase voltage-source-inverter based motor drive plays an important role in controlling large-rated adjustable speed motors of air-conditioners, pumps and compressors.

The PWM waveforms generated by the solid state three-phase motor drives are the source of the EMI noises which can be harmful to other electronic systems on the aircraft, for instance the communication, navigation and surveillance systems. To protect these systems, specified regulations are set for both conducted and radiated EMI emissions. Figure 1.1 and Figure 1.2 show the EMI restrictions in DO160 for different categories of equipment.

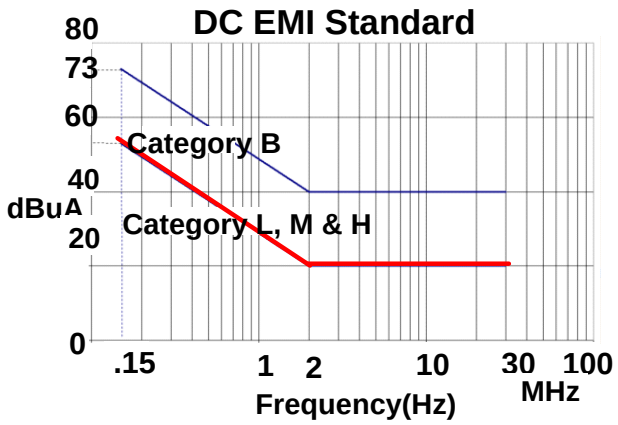

Figure 1.1. Dc side EMI standard in DO160

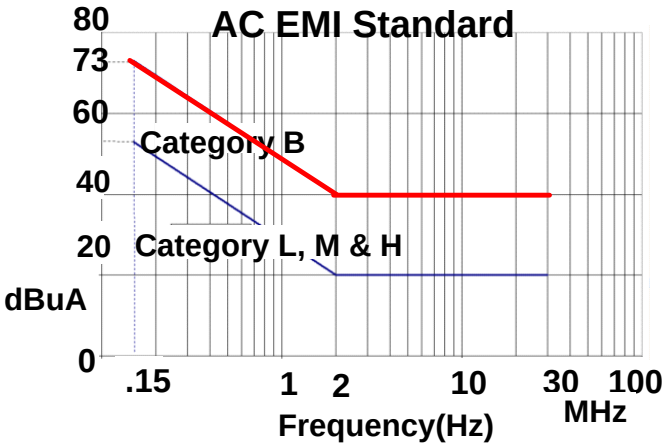

Figure 1.2. Ac side EMI standard in DO160

In Figure 1.1, the red curve of limitation defines the EMI current noise emission level on the power lines. In the dc-fed motor drive system on the MEA, this reflects to the dc input buses. In Figure 1.2, the highlighted upper curve shows the regulation of the EMI noise on interconnection bundles, which is referred to the AC output of the three-phase motor drive. Both standards of the dc and ac sides are ranged from 150 kHz to 30 MHz.

To suppress the conducted EMI noises within the EMI standards, usually EMI filters are required to be added into the system. Consisting of magnetic components like CM choke and DM inductors, these EMI filters are often bulky and heavy; whose weight might take large ratio of the total weight of the entire motor drive system. Considering these filters are carried by the aircraft, the more of their weight means the more of fuels are being consumed for every nautical mile the plane flies. As a result, to save the energy and price of the aircraft, the weight of the EMI filter needs to be reduced. Meanwhile, the filter is still required to carry the large current in the motor drive system. Therefore, an EMI filter of high power or VA density is needed.

The objective of this dissertation is to develop a complete methodology for the high density EMI filter design, which produces lightweight high power EMI filters that can suppress EMI noises well below both dc and ac conducted EMI standards in three-phase motor drive systems.

1.2 Research Approach Introduction

1.2.1 Features of EMI Study

Figure 1.3 shows a typical structure of the power electronics converter system. It includes a power supply, a solid state converter and a load. The connections between the power supply and converter can be either single or multi-phase. The output of the converter can also be either single or multi-phase, including the grounding loop. The power supply provides the energy for

the system. The converter functions as a high efficient conversion tool of electric power format. The load is the component that consumes the power provided by the power supply and converted by the converter.

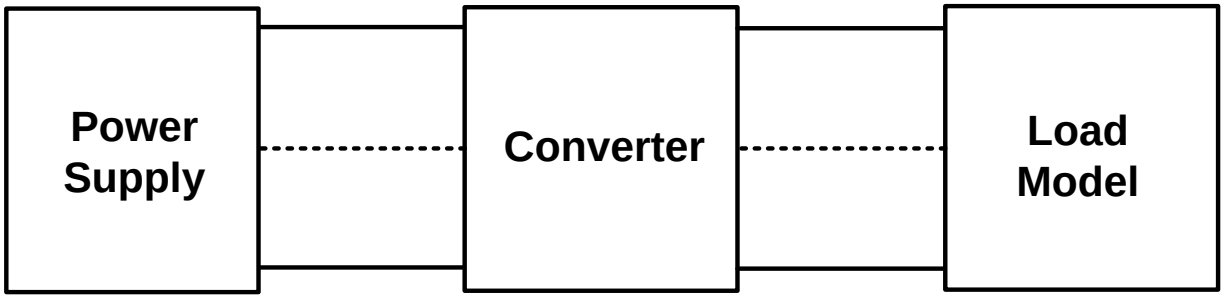

Figure 1.3. A simplified power converter system

However, in the study of EMI and filters, the function of each component in the structure of Figure 1.3 is totally changed. A simplified diagram is drawn in Figure 1.4. As shown in Figure 1.4, the converter is treated as the noise source, generating all the EMI noises. The connections, the power supplies and loads are all known as the noise propagation paths.

This structure in Figure 1.4 actually shows two major features in EMI and filter study. The first one is case-determined. The study of the EMI and filter is highly related to the specified condition, including the EMI standard, the noise source and propagation path conditions. The noise source is determined by the power converter topology, the voltage and current rating, and the modulation and control schemes. The propagation path relies on the power converter layout, the power supply source impedance, the load impedance, and the grounding condition of the system. As a result, EMI filter design methods are often specified to one certain application, for example, the single-phase switching mode power supply (SMPS) [11-19], or active front-end

rectifier [20-24]. Although there are studies under different applications, they cannot be directly used in the three-phase motor drive system.

The other feature of the EMI study is that it is often cut-and-try based. For an effective design method, an accurate model is necessary. However, considering the case-by-case feature of the EMI study, it is very time and effort-consuming to build a high frequency model for the entire system. Since the EMI study focuses on the range of frequency as high as 30 MHz, influence of parasitic components in the system cannot be ignored, for example the grounding impedance from the semiconductor device to the grounded heatsink. These components are not controllable. Meanwhile, they are only known when the system is built and measurements are carried out. Therefore, it is very difficult to predict either the converter EMI noise emission level, or the filter attenuation effect on the EMI noises, before building them.

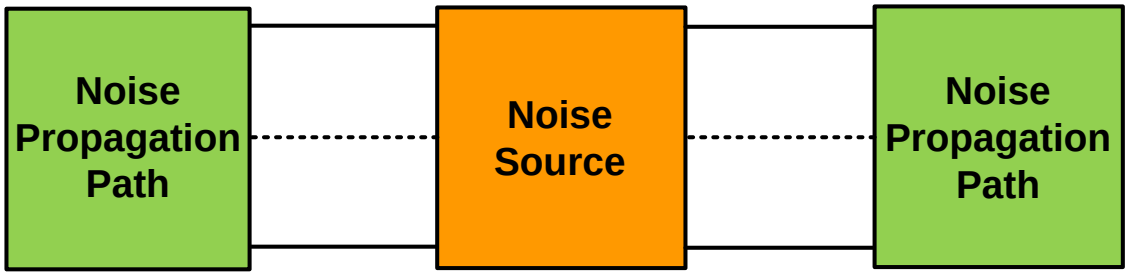

Figure 1.4. A simplified power converter system for EMI study

1.2.2 Conventional EMI Filter Design Method

Figure 1.5 shows a typical structure of the dc-fed three-phase motor drive. The converter is assumed as a traditional two-level VSI PWM motor drive. In the figure, the dashed parts refer to the parasitic grounding capacitance coupling the ground path with the power stage. As required

by the standard, two line-impedance-stabilization-networks (LISNs) are connected at the input end of the DC buses.

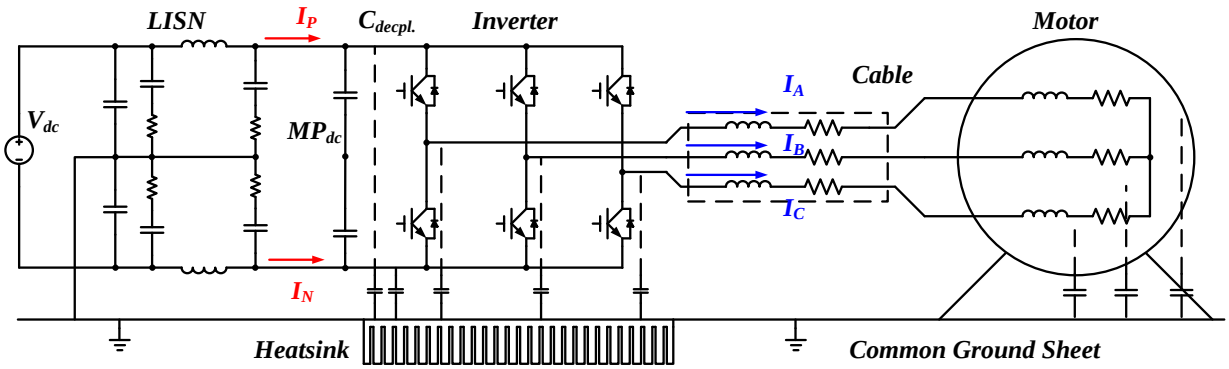

Figure 1.5. Dc-fed three-phase motor drive system

As discussed in [25], in conventional design method, the EMI noise is divided into CM and DM. Then CM filter and DM filter are designed separately according to the CM and DM bare noises. Figure 1.6 to Figure 1.9 show the ways of separating the CM and DM noise on both dc and ac sides.

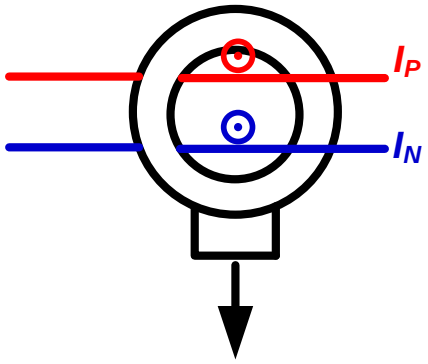

Figure 1.6. DC CM noise acquisition method

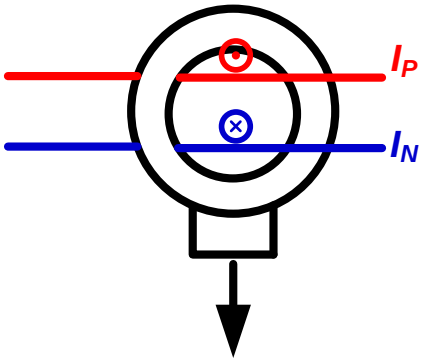

Figure 1.7. DC DM noise acquisition method

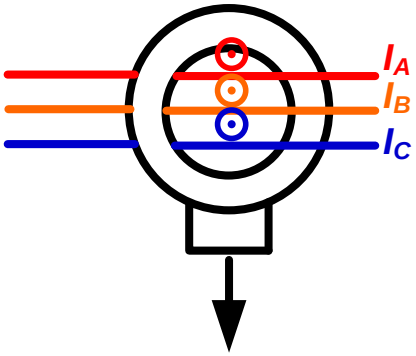

Figure 1.8. AC CM noise acquisition method

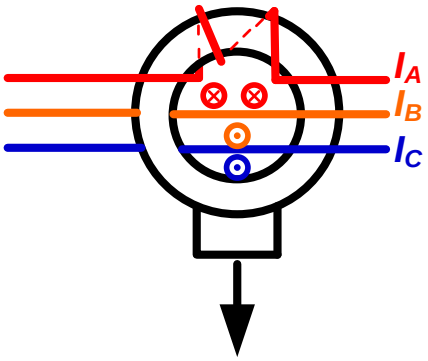

Figure 1.9. AC DM noise acquisition method

According to [26], as the conventional design method goes, typical LC filters are selected. Assuming ideal inductors and capacitors are utilized without influence from parasitic components, the attenuation performance of the filter features with a slope of 40 dB/dec, as shown in Figure 1.10.

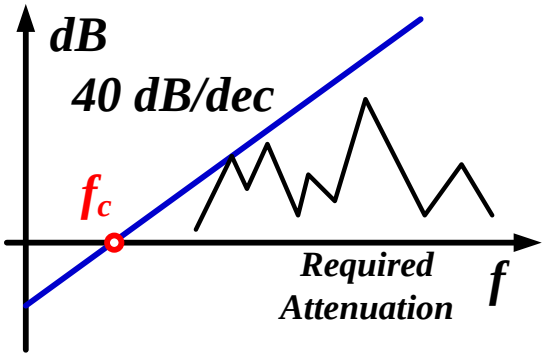

Figure 1.10. LC filter attenuation scheme

As a result, the bare noise of either CM or DM needs to be measured and compared with the standard at first. The part of noise higher than the standard is the part of noise requiring attenuation.

In sum, the conventional method used as a starting point can be simplified as Figure 1.11.

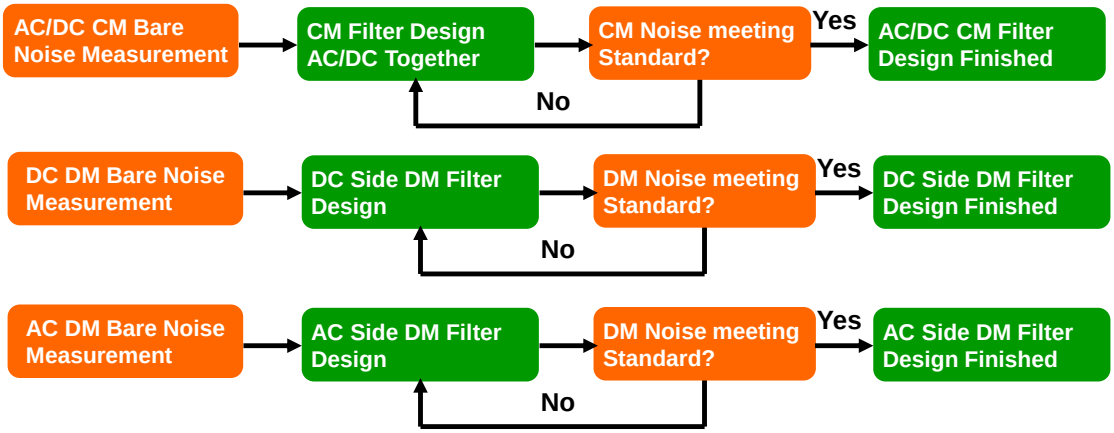

Figure 1.11. Flow chart of conventional EMI filter design method

1.2.3 Prototype EMI Testbed

Figure 1.12 shows the prototype experimental system. One commercial two-level motor drive is selected as the power converter. One set of commercial dynamometer is used as the motor load. Following the EMI Standard, one copper sheet has been installed under the entire power stage as the common ground. LISNs and feed-through capacitors are implemented at the input terminal of dc power. Three-conductor motor feeder is connected and kept from the copper ground.

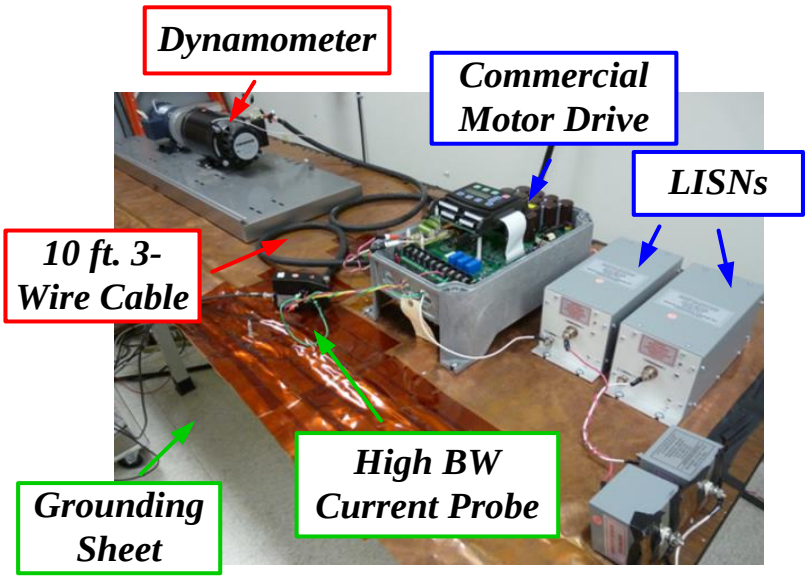

Figure 1.12. Prototype experimental system

1.3 Problem Statement

By using the conventional EMI filter design method and testing in the prototype experimental system, problems have been observed and summarized.

1.3.1 Problem 1: DM Filter Not Functioning

Figure 1.13 shows the circuit of the system with a typical DC DM LC filter. It includes two DC DM inductors and one DC DM capacitor. By adding the LC filter, supposedly the DC DM noise will be effectively attenuated.

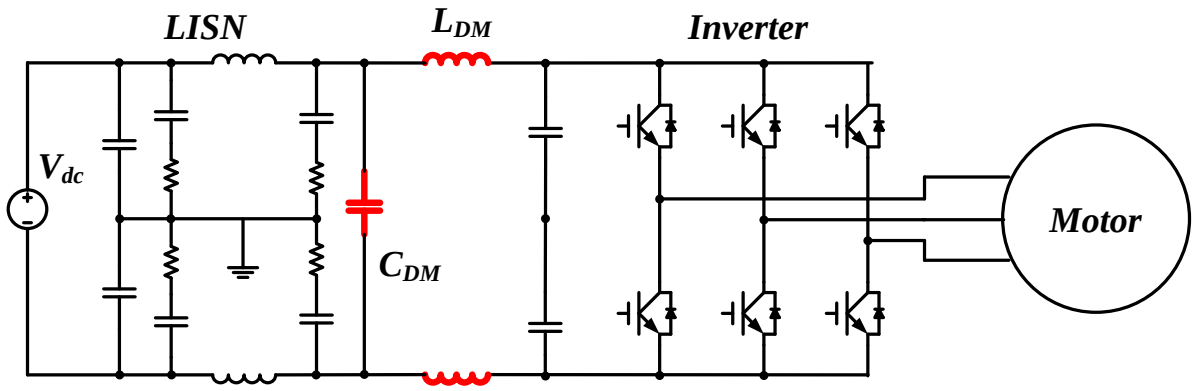

Figure 1.13. Motor drive system with DC DM filter

However, as shown in Figure 1.14, the green curve of the filtered DM noise does not show much difference comparing with the blue curve as the bare noise.

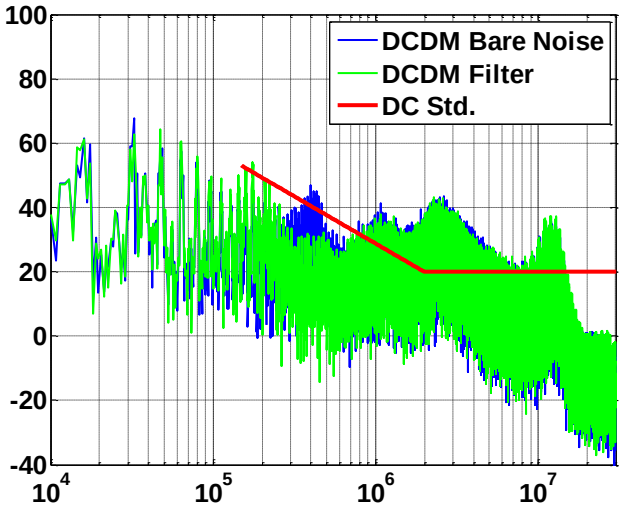

Figure 1.14. DC DM noise comparison: with filter vs. without filter

Similar phenomena have also been observed in AC DM filter design. As shown in Figure 1.15, a three-phase AC DM LC filter has been implemented. Different values of inductor and capacitor have been tested. Assuming the conventional design method is correct, the AC DM noise attenuation will vary as the LC filter changes.

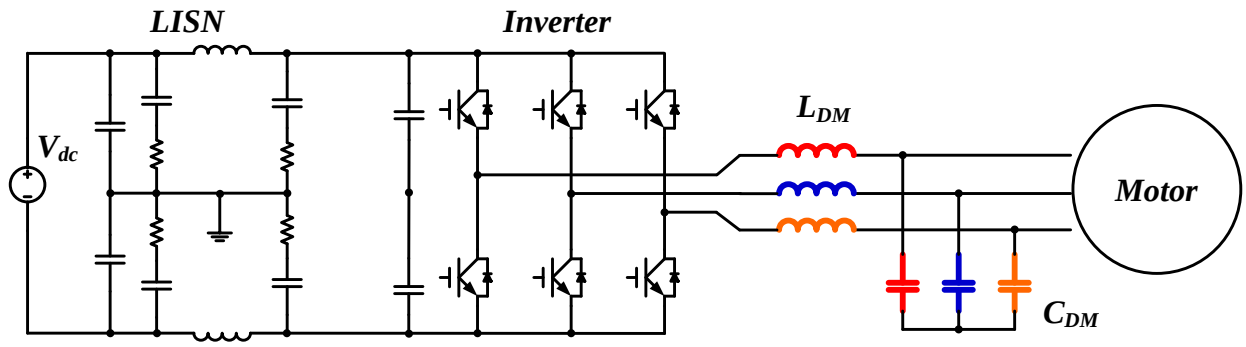

Figure 1.15. Motor drive system with AC DM filter

On the contrary, as shown in Figure 1.16, the spectra of the filtered AC DM noise has one common part cannot be attenuated, no matter what inductance or capacitance is selected. As a summary from Figure 1.14 and Figure 1.16, there is one part of the DM noise cannot be effectively attenuated by DM filter in the motor drive system. DM filter does not function well with the conventional design method.

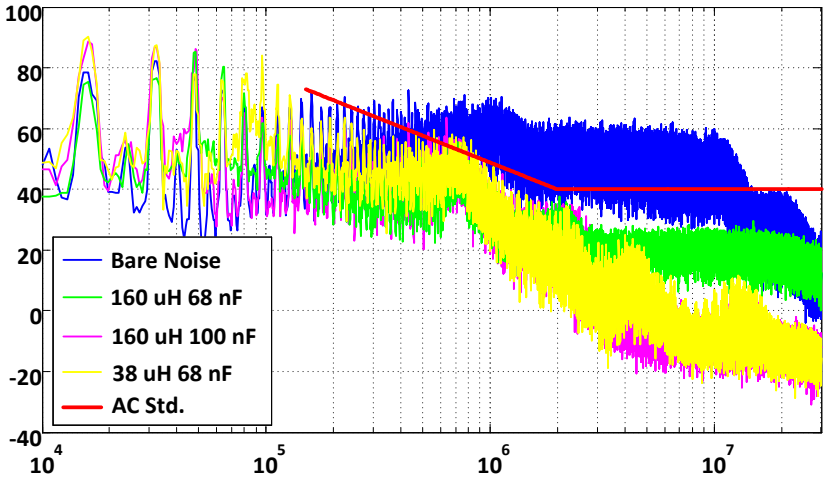

Figure 1.16. AC DM noise comparison: with filter vs. without filter

1.3.2 Problem 2: CM Filter Unexpected Performance

Following the conventional design method, one AC CM LC filter has been implemented into the system as shown in Figure 1.17. According to the calculation, the cut-off frequency of the LC filter is within 30 kHz. However, as shown in Figure 1.18, one resonance at around 400 kHz has been observed.

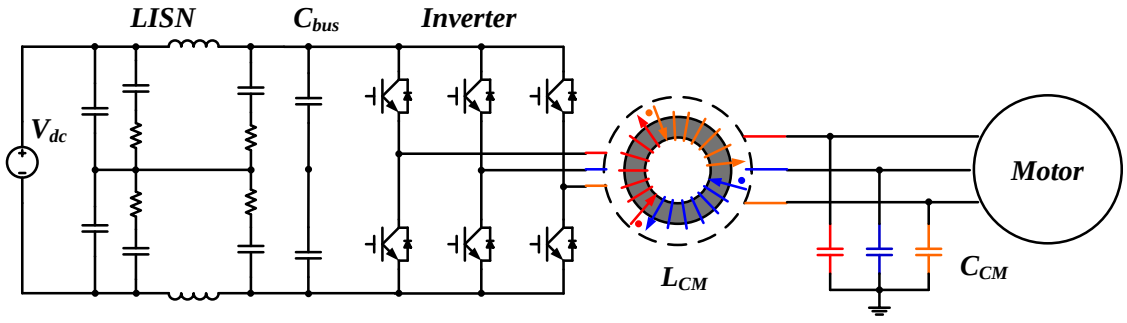

Figure 1.17. Motor drive system with AC CM filter

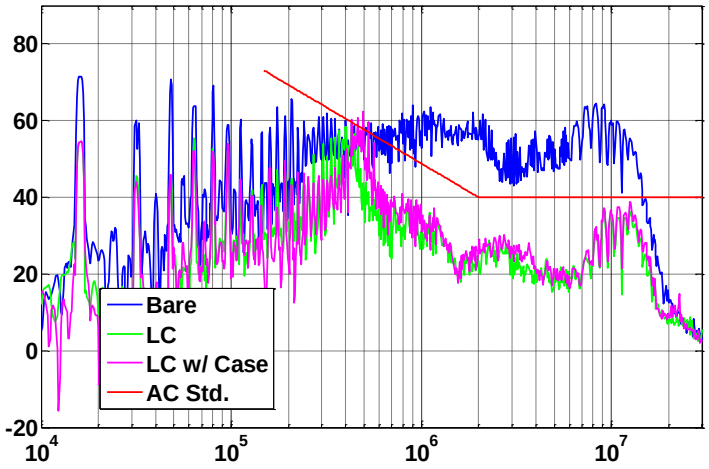

Figure 1.18. AC CM noise: unexpected resonance observed

1.3.3 Problem 3: EMI Filter Thermal Management

As part of the secondary power system on the aircraft, the benchmark motor drive system is 100 kW and 310 V_{llrms}. As a result, the rated DC and AC full load current is 185 Arms. Meanwhile, on the aircraft, the EMI filter needs to share the liquid cooling system of the converter power stage. As a result, a guideline in the EMI filter, especially inductor liquid cooling is needed.

1.3.4 Problem 4: EMI Filter Packaging Influence on EMI Filter

Not included in the conventional design method, the packaging of the EMI filter influences the performance of the noise attenuation. Figure 1.19 shows the DC CM choke in the cooling case with potting. By adding the aluminum case and high-thermal-conductive potting material, the impedance of the choke has been changed.

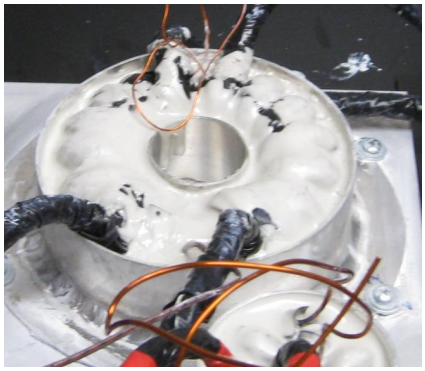

Figure 1.19. DC CM choke with cooling design

The comparison results of the inductor impedance with or without cooling packaging have been shown in Figure 1.20. Comparing with the original DC CM choke impedance, the packaging has influence on equivalent paralleling capacitance and leakage inductance.

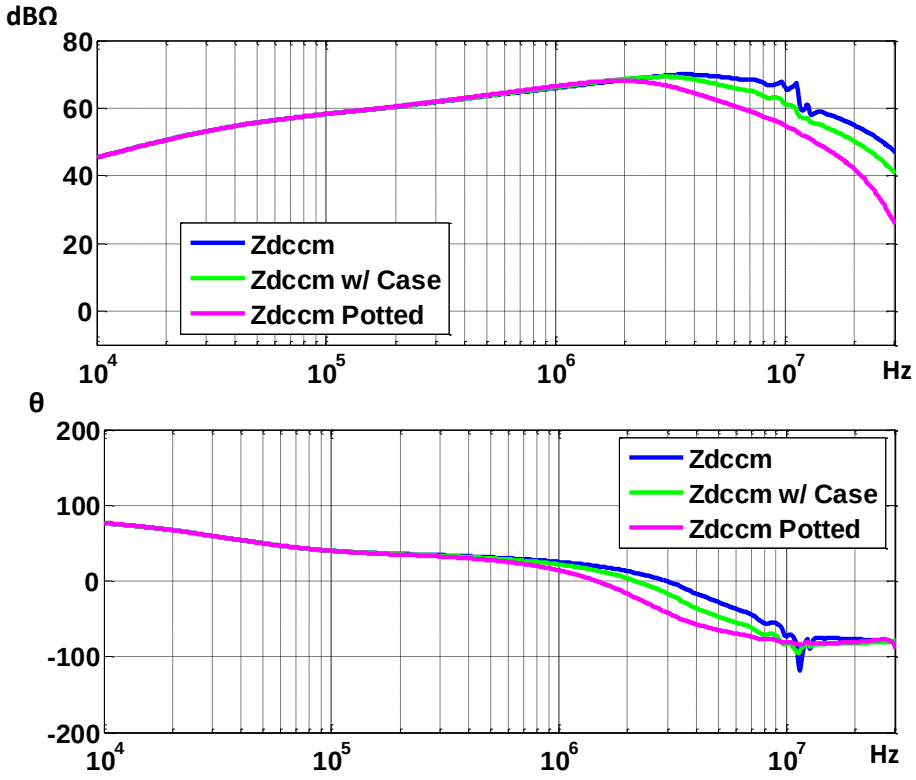

Figure 1.20. CM choke impedance comparison: choke only / with case / with potting

1.3.5 Problem 5: Possible Power Density Improvement

Besides focusing on the EMI filter design itself, the author would like to explore the possibility of reducing the EMI filter weight by improving the motor impedance. Figure 1.21 proposes one potential solution by adding a single-phase inductor between the motor chassis and the ground. In case of safety, this inductor presents relatively low voltage drop at line frequency. Concerning the high frequency CM noise attenuation, this inductor can provide similar performance comparing with three-phase full current CM choke while using only one winding and conducting no power current but just leakage current. Some filter weights are possibly saved by this type of motor end filters.

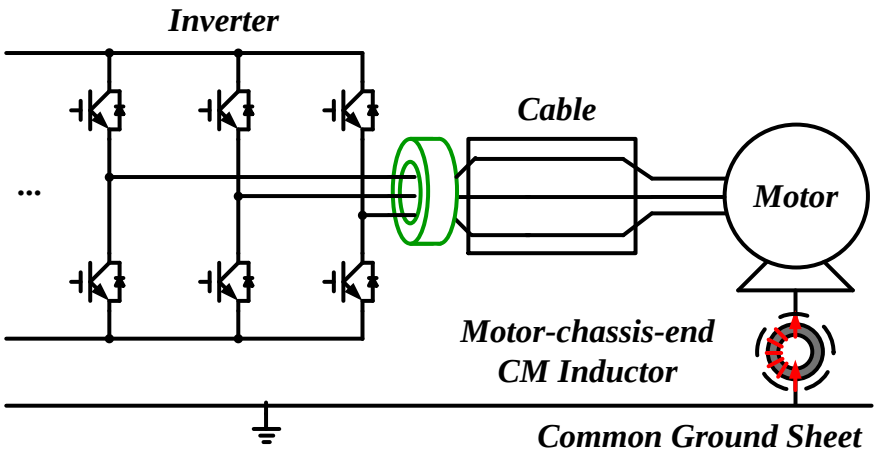

Figure 1.21. One type of motor end EMI filter

1.4 Literature Review

Based on the two features of the EMI study discussed in 1.2.1, the literature review for this work mainly focuses on the EMI analysis and EMI filter design in the specific application of three-phase motor drive system.

H. Agaki and etc. in [27-35] publish a series of papers discussing the EMI and filter design in a diode-front-end three-phase motor drive system. The CM propagation path has been analyzed in these works. A simplified equivalent circuit depicting the CM path is summarized. Practical EMI filter designs are also carried out. One innovative EMI filter topology connecting both the DC and AC side of the motor drive system is proposed.

J. S. Lai and etc. in [36-39] have carried out a series of detailed analysis on the simulation and modeling of the three-phase voltage source inverter. EMI noise can be predicted according to the inverter topology and modulation scheme, as well as system impedance, based on the proposed methods.

As shown in [40-42], studies of N. Hanigovszki and etc. are mainly focusing on the output EMI filter for the three-phase motor drive. As a contribution to the modeling of the system, the high frequency modeling of the components in the motor drive system has been carried out, including the motor, the cable, the IGBT and diode. Conventional technologies for output filters aiming at solving dv/dt problems are reviewed in the works. New topologies of EMI output filter are proposed and evaluated. These works present great insight on the modeling of the system and show more examples of filter design.

Works in [43-45] are for the exact same application as this dissertation proposal focuses on. Y. Maillet and etc. have analyzed the dc side EMI noise of the motor drive system. Meanwhile, high density material for the CM choke is proposed. Some tests on grounding effects and filter topologies have been conducted and discussed. [46-51] aim at solving the EMI problems for both dc and ac sides of the motor drive system. A new EMI filter topology based on the scheme of impedance balancing is proposed. Besides, the damping design of the EMI filter in the motor drive system is analyzed and optimized.

These above works are related to the focus of this dissertation proposal. However, a complete design of the EMI filter meeting the DO160 standard while being lightweight carrying high power rating is not found in any of these literatures. Therefore, in this dissertation, the author decides to pick the general design method as the starting point and try to improve the conventional method.

1.5 Scope of the Dissertation

In Chapter 2, the mixed-mode (MM) noise on the output side of the motor drive system is analyzed. Firstly, conventional EMI noise separation methods for three-phase systems are reviewed. According to the separation, the generation of the MM noises is analyzed thereafter, in specific of every possible switching condition for the three-phase inverter. Based on the prototype system, experiments are designed for validating the existence of the MM noises and its impact on EMI filter design. Possible ways to reduce the impact from MM noise are investigated.

Chapter 3 discusses the noise mode transformation due to system unbalance. The analysis of the intrinsic and EMI filter unbalance existing in the EMI noise propagation path of the dc-fed three-phase motor drive system is carried out. CM path unbalance in the circuit model is investigated with an example switching state in three-phase space vector pulse-width-modulation (SVPWM). Noise transformation from CM to DM is then verified with prototype experiments. The influence of the DM filter component unbalance on the DM propagation path is analyzed with simulation. After that, the transformation of the DM noise to CM is validated with tests. Influence of the unbalance and noise mode transformation on the EMI filter design is discussed and a comprehensive design procedure for high density EMI filter is proposed.

Focusing on an alternative of the conventional inverter-end (IE) EMI filters, Chapter 4 discusses the possibility of implementing an EMI filter on the motor end for the CM noise attenuation. A functional comparison between the inverter and the motor-end CM filter is firstly carried out, concerning the CM noise propagation path in the dc-fed motor drive system. According to their features in the noise propagation, the author focuses on two typical kinds of motor-end CM filters in detail, namely the motor front-end (MFE) filter and the motor chassis-end (MCE) filter. Their performances on improving the output CM impedance and suppressing the CM noise emission are analyzed, based on experimental results from the prototype system. Investigations show that the implementation of the MFE filter has similar functions with the IE CM choke, while attaching the MCE filter with the motor can help save the magnetic size and weight from the conventional IE filter. However, special attentions are needed for the safety and parasitic concerns.

In Chapter 5, a practical liquid-cooling design procedure has been summarized for the magnetic components of EMI filter in high power motor drives.

In Chapter 6, the parasitic influence brought by the liquid-cooling design has been analyzed. A simplified model describing the change of parasitic capacitance and leakage inductance has been built and verified in experiments.

In Chapter 7, a comprehensive design procedure for the high density EMI filter in high power motor drive has been proposed based on the new knowledge from previous chapters. The method has been verified to be effective for high density design with a 100 kW EMI filter and test.

The conclusion of the dissertation as well as possible future work is summarized in Chapter 8.

Chapter 2 Output Mixed-Mode EMI Noise in Three-Phase PWM Motor Drive

2.1 Introduction

Traditional EMI filter design methods divide the emissions into common-mode (CM) and differential-mode (DM) noises [52]. Assuming the two modes of noises are well-decoupled, designs are then carried out separately according to the CM and DM noises for CM and DM filters [53]. Based on this strategy, towards an optimized filter design, literatures have been discussing the noise modeling and filter component size minimization for either the CM [26, 27, 54, 55] or the DM filters [22, 56, 57]. However, since the EMI standards are restricting the total noise before separation, even if both CM and DM filters are optimally designed separately, this design procedure does not necessarily guarantee the success of finding a real high density EMI filter which can suppress the total noise well. The existence of the mixed-mode (MM) noise generates difficulties on the noise recognition and influences the high density filter design [25].

Since discovered in early 2000s, the mixed-mode noise is mainly discussed in the applications of switching mode power supply (SMPS). S. Qu and D. Chen firstly identify the non-intrinsic DM noise in the SMPS as the mixed-mode noise in [11]. Modeling works of the generation schemes and propagation paths of the MM noises are then carried out in [17, 58]. For the attenuation of the MM noise in the SMPS, the effects of X-capacitors and CM chokes are compared and summarized in [17, 59]. More recently, the possible influence of Y-capacitor on the MM noise filtering is also discussed in [60]. Based on the knowledge about the MM noise,

the comprehensive SMPS EMI filter design procedure concerning the MM phenomenon is proposed in 2004 [61] and improved in 2008 [62] and 2010 [63].

On the contrary to the continuous study of the MM noise in single-phase SMPS, limited number of works can be found analyzing the MM noise in the three-phase motor drive systems all through the years. W. Shen and F. Wang [52] have investigated the propagation of the non-intrinsic DM noise in the front-end three-phase diode rectifier side of the variable speed motor drive. Yet for the output side of the motor drive, where EMI standards often focus on, and where bulky three-phase EMI filters are often required, the MM phenomenon and its implication to the EMI filter design have not been fully investigated.

In this chapter, the output side MM noise of three-phase motor drives is analyzed in the dc-fed three-phase voltage source inverter as a benchmark. To start with, the necessity and methods of noise separation have been reviewed in Section 2.2. Conventional way of discriminate CM and DM current noises are introduced. Then in Section 2.3, the method for studying the MM noises is proposed. The MM noise generation scheme in three-phase motor drives is described in each possible switching status of voltage vectors. The relative amplitude of the MM noise referred to the measured CM noise is quantified under ideal assumption of perfectly balanced three-phase impedance. Comparative experiments are designed and carried out in a prototype motor drive system to verify the existence of the MM noise in Section 2.4. To illustrate the influence of the MM noise on EMI filter design, in Section 2.4, one quantified example is selected based on the prototype experimental results. Comparison results show that much extra weight and volume will be introduced if designing the output side EMI filter without concerning the MM noise. Possible ways of reducing the MM noise and its impact have been discussed in Section 2.5. Conclusion and possible future work are included in Section 2.6.

2.2 Three-Phase EMI Noise Separation Method in DC-Fed Motor Drives

With the basic principle of summing and subtracting noises, the three-phase CM and DM emission discrimination methods can be categorized by different realization approaches. External circuits are designed and utilized in [11]. Mathematical model and calculation are carried out in [58]. [17] simplified the method by using high frequency current probes and by changing the wire winding turns of Phase A, B and C to reach the noise separation. In this chapter, this third method is selected. DO160 standard is utilized as the AC side line current constraints.

Figure 2.1 shows a typical structure of the Dc-fed motor drive system. As required from the standard, line-impedance-stabilization-networks (LISNs) and feed-through capacitors are implemented on the DC buses. One common ground made of copper sheet is placed underneath the whole system. On the AC side, three-wire motor cable and motor dynamometer are connected as the output load. Besides the solid path of noise propagation, Figure 2.1 also shows the parasitic grounding capacitance (dash lines) existing between the inverter switches and the heatsink, as well as between the motor windings and motor chassis. Output wires are clamped by a high frequency current transformer, whose signal on secondary side is conveyed to a commercial EMI receiver.

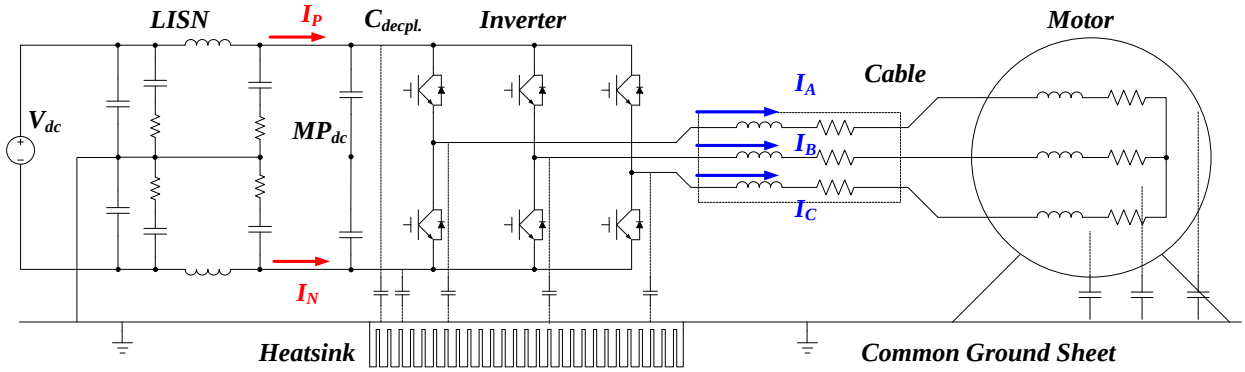

Figure 2.1. Typical structure of noise propagation in three-phase motor drive system

The detailed clamping configurations for CM and DM noises are shown in Figure 1.8 and Figure 1.9. With conventional definitions [52], the CM noise is the common part of the three-phase emissions which share the common path through the ground. As a result, the sum of all three phase currents is captured simultaneously by being clamped together. The remaining part of the line current noise can be acquired by getting two turns of one phase wire and one turn of the other two in an opposite direction. This part of noise is often assumed as the DM noise, which needs to be suppressed by DM filters.

However, this may not be true considering the complexity of the unbalance of the PWM operation and impedance network in the three-phase motor drive system. If any unbalance exists among the three phases, there will be noise propagation path that couples the grounding loop with just one or two of the AC phases instead of all three. According to the acquisition way of this so-called DM noise, the measurement results will then include both the DM noise going through the power line and another part of noise that is conducted along the common ground, but not as common-mode since it is not common for all three phase. This type of grounding noise observed from measurement is typical mixed-mode noise.

$$\begin{cases} I_{ACCM} = \dfrac{I_A + I_B + I_C}{3} \\ I_{ACDM\_A} = I_A - I_{ACCM} = \dfrac{2I_A - I_B - I_C}{3} \end{cases} \tag{2.1}$$

2.3 Output MM Noise Analysis in DC-fed Motor Drive System

2.3.1 Discuss on MM Noise Analysis Method

The conventional three-phase converters equivalent circuits of CM and DM are shown as an example in Figure 2.2 and Figure 2.3. As a tool for analyzing MM noise, the CM circuit has the advantage of considering the grounding path together with all three phases. However, the simplification from a three-phase system to one noise source and one branch of propagation path eliminates the possibility of observing the MM noise from the difference among the three phases. On the other hand, although the DM equivalent circuit specifies the propagation path with different phases, the model simply discards the grounding track. By taking the three-phase-four-wire system into a pure three-wire system, the key path of MM noise through the ground is totally ignored.

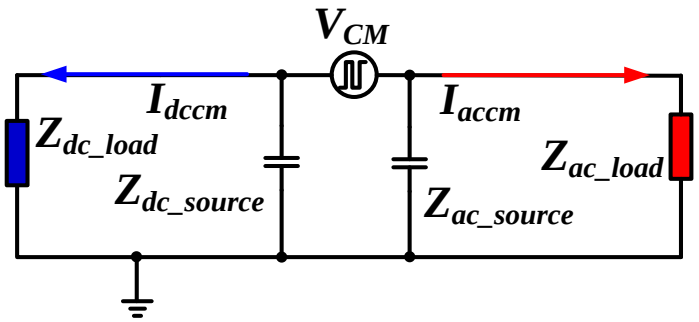

Figure 2.2. CM equivalent circuit

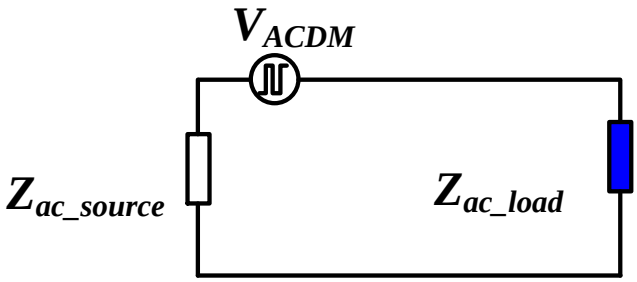

Figure 2.3. AC DM equivalent circuit

An effective MM noise analysis circuit should concern both the grounding path and nonidentical feature of the three-phase noise source. [11, 58] proposes the method with complete circuit analysis for input MM noise in single-phase SMPS, by focusing on the charging and discharging procedures of the parasitic grounding capacitance. [52] utilizes this method in three-phase motor drive application. However the discussion is still limited in the front-end side MM noise with diode rectifier. In this chapter, the authors propose the method of analyzing the motor drive output side MM noise by detailed three-phase circuit with grounding path at different switching conditions.

2.3.2 MM Noise at <100> Condition

The shadow part of Figure 2.4 shows the three-phase gate signal status when the top switch of Phase A and bottom switches of Phase B and C are being turned on. This example status is named as <100> for short. As shown in Figure 2.5 and Figure 2.6, during this time period, the motor parasitic grounding capacitance of Winding A C_{MA} is being charged while C_{MB} and C_{MC} are being discharged. These charging and discharging currents are part of the grounding current, not the intrinsic DM noise due to the line-to-line voltage applied on line impedance of cable and motor, yet captured by the AC DM noise measurement.

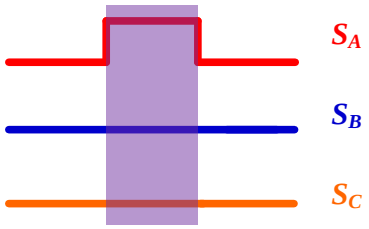

Figure 2.4. Gate signals of voltage vector <100>

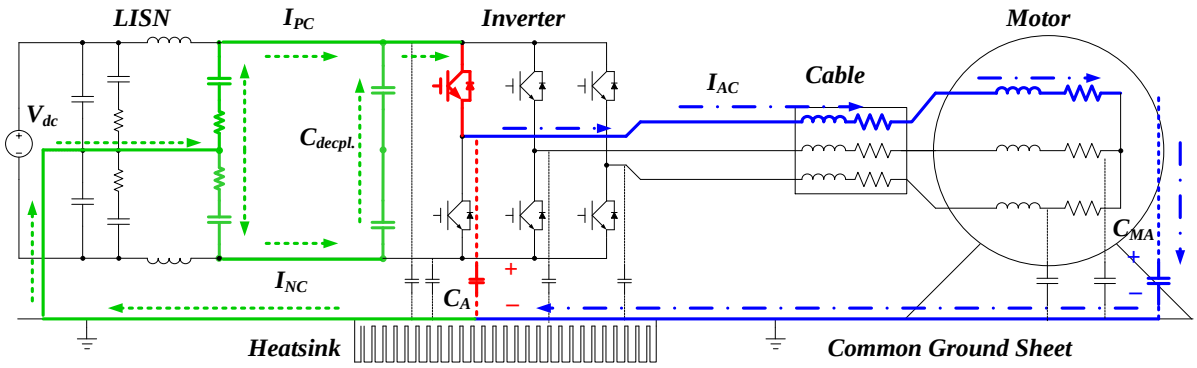

Figure 2.5. Charging of parasitic grounding capacitance during <100>

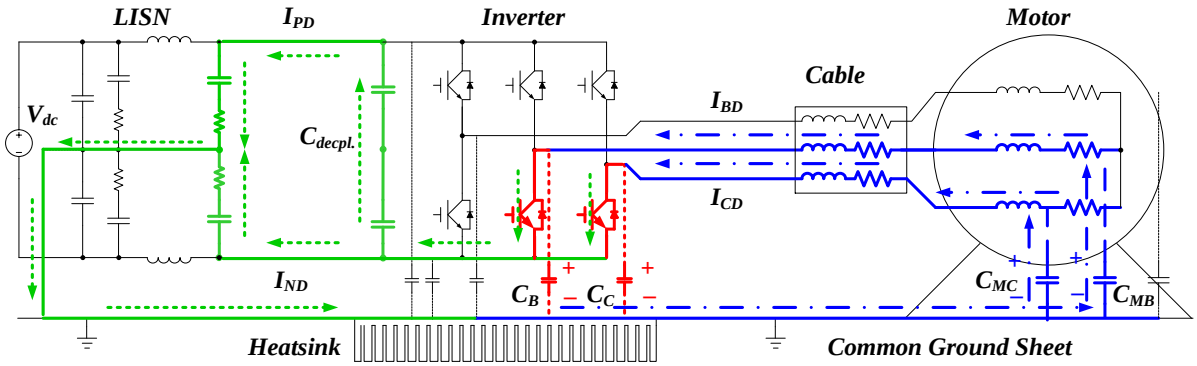

Figure 2.6. Discharging of parasitic grounding capacitance during <100>

A quantitative discussion on the magnitude of these MM noise related to AC CM noise is carried out. Assuming a balanced three-phase motor and three-conductor cable, the impedance on the charging or discharging loops through each phase should be equal to each other. Thus the *Phase A* charging current I_{AC} has the same magnitude but opposite direction with *Phase B* discharging current I_{BD} or *Phase C* I_{CD}. Assuming the magnitude of the charging or discharging current as I_o and the charging direction of I_{AC} as positive, the CM noise can then be deduced as (2.2).

$$I_{ACCM} = (I_{AC} + I_{BD} + I_{CD})/3 = (I_O - I_O - I_O)/3 = -I_O/3 \tag{2.2}$$

With the definition of the AC DM measurement from (2.1), the charging and discharging currents are captured as shown in (2.3). In the equation, the acquired noises are the mixed-mode noise, which is observed in DM measurement but not the intrinsic DM noise for each phase.

$$\begin{cases} I_{MM\_A} = I_O - I_{ACCM} = 4I_O/3 = -4I_{ACCM} \\ I_{MM\_B} = I_{MM\_C} = I_{BD} - I_{ACCM} = I_{CD} - I_{ACCM} = -2I_O/3 = 2I_{ACCM} \end{cases} \tag{2.3}$$

(2.3) quantifies the MM noises with the reference of I_{ACCM} during the time period of <100>. It is shown that in the measurement of AC DM noise of Phase A, there is part of the noise going through the ground with the magnitude of four times of the CM noise. If the measurement is carried out for Phase B and C, the grounding noise part is two times the CM noise.

2.3.3 MM Noise at <110> Condition

Similar analysis can be carried out for the switching condition of <110>, when Phase A and B has the top switches turned on and Phase C the bottom one. As shown in Figure 2.7. Charging of parasitic grounding capacitance during <110>, the charging phenomena of motor grounding

capacitance in Phase A and B lead to two charging current I_{AC} and I_{BC}. On the contrary, as depicted in Figure 2.8, Phase C is the only phase experiencing stray capacitance discharging, with I_{CD}. Still assuming the magnitude of the current as I_O and same definition of the positive direction, the CM noise can be obtained as (2.4):

$$I_{ACCM} = (I_{AC} + I_{BC} + I_{CD})/3 = (I_O + I_O - I_O)/3 = I_O/3 \tag{2.4}$$

Accordingly, the MM noise captured by the AC DM measurement can be summarized as (2.5):

$$\begin{cases} I_{MM\_A} = I_{MM\_B} = I_O - I_{ACCM} = 2I_O/3 = 2I_{ACCM} \\ I_{MM\_C} = I_{CD} - I_{ACCM} = -4I_O/3 = -4I_{ACCM} \end{cases} \tag{2.5}$$

(2.5) shows that when only Phase C is discharging, the MM noise on Phase C is four times of the magnitude of the CM noise, while the other two charging phases are two times.

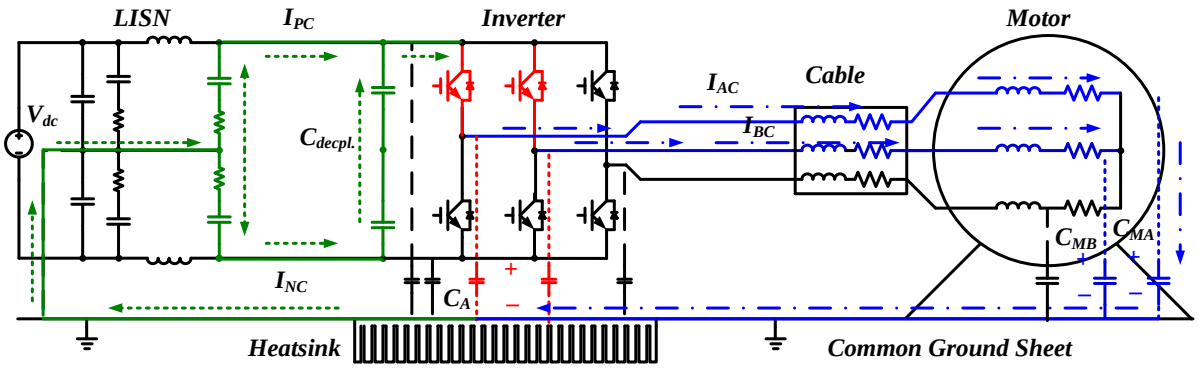

Figure 2.7. Charging of parasitic grounding capacitance during <110>

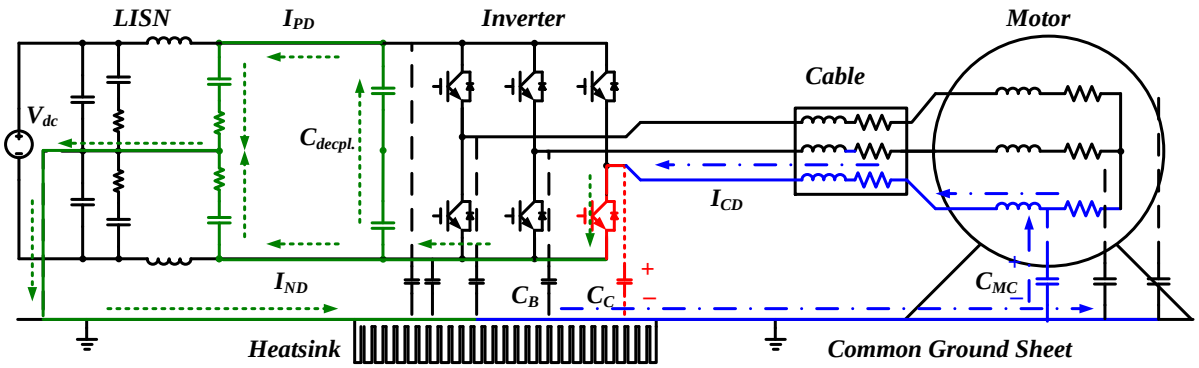

Figure 2.8. Discharging of parasitic grounding capacitance during <110>

2.3.4 MM Noise at <111>/<000> Condition

During zero vectors of <111> or <000>, the conditions are different. As shown in Figure 2.9. Charging of parasitic grounding capacitance during <111>, when all three-phase top switches are turned on, all three-phase grounding capacitances are being charged. Thus the CM current noise can be expressed as:

$$I_{ACCM} = (I_{AC} + I_{BC} + I_{CC})/3 = (I_O + I_O + I_O)/3 = I_O \tag{2.6}$$

Since all three phases are identical for the direction of the current on the output side, the captured MM noise from AC DM measurement is shown in (2.7):

$$I_{MM\_A} = I_{MM\_B} = I_{MM\_C} = I_O - I_{ACCM} = I_O - I_O = 0 \tag{2.7}$$

Similar effect can be found in Figure 2.10. Discharging of parasitic grounding capacitance during <000>, when all three-phase bottom switches are on, which means the three winding-to-ground capacitances are all being discharged. The CM noise is expressed as:

$$I_{ACCM} = (I_{AD} + I_{BD} + I_{CD})/3 = (-I_O - I_O - I_O)/3 = -I_O \tag{2.8}$$

In the same way, the MM noise is calculated by:

$$I_{MM\_A} = I_{MM\_B} = I_{MM\_C} = -I_O - I_{ACCM} = -I_O + I_O = 0 \tag{2.9}$$

As being discussed above, during the zero vector time of either <000> or <111>, there are no MM noises because of the balance achieved by the three phases.

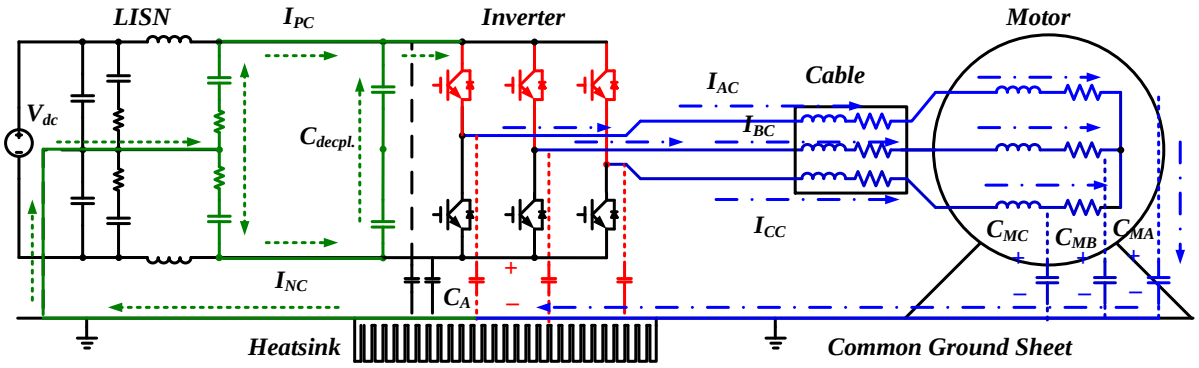

Figure 2.9. Charging of parasitic grounding capacitance during <111>

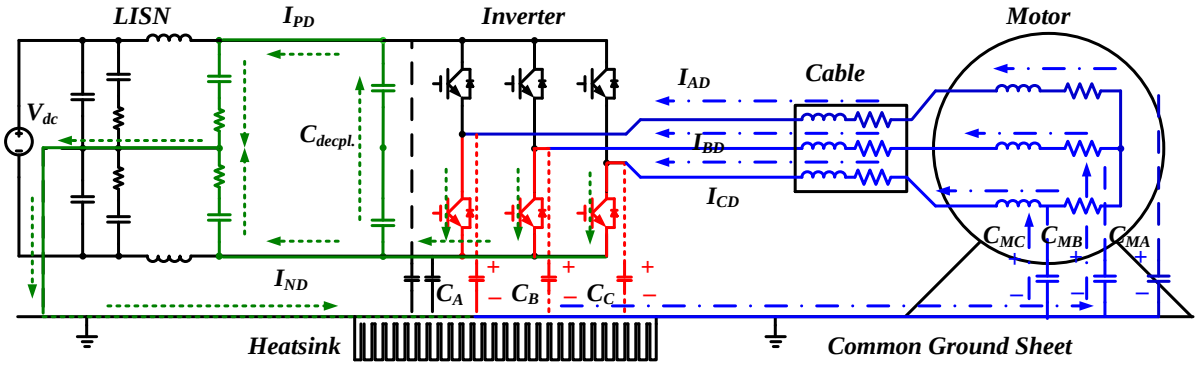

Figure 2.10. Discharging of parasitic grounding capacitance during <000>

2.3.5 Summary of MM Noises

According to the symmetric structure of the three phases, similar study can be carried out during the other non-zero voltage vectors, like <010>, <101> and etc. Table 2.1 summarizes the output MM noise of each phase during every possible voltage vector condition.

Table 2.1: CM and MM Noises Summary for All Possible Switching Conditions

	<000>	<100>	<010>	<001>	<110>	<101>	<011>	<111>
I_{ACCM}	I_O	$-I_O/3$	$-I_O/3$	$-I_O/3$	$I_O/3$	$I_O/3$	$I_O/3$	I_O
I_{MM_A}	0	$-4I_{ACCM}$	$2I_{ACCM}$	$2I_{ACCM}$	$2I_{ACCM}$	$2I_{ACCM}$	$-4I_{ACCM}$	0
I_{MM_B}	0	$2I_{ACCM}$	$-4I_{ACCM}$	$2I_{ACCM}$	$2I_{ACCM}$	$-4I_{ACCM}$	$2I_{ACCM}$	0
I_{MM_C}	0	$2I_{ACCM}$	$2I_{ACCM}$	$-4I_{ACCM}$	$-4I_{ACCM}$	$2I_{ACCM}$	$2I_{ACCM}$	0

When there is zero-vector (<000> or <111>) operating in the inverter, the current on each of the three phases is identical and no MM noise can be found in the measurement. During other switching statuses, the MM noise magnitude on each phase changes from twice to four times of the AC CM noise.

2.4 Motor Drive AC MM Noise Experimental Verification

Literature shows efforts in either obtaining some insightful vision of the MM noise at certain frequency [11], or acquiring the spectrum of MM noise through modeling and calculation [58]. However, a direct measurement of the MM noise spectrum in the standard range of frequency (i.e. 150 kHz to 30 MHz) from experiment is still under development. Focusing on improving the practical EMI filter design, the authors would, instead of keeping on purifying the MM noise from DM noise spectrum, prefer an actual set of experiments which can validate the MM

phenomena and their impact on the selection of EMI filters, since this is more straightforward for helping designing the filter.

Figure 1.12 shows the setup of a prototype motor drive system. The testbed is constructed according to the Standard DO160, including the DC input side feed-through capacitors and line-impedance-stabilization-networks (LISNs). One commercial motor drive from Vacon® is utilized as the power stage. On the output side, one 10 feet 3-conductor cable is applied with standoff, keeping it certain distance away from the common ground of copper sheet. One set of dynamometer with induction machine is connected as the motor load. During operation, 540 V_{dc} is applied to the motor drive. With 16 kHz switching frequency, the induction machine is running at 60 Hz with 230 V_{llrms}.

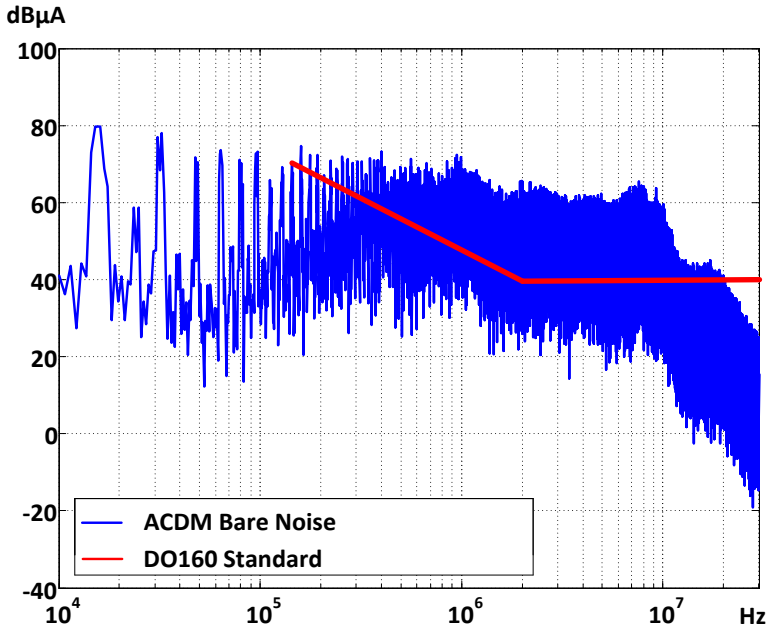

Figure 2.11. AC DM bare noise in prototype system

Figure 2.11 shows the measured results of ac output side DM bare noises. The DO160 standard emission limit is also drawn in the spectrum as a reference. As shown, the DM noise on the ac output side has exceeded the DO160 limit. According to traditional filter design methods, one three-phase LC filter is implemented to the output side of the motor drive, as shown in Figure 2.12. With three 140 µH DM inductors and three 50 nF film capacitors in star-connection, attenuation of the AC DM noise is expected beyond the crossover frequency of 60 kHz. As shown in Figure 2.13, the green curve is the AC DM noise after adding the LC filter. Beyond the over shoot around 60 kHz of crossover frequency, attenuation can be found beyond 60 kHz.

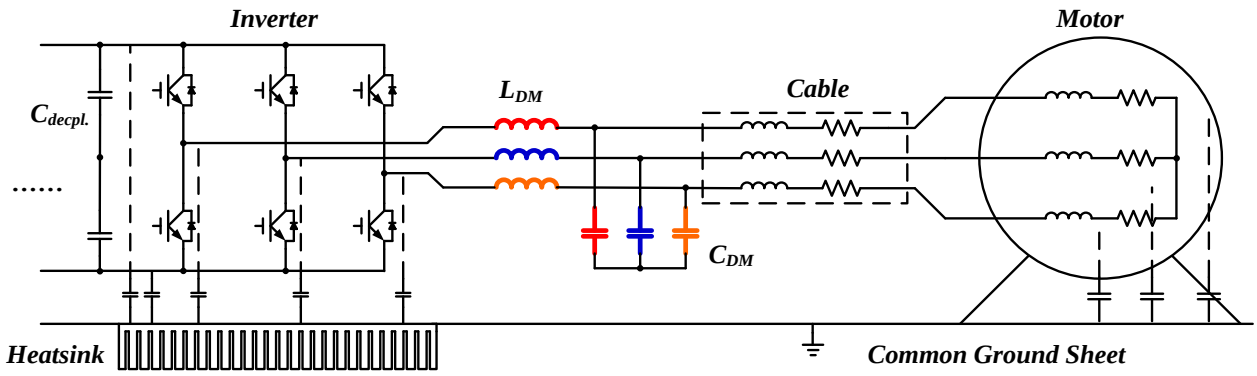

Figure 2.12. Ac side three-phase DM LC filter

From traditional filter design method, the lower the crossover frequency, the higher attenuation the LC filter will achieve. However, as the authors try to increase the DM inductance or capacitance, the AC DM noise does not get suppressed further. In fact, the AC DM noises with different LC filters show similar emission. As shown in Figure 2.14, different AC DM LC filters have been tried. With three 160 µH DM inductors and three 68 nF film capacitors, the crossover frequency has been decreased to around 48 kHz, which can be observed. However, the

noise beyond that is similar with the previous test results shown in Figure 2.13. By further increasing the DM capacitance to 100 nF and reducing the crossover frequency to around 40 kHz, similar phenomena has been found. The attenuation of the filter does not show much difference comparing with the original 140 µH DM inductors and 50 nF DM capacitors.

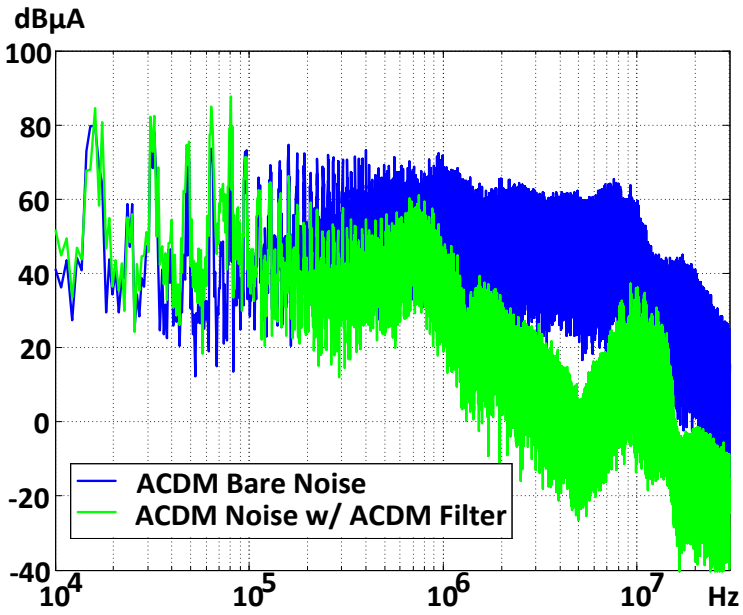

Figure 2.13. AC DM noise with AC DM LC filter

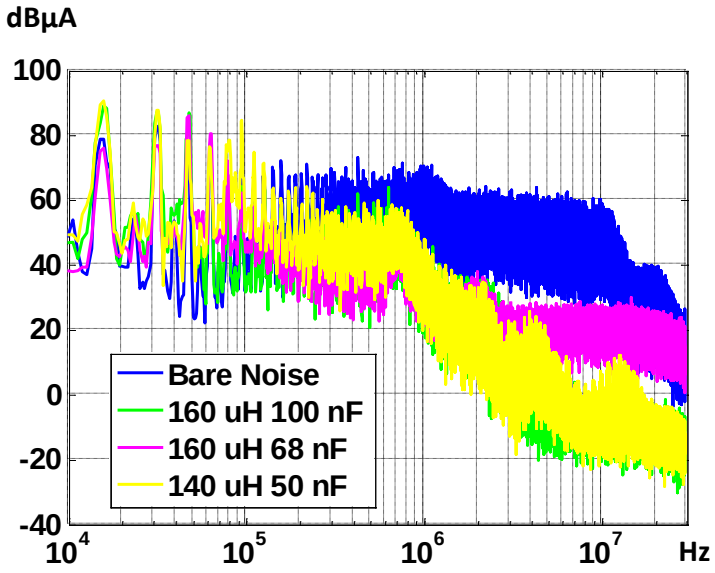

Figure 2.14. AC DM noise with different AC DM LC filters

However, when a simple CM LC filter is added into the circuit, change in the DM noise spectrum happens. As shown in Figure 2.15, a three-phase CM choke of 200 uH CM inductance has been put in series with the 140 µH DM inductors. At the same time, the three DM capacitors have been grounded at the common point, which makes the 50 nF capacitor act also as CM capacitors. As a result, a CM LC filter is realized in the motor drive system. Considering the leakage inductance of 3 µH from the CM choke, there is no significant influence on the crossover frequency of the DM LC filter. Based on the knowledge of conventional EMI filter design, this new filter structure will only filter the ac output CM noise. No significant change in DM noise spectrum is expected. However, as shown in Figure 2.16, the magenta curve of the DM noise with both CM and DM LC filters is further attenuated.

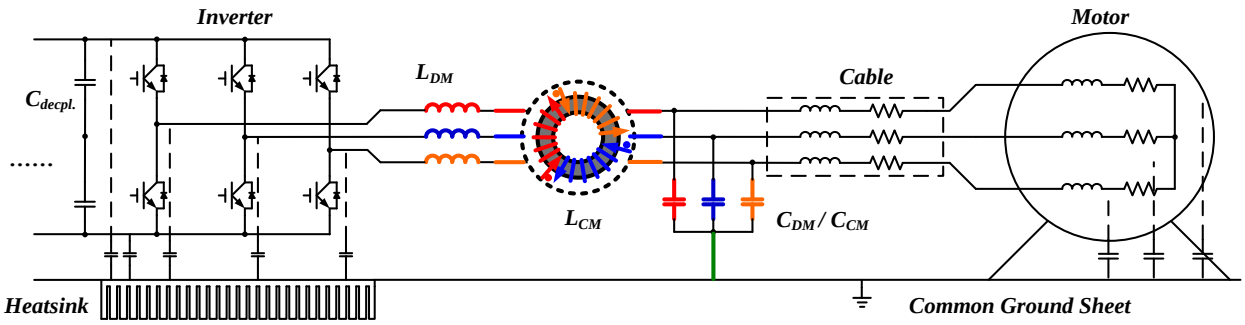

Figure 2.15. Ac side AC CM and DM LC filter

Figure 2.16 is showing the fact that the CM filter is helping attenuate the DM noise, which actually validates the existence of the MM noise in the motor drive system. The previous unsuppressed noise in Figure 2.14 is mainly the MM noise transferred from the CM spectrum. The CM filter in Figure 2.15 attenuates the CM noise. As a result, the MM noise is largely suppressed. Hence the green curve in Figure 2.16 get further attenuated, considering a large part of it is the MM noise which has been attenuated. The magenta curve in Figure 2.16 shows a 40 dB/dec shape until 1 MHz, which is within the expectation of the AC DM LC filter insertion gain.

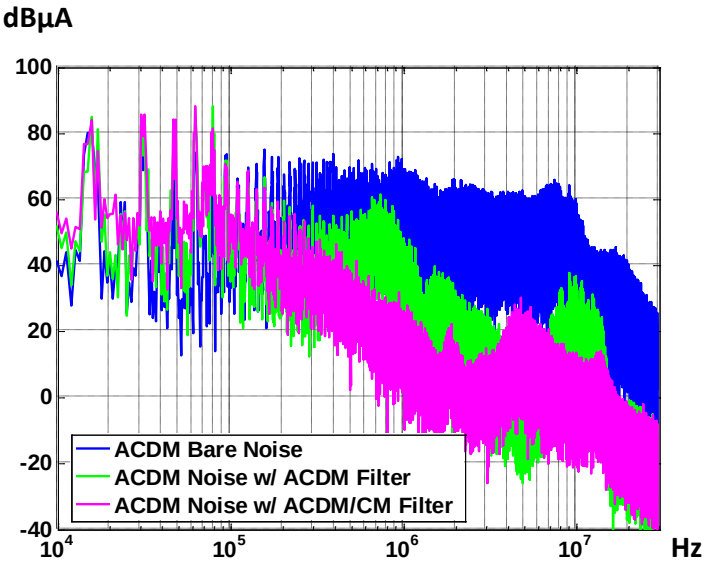

Figure 2.16. AC DM noise comparison: with AC DM filter vs. with AC CM and DM filter

2.5 Discussion on Impact of MM Noise on Filter Design

As discussed in Section 2.4, the green curve in Figure 2.16 is not only intrinsic ac DM noise. Part of it is the MM noise going through the ground. Considering its characteristics, no so-called MM filter is needed to attenuate it. Typical CM filters either increasing or bypassing the output grounding impedance will help suppress the MM noise. If CM noise is well attenuated, MM noise will not cause total noise exceeding standards. Meanwhile, like the discussion in SMPS, DM capacitors, as part of traditional DM filter, will create low impedance path among phases, making all three phases balance, which puts an end to the MM phenomenon unless intrinsic unbalance existing in cable and motor. In short, the MM noise is not an extra type of noise decoupled from the line noise of three-phase, and it does not require extra filtering itself.

However, the existence of the MM noise will influence the DM filter design by misleading designers to select DM inductors and capacitors based on MM noise instead of DM noise. As

shown in the example in Section IV, the MM noise will give filter designers a misconception of higher DM noise than the real value. This misrecognition of the DM noise will introduce larger DM filter than needed.

If the designers are not familiar with the feature of the MM noise and its influence, following the procedure proposed in [64], more and more DM inductance and capacitance will be added. However, this action of reducing crossover frequency will not help attenuate the DM noise until the DM inductance is large enough to act as a CM inductor and suppress the MM noise. Considering the test result shown in Figure 2.16, it is conservative to assuming 600 μH DM inductance is needed to achieve this. Around 4 times of the DM inductance is needed. The higher power rating the system has, the bigger and heavier these three DM inductors will be comparing with CM choke. A design of 100 kW, 200 Arms, 400 Hz motor drive application is selected as an example. As can be found in Figure 2.17, without understanding the MM noise, two more times of weight is added into the design.

As discussed above, no special filter is needed to suppress the MM noise. If both CM and DM noises are well attenuated, the MM noise is suppressed. However, to avoid the overdesign like the example in Figure 2.17, the EMI filter design procedure should be reconsidered. In case of the existence of high level of MM noise emission, it is recommended to implement both CM and DM filter when checking if the DM noise is attenuated by the designed DM filter. When CM noise is suppressed by the CM filter, the influence of the MM noise on DM bare noise measurement will be minimized.

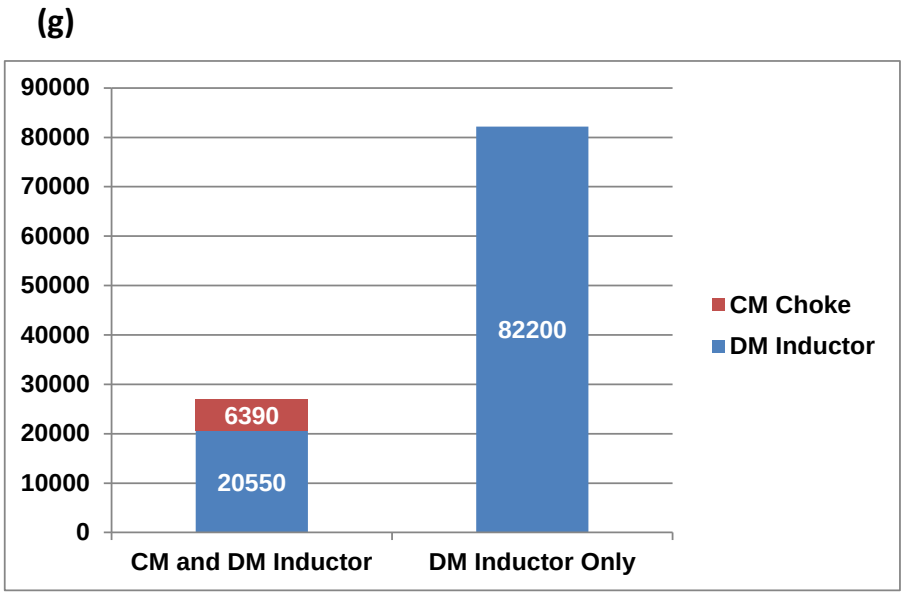

Figure 2.17. Example design comparison: with and without considering MM noise

2.6 Conclusions

The MM noise is one key factor influencing the EMI filter design. In this chapter, the MM noise has been analyzed on the output side of the three-phase motor drive system. Being different from the study of CM and DM noises, one analysis method is proposed for characterizing the MM noise. The generating scheme as well as amplitude and direction of the MM noise at every possible switch condition in three-phase inverter operation is analyzed and summarized under ideal condition when all three phases are perfectly symmetric. According to the propagation feature of the MM noise, one set of comparing experiments are designed and the existence of the MM noise is verified. Discuss on the impact of the MM noise is carried out with one example filter design. The example shows that if not concerning the MM noise, DM filter much bigger than needed might be produced according to traditional design method.

Chapter 3 EMI Noise Mode Transformation Due to Propagation Path Unbalance

3.1 Introduction

Besides the MM noise discussed in Chapter 2, one more phenomenon that may cause filter overdesign or unnecessary iteration is the transformations of the noise mode between the CM and DM. The studies of the noise mode transformation (NMT) are mainly in the area of switching mode power supply application. The analysis of NMT can be divided into two parts. One is focusing on the general characterization of the NMT without specific converter application. S. Wang and etc. [65-70] have discussed the filter component unbalance and its impact on the filter insertion gain through NMT. The other part of the study concentrates on the EMI filter design practice. Comparison of EMI filter design in SMPS applications has been carried out in [71-76].

In this chapter, the system unbalance and noise mode transformation in three-phase VSI motor drives are analyzed. In Section 3.2, the DC CM noise path unbalance is studied. The corresponding CM noise transformed to the DM spectrum can then be characterized accordingly. Experimental verification of the DC CM noise transformation is verified in a prototype system. Then in Section 3.3, the possible factors causing DM noise propagation unbalance are discussed.

The transformation of AC DM noise to CM is observed through equivalent circuit simulation. Section 3.5 gives the conclusion of the work.

3.2 DC CM Noise Propagation Unbalance and DC CM Noise Transformation

Figure 3.1 shows a typical structure of the dc-fed motor drive system. The dashed lines with capacitors indicate the paths of CM noise propagation, including the parasitic grounding capacitances. For the DC side propagation path, the line-impedance-stabilization-networks (LISNs) are also included. As part of the EMI regulation, the input impedance of the LISN is usually defined in the standard [25]. However, the grounding branches of the highlighted parts in Figure 3.1 are not strictly regulated. For commercial products, the tolerance of the resistor and capacitor is varied from 10% to 20%, which means there is an expected difference between the positive and negative grounding impedance.

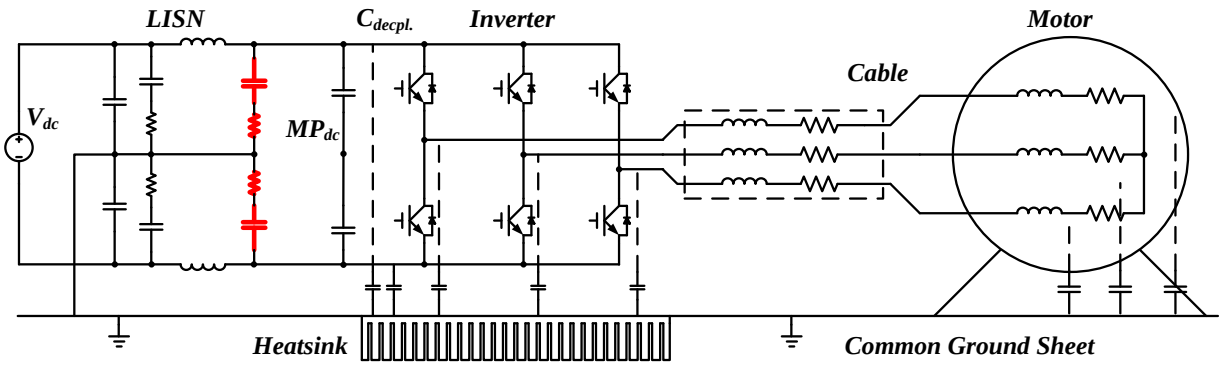

Figure 3.1. LISN schematic with dc-fed three-phase motor drive

Figure 3.2 and Figure 3.3 show the CM noise propagation path when one top switch and two bottom switches are conducting. As shown in the figures, on the power stage side, the decoupling capacitor at the inverter input end helps balance the positive and negative bus. However, if the grounding branches of the LISNs, namely the CP & RP and CN & RN, are different, the charging or discharging currents of the positive and negative buses cannot be identical. As a result, the total grounding currents going through the positive bus and negative bus are different, as shown in (3.1).

$$I_{PC} + I_{PD} \neq I_{NC} + I_{ND} \tag{3.1}$$

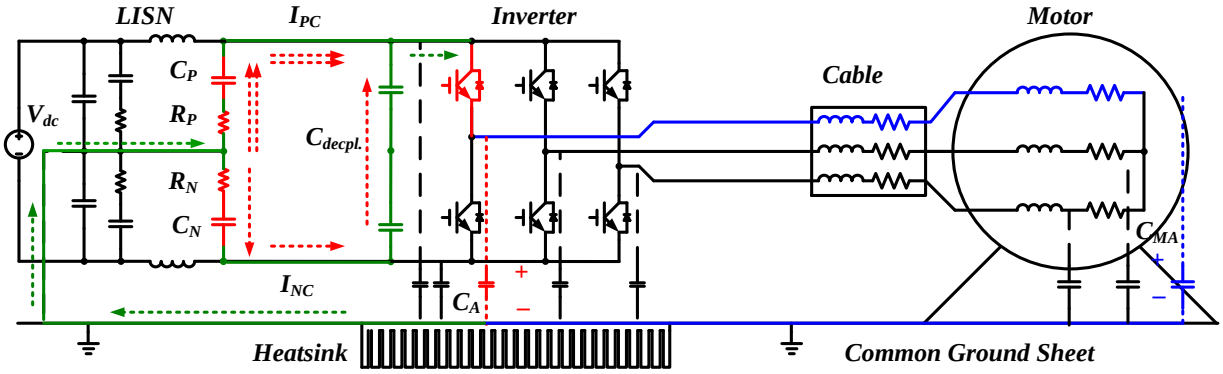

Figure 3.2. Dc side grounding capacitance charging during <100>

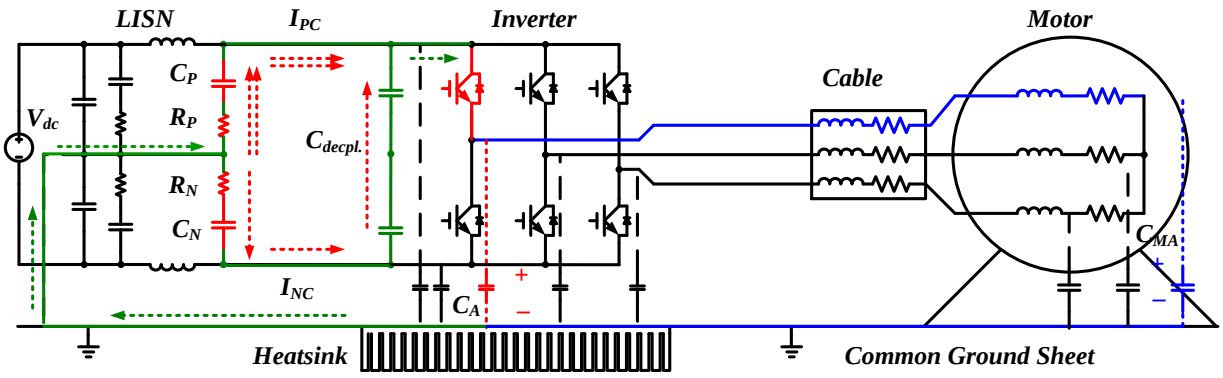

Figure 3.3. Dc side grounding capacitance discharging during <100>

Since the grounding current going through the positive and negative buses are different, the DC DM noise measurement will include this grounding current difference. Therefore, part of the CM noise is transferred to the DM spectrum, which is also called the mixed-mode (MM) noise referred to [11]. Since originated from the CM noise, no extra so-called “MM filters” are needed, since it will be well attenuated if the CM noise can be filtered by a typical CM filter. But if this MM noise is not well configured, it will mislead the designer by applying more and more DM filter and cause filter overdesign, because this part of noise cannot be effectively suppressed by DM filter.

Figure 3.4 shows the system circuit with DC DM filters. A series of typical DM LC filters have been fabricated and implemented into the system.

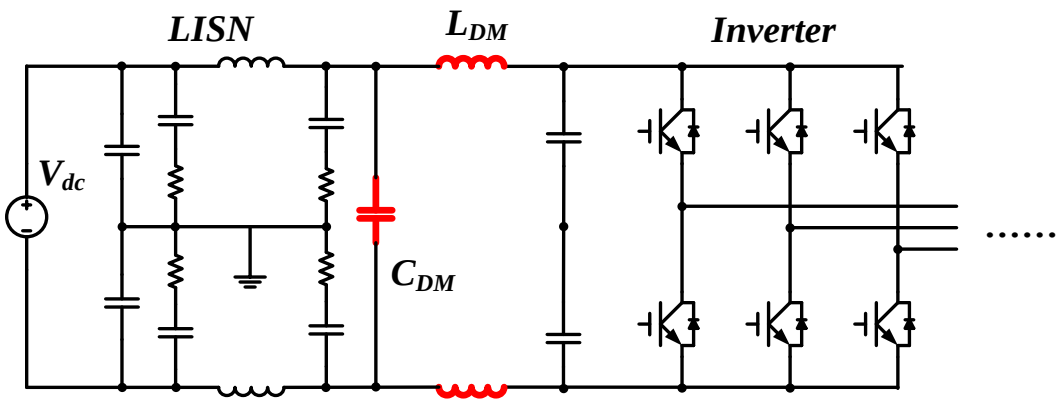

Figure 3.4. Motor drive system with DC CM LC filter

Figure 3.5 displays the DC DM noise comparison results before and after adding the DM filters. The blue curve shows the system bare DC DM noise without any filter. The green one stands for the DM noise when adding the filter of 10 μH and 50 nF. The magenta curve is for the DM noise with 10 μH and 15 μF. Figure 3.5 shows that the DM filters are effective in filtering the noise, since both the green and magenta curves have a part of noise lower than the blue bare noise, beyond their own cut-off frequency, namely 225 kHz for the green one and 13 kHz for the magenta one. However, both filters stop functioning as attenuating DM noise beyond around 500 kHz. As can be seen, the green and magenta curves have similar level of emission comparing with the blue bare noise between 500 kHz to 2 MHz. Beyond 2 MHz, there are influence from parasitic components, which will cause some difference, but still it is not as expected from a typical LC filter.

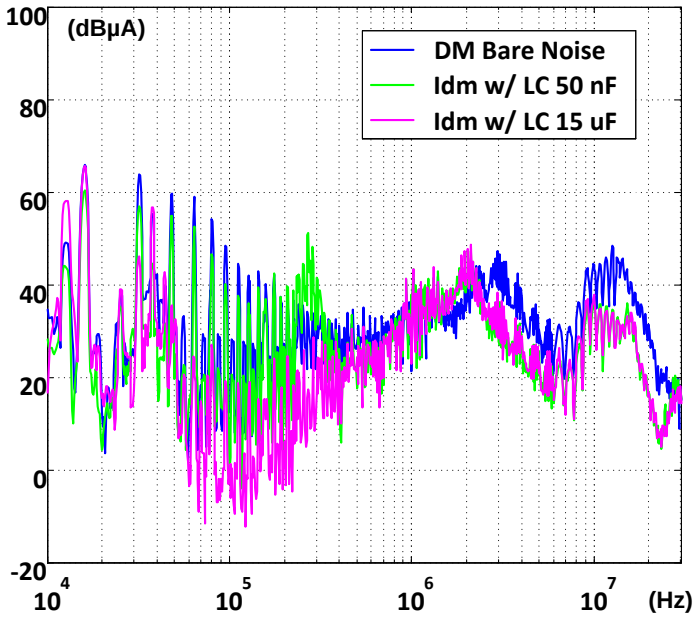

Figure 3.5. DC DM noise comparison: with and without DC DM filter

As a comparison, one CM filter is added into the system with DM filter in it, as shown in Figure 3.6. One DC CM choke is implemented, whose leakage inductance is 10 μH, standing for the DM inductors. Grounding capacitors of 50 nF are added on both positive and negative sides. Comparing with Figure 3.4, the new system has both DC CM and DC DM filters.

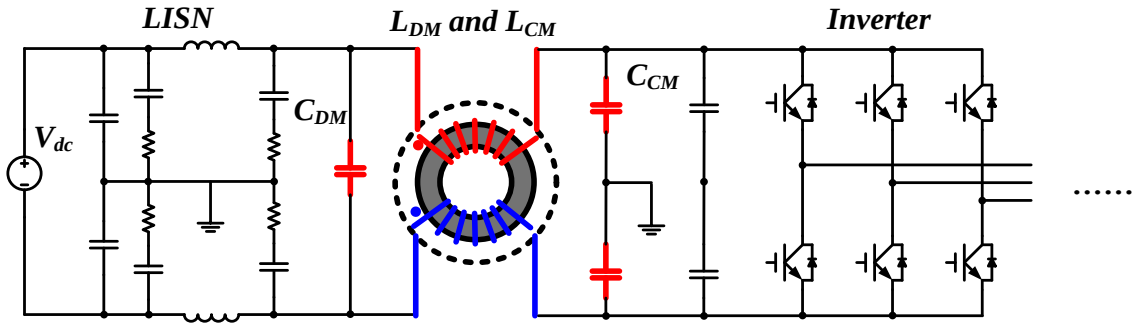

Figure 3.6. Motor drive with DC DM and DC CM filter

Figure 3.7 shows the DC DM noise results after adding the DC CM filter. As the new magenta curve representing the DC DM noise after adding both CM and DM filters, it is observed that the previous un-suppressed noise are well attenuated, which indicates that this part of noise can be only filtered by CM filter instead of DM filter, which is the transformed noise from CM.

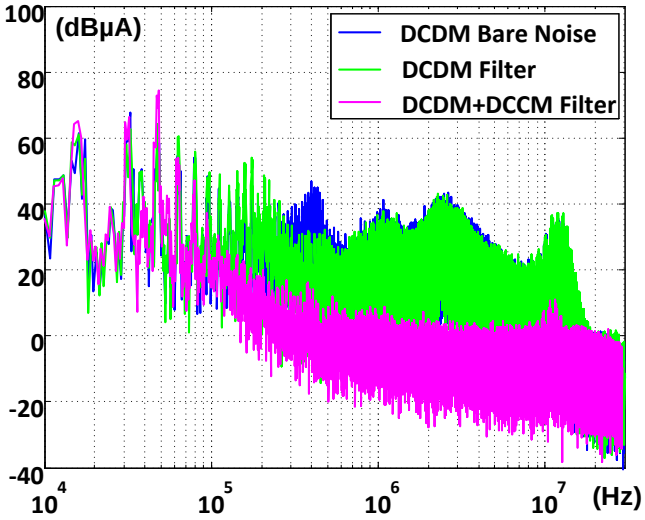

Figure 3.7. DC DM noise comparison: with DC DM filter vs. with both DC CM and DM filter

3.3 DM Noise Propagation Unbalance and DM Noise Transformation

In DM noise propagation path, the discrepancies among the three-phase components of the DM filter are the main contribution to the noise propagation path unbalance. In a system with a typical DM LC filter as shown in Figure 3.8, usually it is assumed that all three phases have identical value of DM inductance and phase-to-phase capacitance. However, in practice, this assumption is difficult to approach. The accuracy of the values of the inductance and capacitance is limited by the manufacturing technics and prices. For example, normally there is a minimum

of 5% tolerance for commercial film capacitors. Concerning the tolerance of the core parameters and winding conditions, three perfectly identical DM inductors are not easy to realize either. These discrepancies in inductors and capacitors would result in the unbalance of the DM noise path.

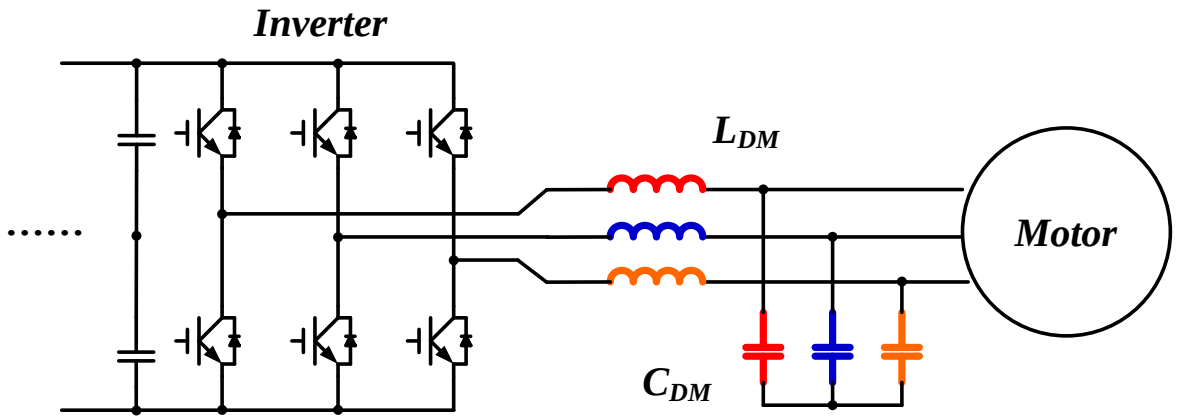

Figure 3.8. Ac side DM LC filter

This unbalance of the DM noise path will introduce transformation of the DM noise into CM spectrum. If the DM noise level is low, this transformation will not cause problems in CM filter design. However, the DM LC filter often brings in DM noise resonance at its cut-off frequency. The resonance peak is of high emission level and can be observed influencing the CM noise spectrum.

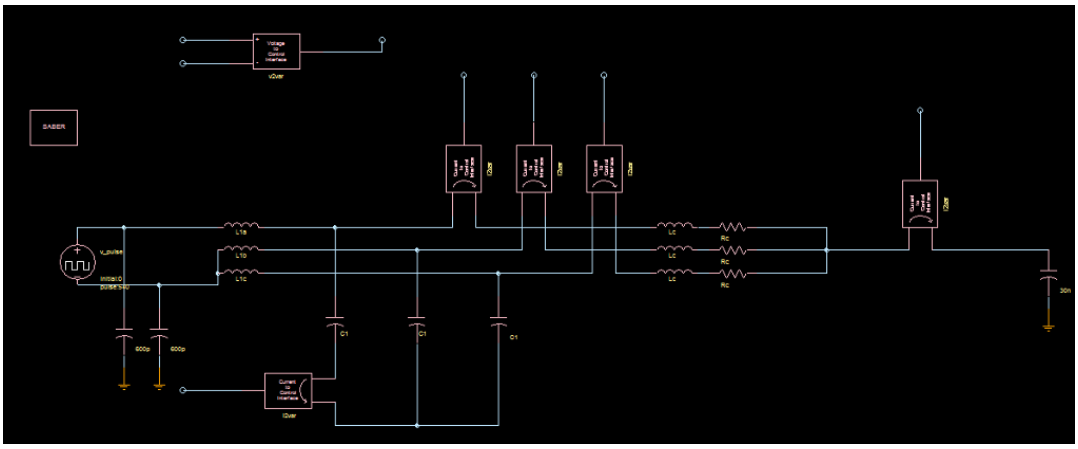

Figure 3.9. CM noise analysis in simulation

One simulation file is set up in Synopsis Saber® as shown in Figure 3.9 for the condition when only one top switch is conducting. The current going through the grounding capacitance of the motor (30 nF from commercial motor measurement) can then be treated as the CM current. As shown in Figure 3.10, if purposely unbalancing the three DM inductances from 0% to 20%, the DM LC resonance can be found in this CM current, which shows the existence of the DM to CM noise transformation. The more unbalanced the system, the more DM noises are transferred to CM measurement.

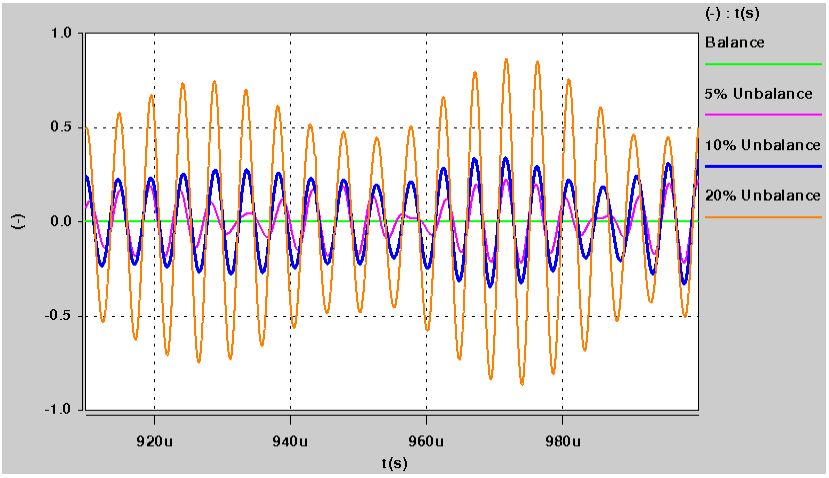

Figure 3.10. CM current simulation result at <100>

To get a better view of this unbalance and its influence on DM noise transformation to CM, a typical CM LC filter is added into the prototype motor drive system, including three 50 nF Y-capacitors and two three-phase CM choke both having 200 μH CM inductance but slightly different leakage inductance. One is 2.5 μH and the other is 3.5 μH. The equivalent circuit is shown in Figure 3.11.

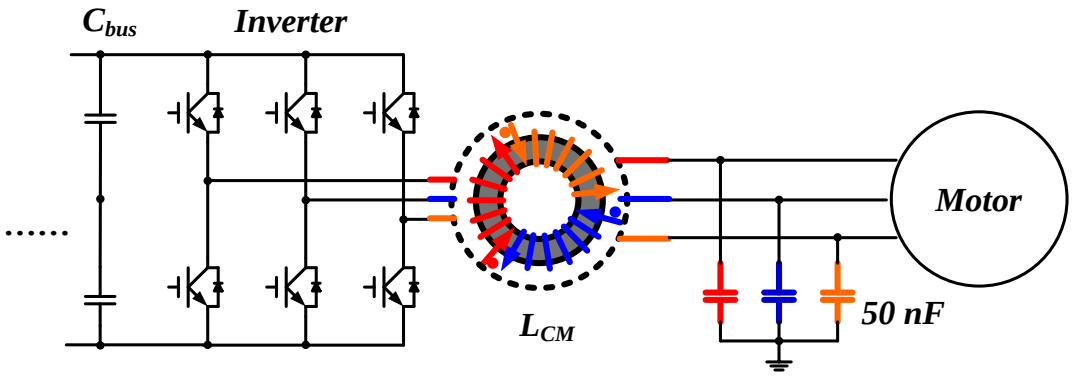

Figure 3.11. Ac side CM LC filter

Figure 3.12 shows the AC CM noise measurement results comparison from the spectrum analyzer. The blue curve is the AC CM bare noise. The green and magenta curves stand for the AC CM noise after implementing two different LC filters. The green one has bigger leakage inductance and the magenta one has smaller value. Resonance peaks can be found in the two attenuated CM noise curves, at 380 kHz (green) and 450 kHz (magenta) accordingly. In Figure 3.13, the impedance of the leakage inductances of the two CM chokes are compared with the grounding capacitance of 50 nF. The two crossing points of the three impedance curves are also at 380 kHz and 450 kHz, which represent the resonance frequencies of the leakage inductance of the CM LC filter and phase-to-phase capacitor. This indicates that the resonance peaks in Figure 3.12 are caused by the resonance of impedance in Figure 3.13. In the other way, this resonance in the CM spectrum is the DM resonance. The DM noise has been transformed to the CM spectrum.

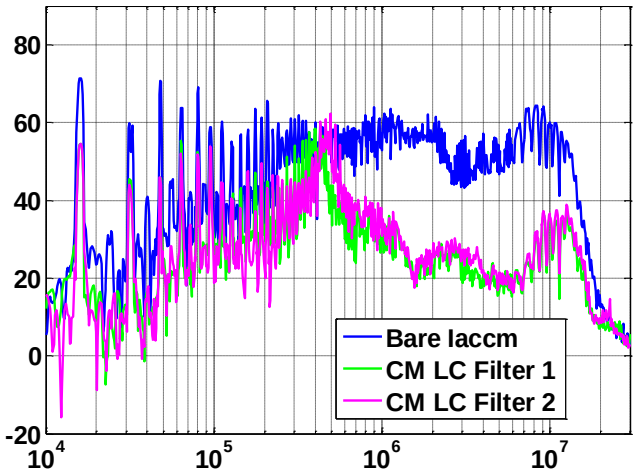

Figure 3.12. AC CM noise comparison: with and without CM LC filter

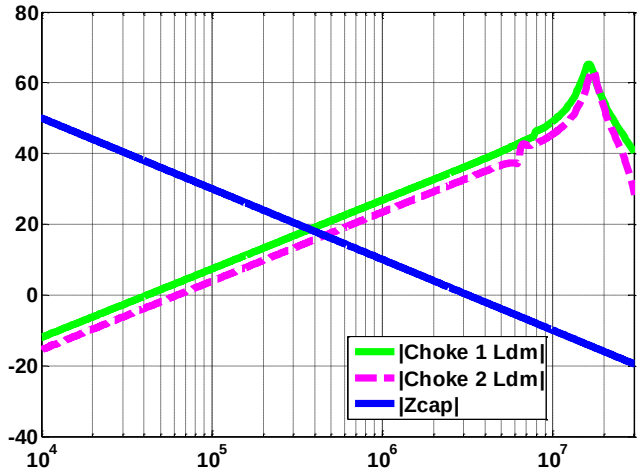

Figure 3.13. Leakage inductance and CM capacitor impedance

3.4 Conclusion

The noise transformation is one key factor influencing the EMI filter design. In this chapter, focusing on the motor drive system, the reason of noise transformation is discussed. For the CM noise emission propagation path, the unbalance from the LISNs grounding branches introduces CM noise transformation to DM. Meanwhile, the component value difference among three phases in DM filters causes DM noise path unbalance and results in DM noise transformation to CM spectrum. Experimental results have verified the existence of both CM and DM noise transformation. A comprehensive design method considering the effects of unbalance and noise transformations is proposed.

Chapter 4 Motor-end EMI Filter on Output Common-mode Noise Suppression

4.1 Introduction

For the suppression of the CM noise, the traditional method is to add EMI filters on the output terminals of motor drive, or inverter-end (IE) filters [29, 57, 77]. This method is proved to be effective in CM noise attenuation. However, as the essence of EMI filters, inductors and capacitors usually bring in extra weight and volume into the system, which is undesirable in transportation applications like the electric vehicles and the more-electric aircrafts [20]. Meanwhile, the filter design method is often not easy to conduct. Because of the difficulty in predicting the system original "bare" CM emissions without the knowledge of the high frequency impedance information of the system, especially cable and motor, most of the filter design procedures only start after the fabrication of the motor drive power stage. And these procedures are frequently accompanied with time-consuming iteration tests, since the attenuation effect of the filters are also influenced by the unknown system impedance information.

In other words, if the impedance information of the cable and motor can be obtained, or even modified through attaching EMI filters at the motor end, the CM noise emission can be not only predicted, but even designed to be reduced. With a better and known impedance of the motor and cable, efforts in filter design can be saved, and weights of the conventional IE filters can also be

reduced with a more systematical design. An effective way of knowing and modifying the cable and motor impedance is by adding an EMI filter at the motor end. If there is impedance mismatch between the filter and the cable and motor in the conducted EMI frequency range, impedance will be shown as the filter impedance.

The structures of the motor-end EMI filter have been studied since late 1990s. G. Skibinski [78] proposed an RC damping topology at the motor end of the long cable for the motor terminal overvoltage suppression. In 1999, N. Aoki etc. [56] derived analytical design approaches for two types of motor-terminal damping networks, with the similar purpose of the long-cable overvoltage attenuation. Later on, the motor feed cable terminators [79] as well as the surge and EMI noise control board [80] are also developed with the idea of adding passive components at the motor end. These are all effective practices of applying motor-end filters; however, their first concern is the differential-mode overvoltage at the motor terminals, not the common-mode EMI noise emission.

This chapter discusses the application of the motor-end filter for the CM noise attenuation. In Section 4.2, the possible structures of the motor-end filter have been discussed, and compared with the inverter-end (IE) filters. According to the analysis of the CM noise propagation path and the emission acquisition method, the motor-end topologies have been categorized as motor-front-end (MFE) and motor-chassis-end (MCE). Focusing on the CM noise suppression, this chapter concentrates on the condition when there is minor effect from the cable length and the cable grounding parasitic impedance. In Section 4.3 and 4.4, detailed analysis of the MFE and MCE filters are described separately, with example filters designed and tested in a prototype motor drive system, compared with a conventional IE CM choke. The benefits and restrictions of the two types of motor-end filters are summarized in the conclusion.

4.2 Motor-End EMI Filter Implementation Discussion

The output CM current emission is determined by both the PWM CM voltage and the CM noise propagation path impedance [36, 77]. One typical circuit configuration of a dc-fed motor drive system is illustrated in Figure 4.1. The blue and red dashed lines indicate the propagation path of the CM noise emission for both the output and input sides.

The output CM current noise is captured through a high-frequency current transformer (CT). As shown in Figure 4.1, the CM voltage acts like a noise source which applies to the propagation path impedance. Accordingly, an equivalent single-phase circuit can be derived in Figure 4.2. In it, the input side CM path is simplified as the DC load impedance Z_{dc_load}, while the output side as the AC load impedance Z_{ac_load}. The IGBT-to-heat-sink parasitic capacitances are named as the source impedance for both the DC (Z_{dc_source}) and AC (Z_{ac_source}) sides. Therefore, the output CM emission can be written as (4.1).

$$I_{cm} = \frac{V_{cm}}{Z_{ac\_source} // Z_{ac\_load} + Z_{dc\_source} // Z_{dc\_load}} \times \frac{Z_{ac\_source} // Z_{ac\_load}}{Z_{ac\_load}} \tag{4.1}$$

Equation (1) shows that both the V_{cm} and the impedances contribute to the CM noise emission. Conventional inverter-end filters mainly focus on modifying the noise source impedance, by increasing it with series-connected three-phase CM chokes, or by creating a low impedance bypassing path in it, like the grounding capacitors, so that the high frequency CM noise emission is not going through the current transformer.

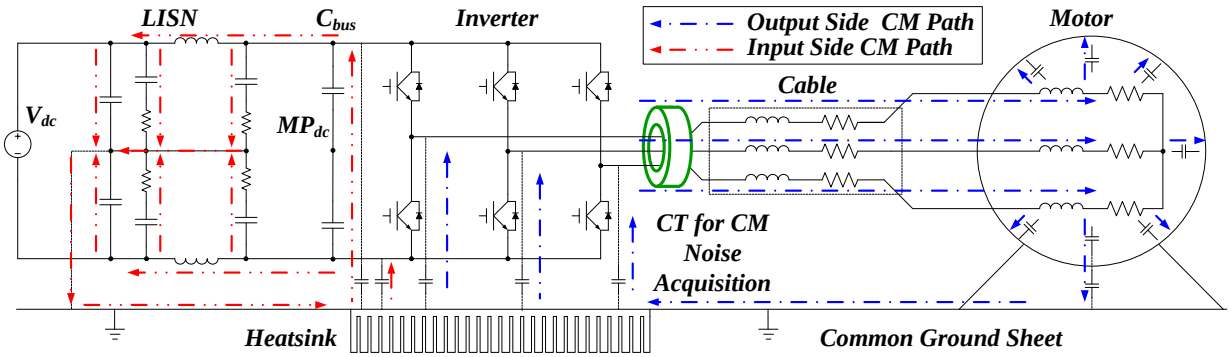

Figure 4.1. AC CM noise measurement in three-phase motor drive system

On the contrary, a motor-end filter aims at altering the load impedance Z_{ac_load} so that the I_{cm} in (4.1) can be reduced. Since the EMI noise is measured at the output terminal of the motor drive, the bypassing-branch topology is not applicable for the motor-end filters. On the other hand, because of the relative high impedance of the Z_{ac_source} and Z_{dc_source} in Figure 4.2, a higher Z_{ac_load} will introduce lower level of the I_{cm} emission. Hence the motor-end filters are targeting on increasing the output impedance Z_{ac_load} through series-connecting passive components with high impedance at high frequency range. Consequently, inductors are selected and two kinds of CM inductor-based motor-end filter connections are mainly analyzed in this chapter. The first one is by inserting a three-phase CM choke at the three input terminals of the motor, with the name of the motor-front-end (MFE) filter, which is shown in Figure 4.3. The other one is by connecting an inductor between the motor chassis and the ground, which is called the motor-chassis-end (MCE) filter and shown in Figure 4.4.

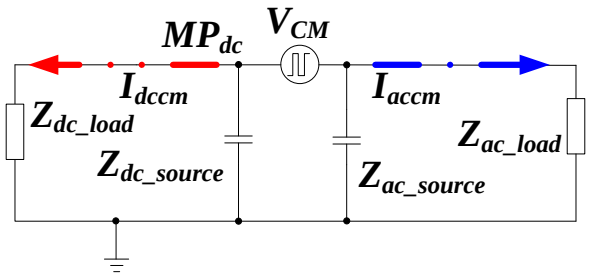

Figure 4.2. Simplified single-phase CM equivalent circuit

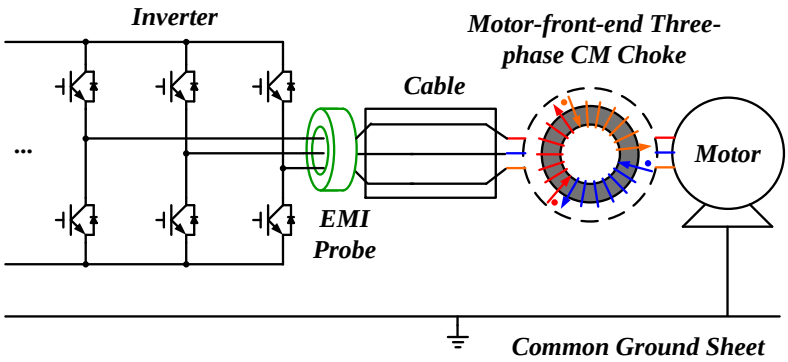

Figure 4.3. Conventional motor front-end (MFE) EMI filter

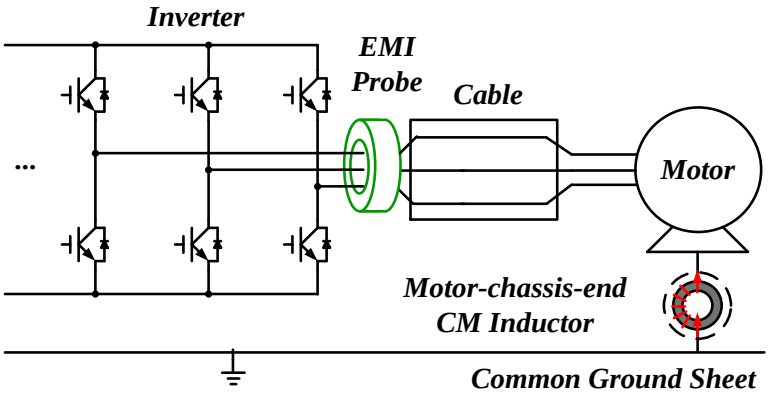

Figure 4.4. Motor chassis-end (MCE) EMI filter

4.3 Motor-Front-End (MFE) Filter Design and Analysis

The major difference of the MFE filter from the IE CM inductor is the location of the CM choke. In the case with a three-wire unshielded cable shorter than 10 feet, the long-cable effect and cable grounding impedance can be both neglected [81], which simplifies the AC side path as a series-connecting circuit. Thus the functions of the IE and the MFE filters are similar, with the attenuation on CM noise written as (4.2). In it, the Z_{ac_L} stands for the impedance of either the IE or the MFE CM choke.

$$Att = dB\left(\frac{Z_{ac\_source}//\left(Z_{ac\_load}+Z_{ac\_L}\right)+Z_{dc\_source}//Z_{dc\_load}}{Z_{ac\_source}//Z_{ac\_load}+Z_{dc\_source}//Z_{dc\_load}}\times\frac{Z_{ac\_source}//Z_{ac\_load}}{Z_{ac\_source}//\left(Z_{ac\_load}+Z_{ac\_L}\right)}\times\frac{Z_{ac\_load}+Z_{ac\_L}}{Z_{ac\_load}}\right) \quad (4.2)$$

Table 4.1: Example MFE and MCE Inductors

	MFE Inductor	***MCE Inductor***
Core	F1AH0706	F1AH0706
Material	Finemet®	Finemet®
Winding	3	1
Turns	9	9
Wire Gauge	17 AWG	17 AWG
Core OD	68 mm	68 mm
Core ID	19 mm	19 mm
Core Height	30 mm	30 mm

An example three-phase CM choke is wound with the information shown in Table 4.1, which is used as either the IE filter or the MFE filter. The impedance of the choke is compared with the Z_{ac_load} of the prototype system in Figure 4.5, together with the modified output impedance after implementing the IE or the MFE filter. Since the choke impedance is much higher than the

original motor and cable impedance beyond 100 kHz, the Z_{ac_load} can be changed to approximately the choke impedance with series-connection. The MFE filter, as the green curve shows, has similar performance on the Z_{ac_load} improvement with the conventional IE filter, from 150 kHz to around 2 MHz. Beyond 2 MHz, the MFE filter is influenced by the cable grounding parasitic, with around 10 dB lower magnitude than the IE filter, but still higher than the original Z_{ac_load}, which means benefits on the CM noise attenuation. Figure 4.6 illustrates the measured output CM noise emissions. Compared with the system bare CM noise without any filters in the blue curve, both the IE filter and the MFE filter show similar contributions on the CM noise suppression between 200 kHz and 2 MHz, which matches with the impedance measurement results. Though not as large, the MFE filter still introduces some further attenuation beyond 2 MHz and till 10 MHz, which is also consistent with the impedance comparison results in Figure 4.5.

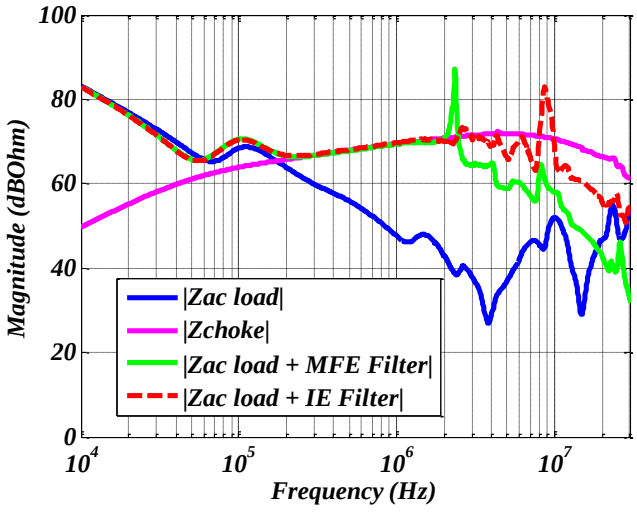

Figure 4.5. Output impedance comparison: with MFE filter vs. with IE filter

4.4 Motor-Chassis-End (MCE) Filter Implementation Practice Discussion

For safety concerns, the motor chassis is usually directly grounded or guarded with special attention [82]. The discussion in this chapter is under the condition of the guarded motor frame. As shown in Figure 4.6, the MCE filter effectively avoids conducting the main current going through the cable, which can largely save the size and weight of the EMI filters in high power applications. Moreover, only one winding is required in the MCE connection, which can further reduce the weight of the three-phase CM choke with three windings.

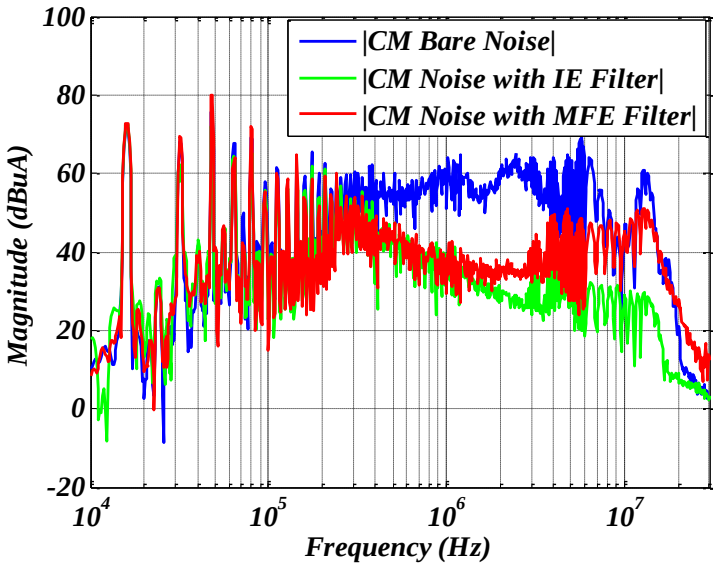

Figure 4.6. CM noise comparison: with MFE vs. with IE filter

One demo MCE filter is wound as shown in Table 4.1. For comparison with the MFE and the IE choke, same core and winding turns are selected. As a result, the impedance of the MCE inductor is in agreement with the MFE choke until 5 to 6 MHz in Figure 4.7. The difference of parasitic winding capacitance results in the discrepancies beyond 6 MHz. When connecting to the motor chassis, as illustrated in Figure 4.8, the MCE inductor can help increase the system

Z_{ac_load} as much as the IE choke, however only in the range within 2 MHz. In the higher range of frequency, the impedance improvement effect of the MCE filter is reduced due to the parasitic capacitance coupling between the motor chassis and the common grounding, together with the cable grounding parasitic capacitance.

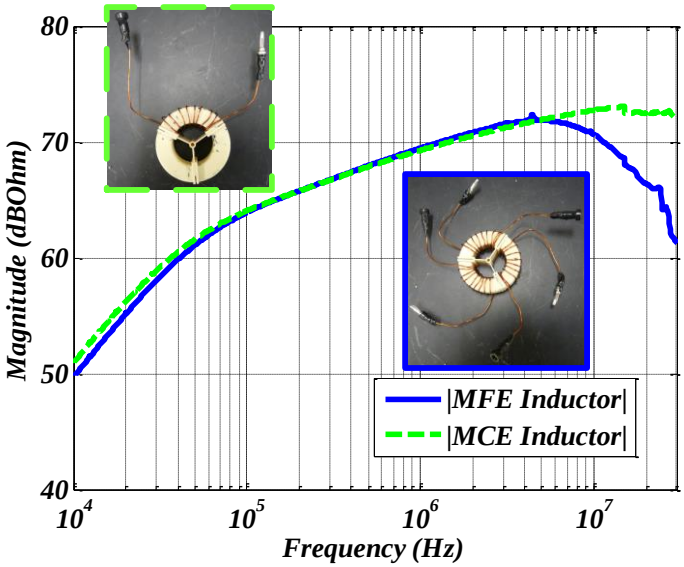

Figure 4.7. Impedance comparison of example MFE and MCE inductors

Figure 4.9, Figure 4.10 and Figure 4.11 list three typical cases of interactions between the motor chassis and the ground. Considering the capacitance between the motor chassis and the common grounding sheet is the major factor influencing the effect of the MCE filter, the relative position of the motor chassis and the copper sheet is varied. In Case I, the motor and base is put away from the common copper grounding sheet. In Case II, the whole motor load is located directly on the copper sheet. In Case III, the chassis is set right under the copper sheet.

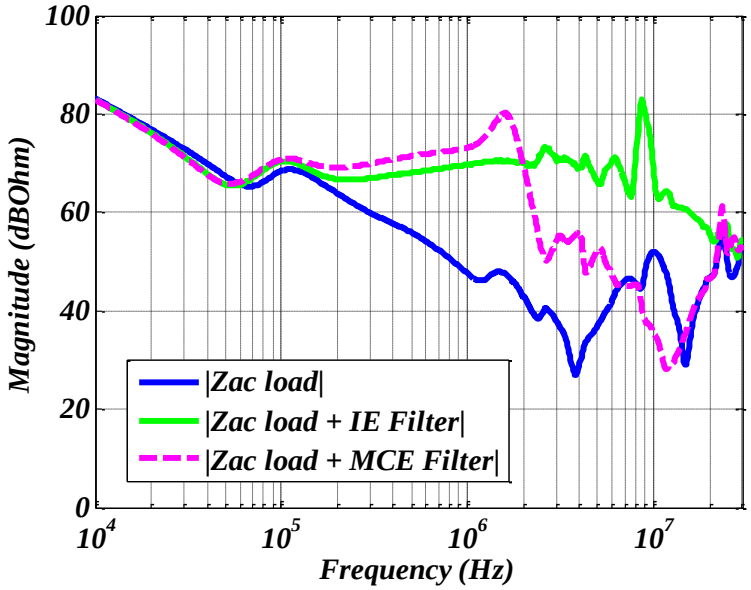

Figure 4.8. Output impedance comparison: load with IE filter vs. load with MCE filter

The MCE filter is added between the motor chassis and the common ground. Figure 4.12 shows the measured output CM impedance of the three different cases, comparing with the original AC load impedance. From the measurement results, the location of the motor chassis to the grounding sheet influences the performance of the MCE filter.

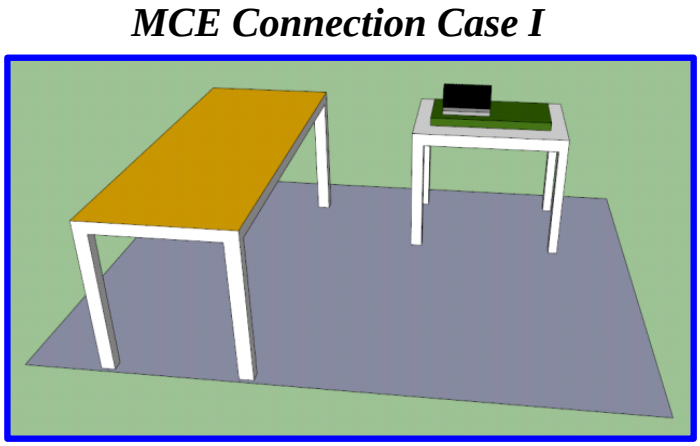

Figure 4.9. MCE layout: Case 1

MCE Connection Case II

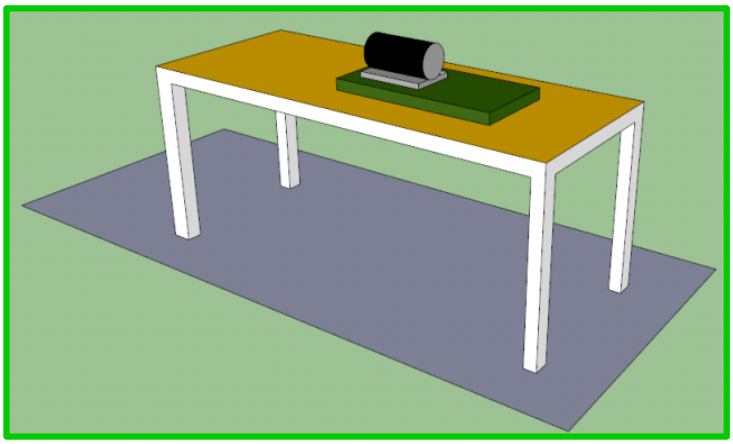

Figure 4.10. MCE layout: Case 2

MCE Connection Case III

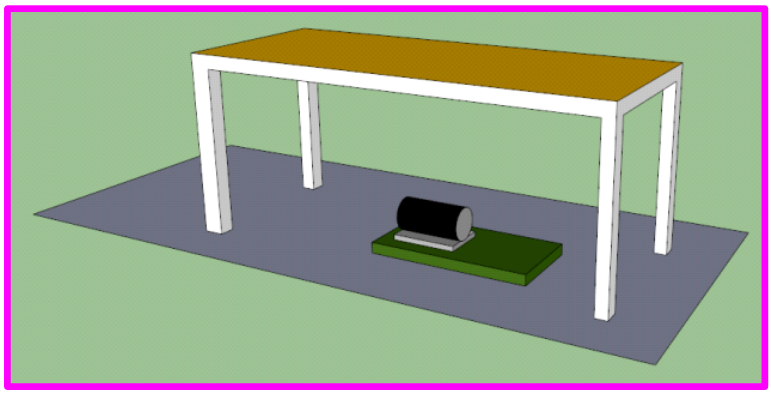

Figure 4.11. MCE layout: Case 3

However, even if there is side effect from the parasitic impedances, there is still around 10 dB benefits of the CM impedance comparing with no filter added, as shown in the red curve.

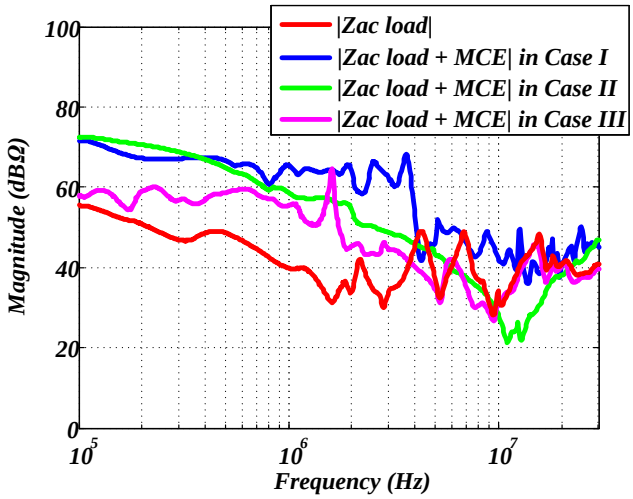

Figure 4.12. Output impedance comparison with different layout cases

Figure 4.13 shows the CM noise emission of the system with the MCE filter, comparing with the traditional IE filter. As expected from the impedance comparison in Figure 4.12, the magenta curve (the MCE filtering results) still has around 10 dBμA attenuation from the blue one of the original system bare noise, although not as great as the suppression from the conventional IE filtering results at the high frequency range.

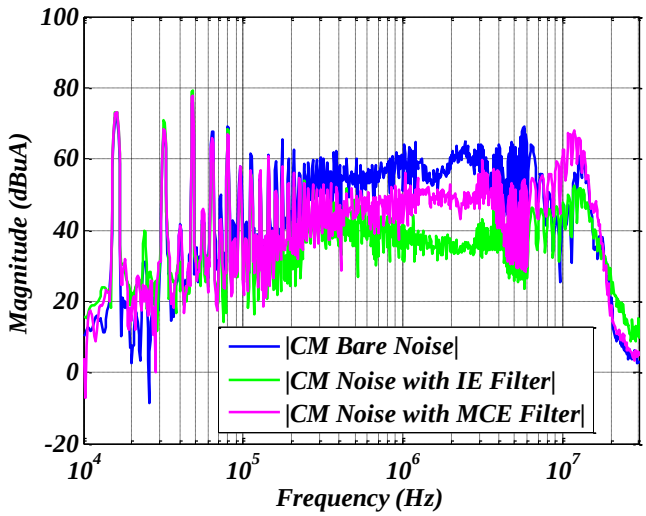

Figure 4.13. CM noise comparison: with IE filter vs. with MCE filter

4.5 Conclusion

This chapter discusses the effects of applying the motor-end EMI filter for conducted CM noise suppression. Two typical types of motor-end filters are analyzed and compared based on prototype system experiments. Although suffered from grounding parasitic impedance influence beyond around 2 MHz for both, the MFE and MCE filters show benefits in high power high density motor drive design. Under the condition of short, unshielded three-wire cable feeding, the MFE filter has similar noise attenuation performance with the IE CM choke, which can help save the steps of the conventional inverter-end EMI filter design and iteration, since the system bare noise can be reduced. The MCE filter is also a potential option in saving the magnetic weight of the conventional IE filter by conducting only CM noise current in only one winding.

Chapter 5 A Practical Liquid-Cooling Design Procedure for Magnetic Components in High Power Dc-Fed Motor Drives

5.1 Introduction

Magnetic components in dc-fed motor drives mainly include common and differential-mode inductors of electromagnetic interference (EMI) filters, and sometimes interphase inductors for the interleaved topology. For high power motor drive systems, thermal is usually one key factor limiting the power density of these magnetic components, and therefore the power density of the entire system [20]. To approach high density design, especially in applications of hybrid and electric vehicle and more-electric-aircraft, liquid-cooling is one important and effective thermal management method [83-85].

Inductors have three-dimensional heat source and uneven surface of loss dissipation. As a result, different methods need to be considered, other than directly putting the inductor on the cold plate, as in the practice of semiconductor device cooling design. Encapsulations are usually applied to inductors before attaching them to the cold plate [86]. These enclosures can create a more intimate contacting surface with the coldplate. Meanwhile, the relatively-higher-thermal-conductivity potting materials are supposed to fill all the air gaps between winding turns and between the winding and the core. Therefore, the heat source can be treated as a solid one.

Regional hot spot in the inductor can be avoided. [87-94] have indicated industrial efforts on several types of encapsulation methods for different shapes of inductors. For detailed thermal model study, [95] and [86] have carried out finite element analysis based on three-dimensional multiphysics software. These methods of liquid-cooling design are proved effective in matching with test results. However, from a practical magnetic designer's point of view, these methods are not straightforward enough in guiding the design procedure, mainly in three aspects.

Firstly, in the cooling setup building process, there are unpredictable factors that would influence the thermal performance. As shown in [86] and [95], potting is one key step in the cooling realization. Considering the viscosity of the potting material before curing, there might be voids in the final fabrication. These air voids would have negative impact on the thermal conductivity of the encapsulation. It is difficult to model these influences in simulation without doing any tests. [86] has raised the hybrid method combining both 3D simulation and practical measurement to develop the encapsulation model. Based on this method but aiming at potting evaluation, the author would recommend a simplified method to verify the thermal performance of potting process.

Meanwhile, detailed FEA simulation models are usually needed. To reach required accuracy, time-consuming initial condition setting and parameter tuning are often inevitable. These methods would work well with one inductor cooling design. However, when there are multiple design tasks including CM, DM and interphase inductors, it would take much longer time to build models for each of the inductors since they are different in shape, material and heat source. In this work, an experiment-based practical thermal model characterization method is suggested.

Last but not least, the uncertainty of the loss model of the inductors needs to be considered. In the application of motor drive systems, the core and winding loss are not easy to characterize

since the excitations are usually non-sinusoidal. There are methods estimating the core [96-99] and winding losses [100, 101] under certain operation conditions. However, the interaction between the loss and component temperature always requires special attention [86]. That's why people usually go back to 3D multiphysics FEM for predicting the final loss of the inductors at steady state, which can be very accurate with the penalty of large amount of efforts and time consumed. At the same time, if any thermal failure happens to these inductors, possible damage might occur to other components in the system. Iterations on building the power stage together with the inductors are essentially expensive and time-consuming considering high power applications. Considering both aspects, tests that can emulate the excitations of inductors in the final systems are necessary, before final magnetic implementation and system-level thermal tests. In this chapter, a general purpose thermal testbed has been built to emulate real conditions of high power motor drives. Practical thermal tests can be carried out based on this testbed to characterize the loss of the inductor in condition of the final system, before really implementing the components into the final system and running system-level tests.

This chapter is organized in the following way. In section 1, the commonly-used encapsulation method for inductor is introduced. Based on previous study, a simplified one dimensional thermal model is built. Initial design of the inductors can be carried out according to the model. In section 2, a simplified evaluation test can be carried out to ensure the potting process is correct and effective. Cooling models of different inductors are developed based on experiments in section 3. In section 4, before putting the components into final system, a testbed has been built, emulating the excitations on the inductors in the final system. An example interphase inductor has been tested. The comparison with the final system test results shows good agreement.

Section 5 combines the techniques explained in Section 1 to 4 and summarizes a practical liquid cooling design procedure for the magnetic components in high power motor drives.

5.2 Inductor Liquid Cooling Introduction

Different patterns of encapsulation methods for inductors have been invented since. Among these different cooling designs, the basic idea is the same, as shown in Figure 5.1.

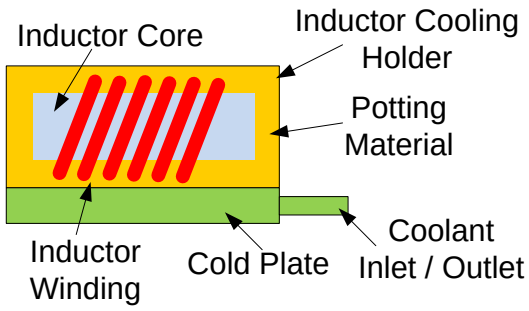

Figure 5.1. Inductor liquid cooling structure

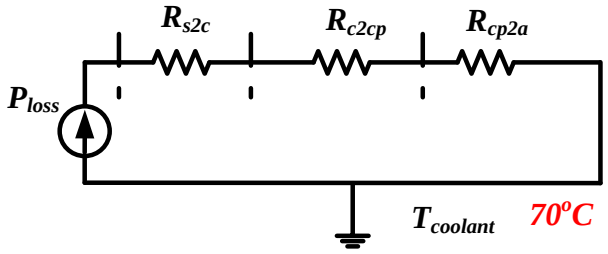

Figure 5.2. A simplified thermal model for inductor liquid cooling

Relatively high conductivity materials like copper or aluminum have been selected as the enclosure of the inductor. These cases have flat and smooth surface contacting with the cold plate. Thermal interface materials like thermal greases are selected to fill possible air gaps

between the case bottom surface and the cold plate. Inside the case, the wound inductor is held. Thermal conductive but electrical insulated materials like thermal epoxies are selected to fill the spaces between the inductor and the case. As summarized in [86], the major heat transferring path lays in the vertical direction, from the heat source of the inductor winding and core to the bottom of the case and finally reaches the ambient media of liquid coolant. As a result, a simplified one dimensional thermal model of the system can be summarized as shown in Figure 5.2.

In the equivalent thermal circuit, the current source stands for the simplified heat source of the inductor. The thermal resistance of R_{s2c} represents the media between the heat source of the inductor and the case enclosure. In it, it is mainly the potting material. Considering the temperature drop on this layer, the thinner potting material has the better cooling performance. In practice, the feasible minimum dielectric thickness can be assumed. In the design example, one epoxy-based potting material named Duralco® 128 is selected. According to its material datasheet, a 1 mm layer is applied on the internal surface of different shapes of aluminum cases, as shown in Figure 5.3.

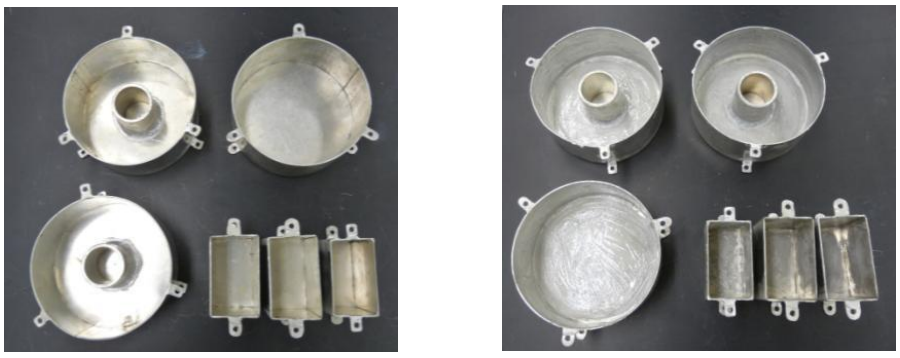

Figure 5.3. Cooling cases for CM and DM inductors

Hipot tests can be carried out for these layers, ensuring the insulation of at least 2000Vac, as shown in Figure 5.4.

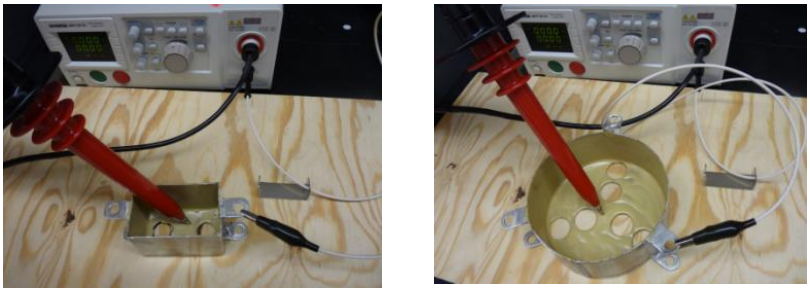

Figure 5.4. Hipot tests for CM and DM cases with potting

As a result, according to (5.1), the thermal resistance can be estimated:

$$R_\theta = \frac{l}{A \times k} \tag{5.1}$$

In (5.1), l stands for the thickness of the potting material. *A* represents the contacting area of the surface. *k* indicates the ideal thermal conductivity of the potting material referring to its datasheet.

R_{c2cp} in Figure 5.2 stands for the thermal resistance between the case bottom layer and the cold plate. In practice, the thickness of the metal case needs to be concerned. For high density design, the thickness is often defined as 1/16". According to (5.1) with the metal thermal conductivity, the case bottom layer thermal resistance can be obtained. The thermal resistance of the TIM can be looked up from its datasheet. Considering the footprint of the example inductors are normally over 30 $inch^2$, the thermal resistance of the TIM layer is within $0.1^oC/W$

The last part of the thermal model in Figure 5.2 is the thermal resistance between the top surface of the cold plate and the coolant. This is a standardized parameter which can be looked

up in the datasheet of the commercial cold plate. In this work, a Hi-Contact® series cold plate from Aavid® is selected. According to the coolant flow rate and pressure drop, the thermal resistance R_{cp2a} can be identified as 0.01°C/W.

As a result, based on this simplified thermal model, the relationship between the temperature rise at the bottom of the inductor and the total loss of the inductor can be identified. This is not an accurate model. It ignores the difference of the temperatures at different spots of the inductor. The heat transfer at the horizontal direction is also neglected based on the thermal resistance comparison in [86]. The potting process is also assumed to be perfect, without any voids. An initial design can be carried out for the selection of the core and winding size of the inductor.

In an example design of the DC CM inductor, with the calculation loss of 300 W when carrying 200 A_{dc}, the design of the case can be shown in Figure 5.5. The picture of the DC CM choke is shown in Figure 5.6.

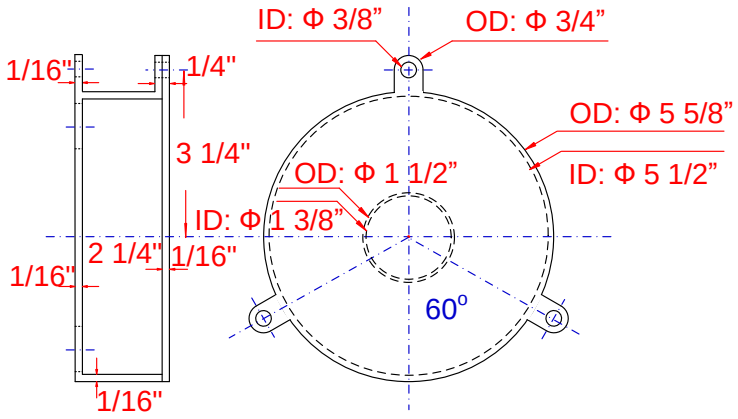

Figure 5.5. Design of cooling case for CM choke

Figure 5.6. CM choke before put in the cooling case

5.3 Potting Procedure Evaluation

To ensure the expected thermal conductivity of the potting material, evaluation tests are needed. In [86], a method is proposed by adding a resistor-based heat source at different surfaces of the potted case.

However, in real case, the heat source is inside the case, in the midst of the potting material. As a result, the author recommends a new by building a round shape of resistor as shown in Figure 5.7 and Figure 5.8. This resistor is emulating the shape of the heat source of the inductor. It is buried in the case with potting material. To reduce possible voids in the potting material, a vacuum container and a pump are utilized as shown in Figure 5.9.

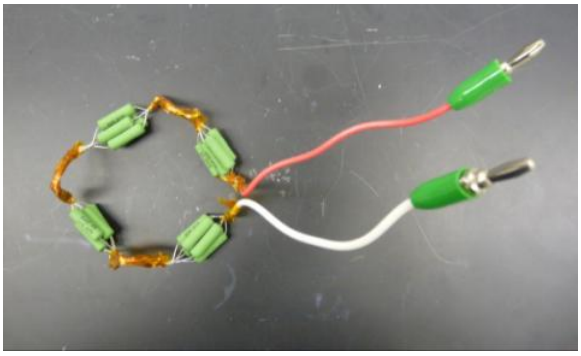

Figure 5.7. Ring shape resistor heat source

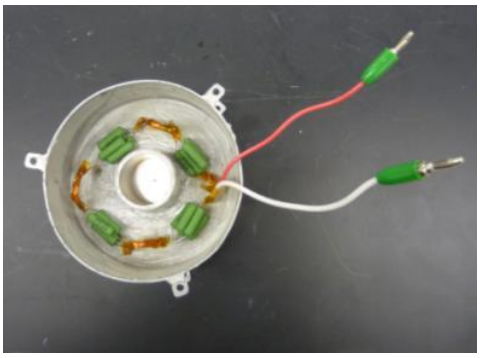

Figure 5.8. Ring shape resistor in CM cooling case

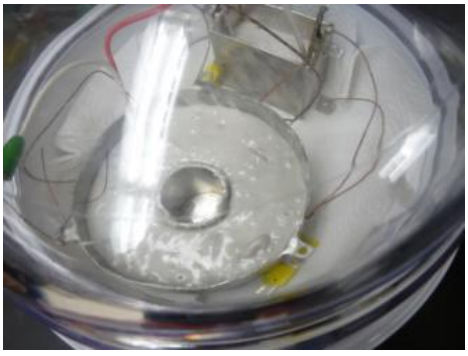

Figure 5.9. Potting in vacuum container

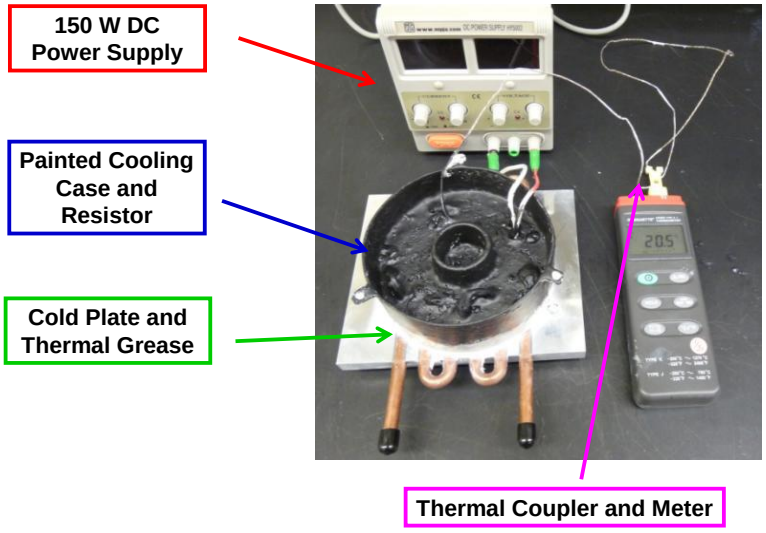

Figure 5.10. Thermal test setup for potting evaluation

To verify the potting results, dc power can be applied to the case as shown in Figure 5.10. The temperature rise of the resistor will indicate the cooling performance of the setup. As shown in the simplified one dimensional cooling model, the thermal resistance of the potting material can be estimated as 3.5 to 3.8 W/m/k. The calculated result from the size of the case and the potting material datasheet is around 4 W/m/k. This test verifies the processing procedure of potting.

5.4 Thermal Model Evaluation

After evaluating the potting process, the same process of potting can be applied to the designed CM choke. Figure 5.11 shows the setting of the thermocouples on the DC CM choke before winding.

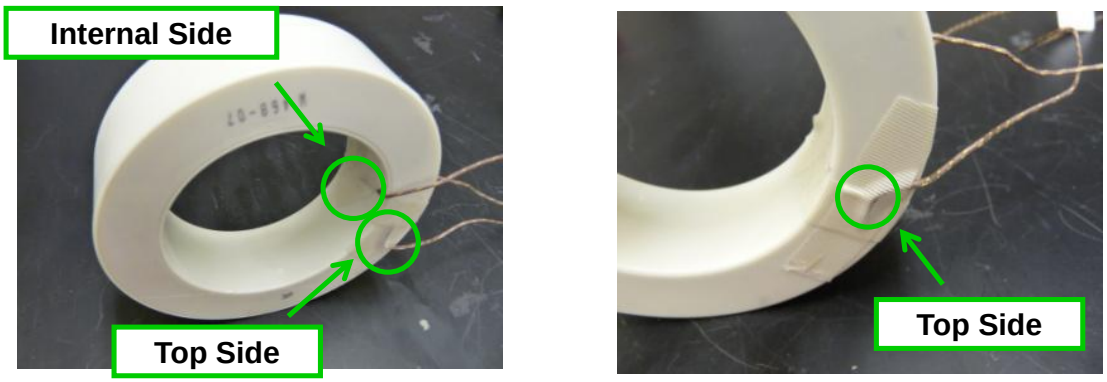

Figure 5.11. Thermocouple attachment on the surface of core

Figure 5.12 illustrates the DC CM choke after putting in the case. Figure 5.13 shows the final look of the choke after potting.

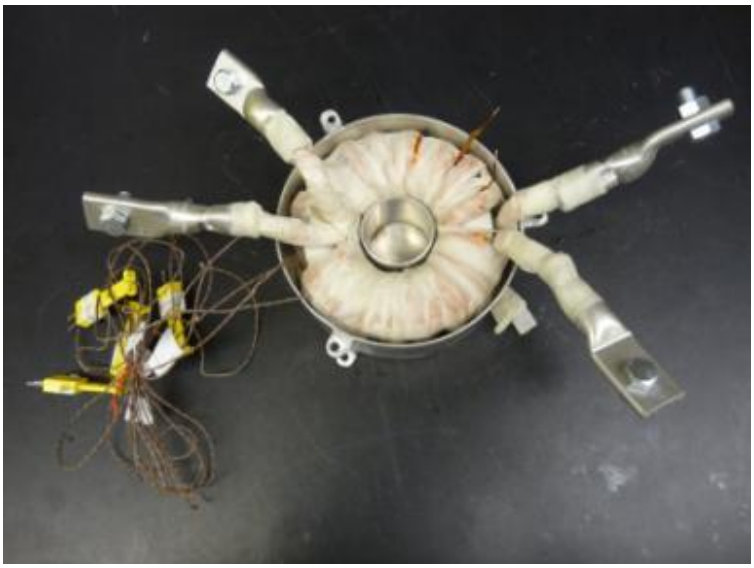

Figure 5.12. DC CM choke in cooling case

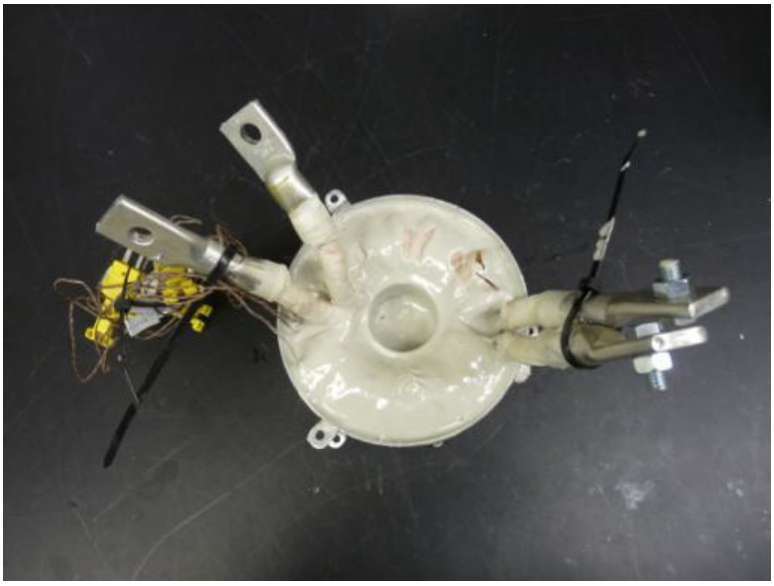

Figure 5.13. DC CM choke in cooling case with potting

For thermal model evaluation, dc current tests are preferred since the loss of the inductor can be easily recognized. A 5 V 500 A_{dc} power supply is applied. The testing schematic is shown in Figure 5.14.

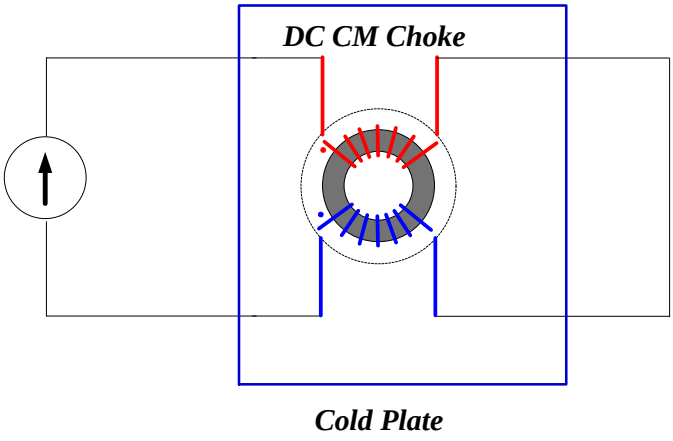

Figure 5.14. DC CM choke thermal model evaluation test schematic

Figure 5.15 shows the setup of the thermal test after mounting the case on the cold plate. For better infrared imaging, the surface of the potted choke is painted black.

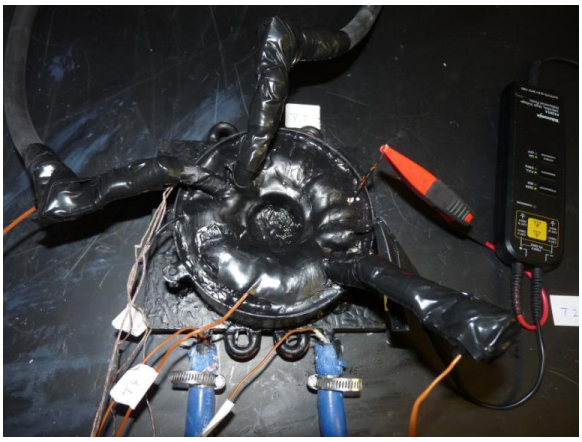

Figure 5.15. DC Cm choke thermal model evaluation test setup

In Figure 5.16, the thermal images of the choke carrying different dc currents have been captured.

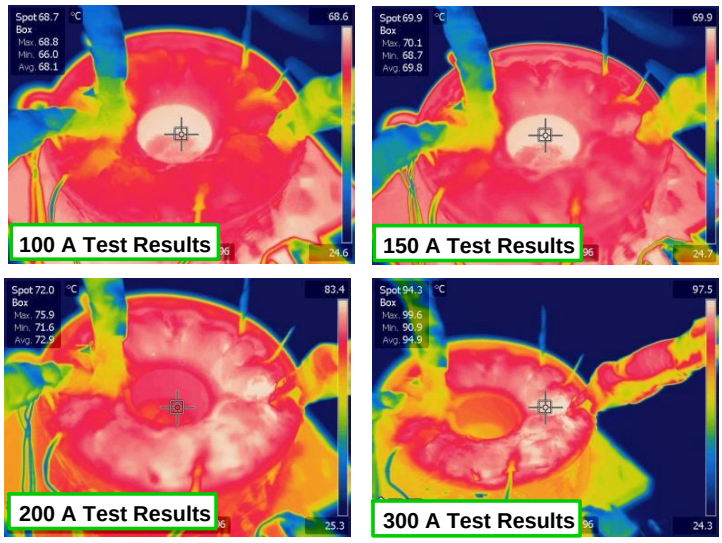

Figure 5.16. DC CM choke thermal model evaluation test results

By testing the DC CM choke at different dc current rating, the loss dissipated by the setup can be obtained. As a result, the relationship of the temperature with the loss can be summarized as Figure 5.17.

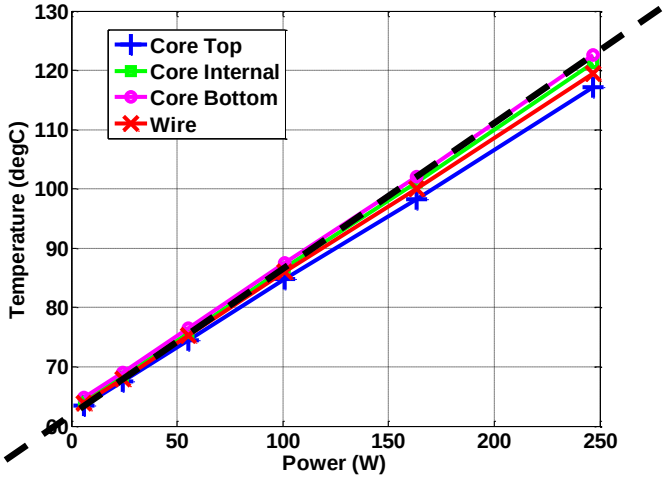

Figure 5.17. DC CM choke thermal modeling

From Figure 5.17, it can be found that there is almost a linear relationship between the temperatures of different spots of the inductor and the loss. Although there are temperature differences among the different spots, they are around the tolerance of the thermocouple tolerance. For a conservative design, the thermal model of the DC CM choke can be estimated as the hot spot of the core bottom results shown as the black dash line, which is around 0.24 ^{o}C/W.

Similar thermal model evaluation can be carried out for other inductors with different shapes. Figure 5.18 shows the design of three DM inductors. Smaller cases are applied considering the smaller size of the core and wires.

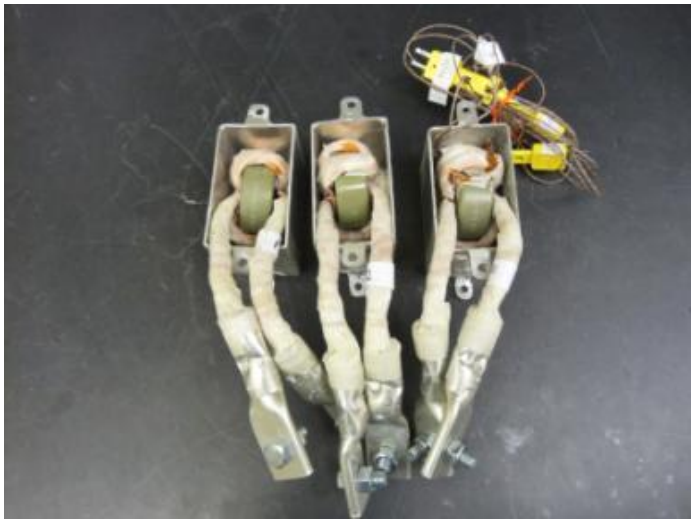

Figure 5.18. DM inductors in cooling cases

Similar testing setup can be built for the characterization of the DM inductors, following the schematic of Figure 5.19.

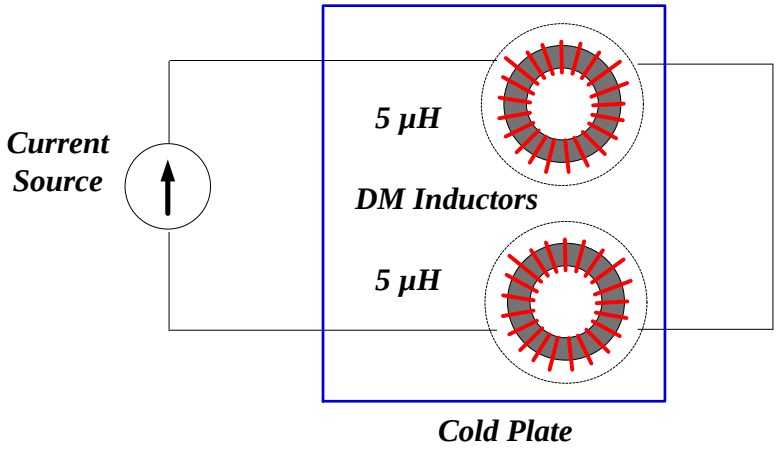

Figure 5.19. DM inductors thermal model evaluation test schematic

The thermal image of DM inductor carrying 100 Adc is shown in Figure 5.20.

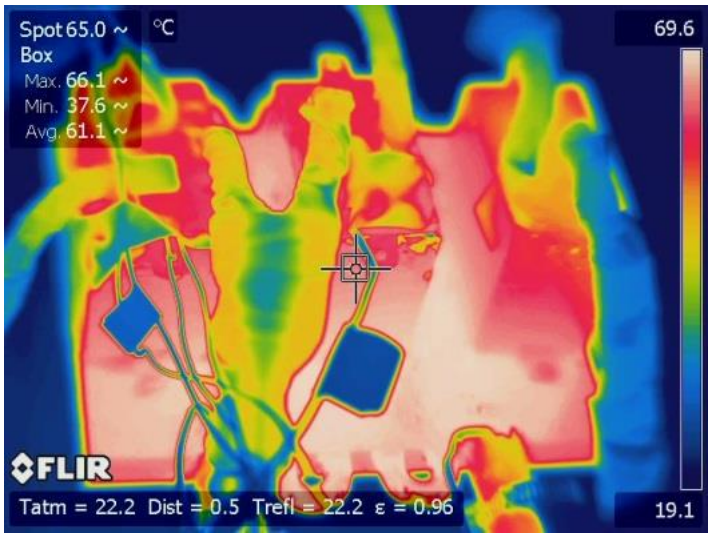

Figure 5.20. DM inductors thermal imaging during tests

The thermal model can also be summarized as shown in Figure 5.21.

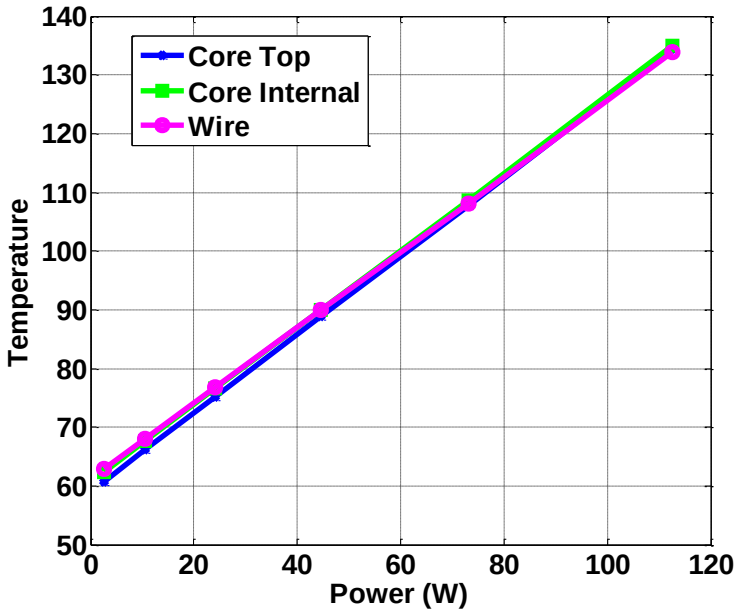

Figure 5.21. DM inductor thermal modeling

Considering the contacting area of the DM inductor cooling setup is smaller than DC CM choke, the equivalent relationship between the temperature and the loss is higher as 0.67^{o}C/W.

5.5 Loss Characterization and Final System Emulation

Even after getting the thermal model of the cooling setup, it is not carefree to directly implement the magnetic component into the final system. Considering the difficulty of core and winding loss estimation, there is still the possibility of overheating the inductors to its limit. The analysis of the loss evaluation is based on an example interphase inductor design. Figure 5.22 shows a typical interleaving structure of two-level voltage source inverter.

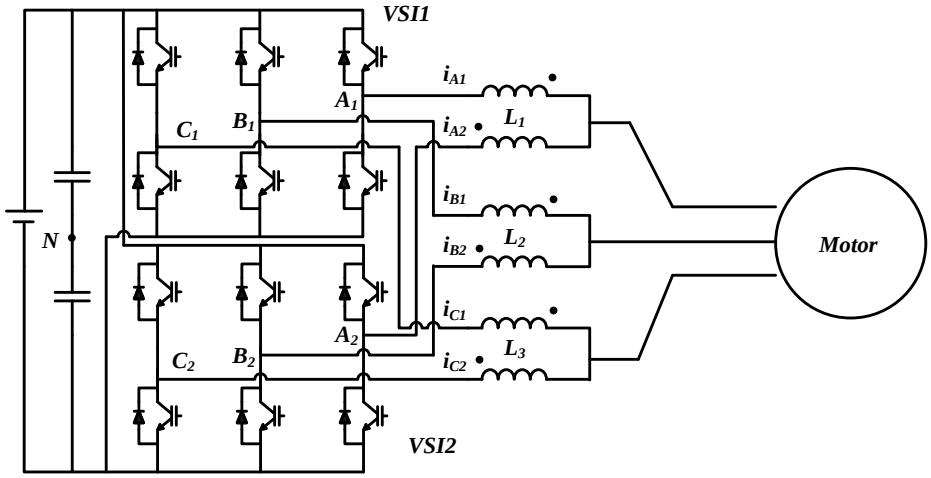

Figure 5.22. Interphase inductors in interleaved motor drive system

As discussed in [51], the interleaved topology has the benefits of eliminating certain orders of switching frequency harmonics. However, to reach such advantage, special attentions are needed at the interphase point of the two interleaved inverters. Because of the phase-shifting of the two carrier waves as shown in Figure 5.23, there are dc bus volt-second applied between the output

of the same phase of *VSI1* and *VSI2*. Interphase inductors are thus required to suppress the circulating current generated by the interphase volt-second, which is illustrated in Figure 5.24.

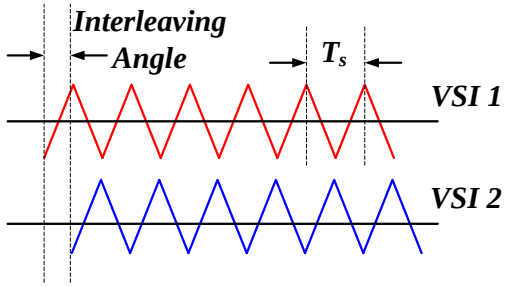

Figure 5.23. Carrier waveform of interleaved motor drive system

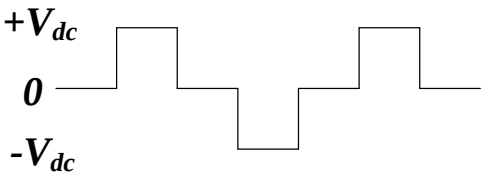

Figure 5.24. Voltage waveform applied to interphase inductors

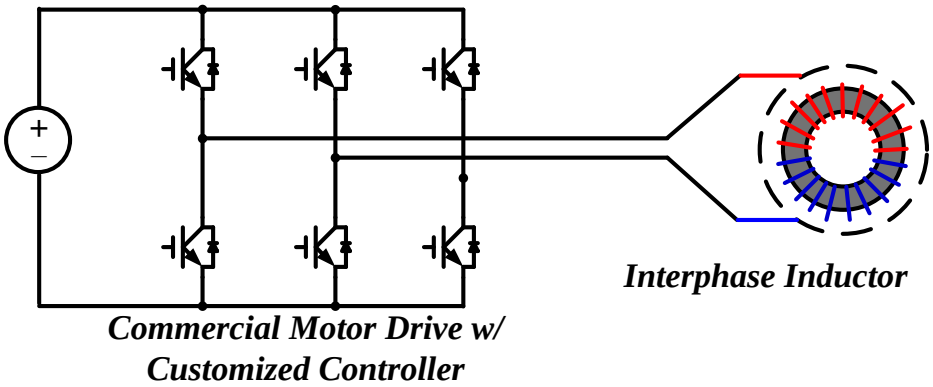

Figure 5.25. Emulation testbed circuit scheme

If the interphase inductor is overheated to insulation or saturation limit, overcurrent may occur through IGBT devices and causing power stage damage. To avoid such happen in final tests, an emulating testbed circuit is designed as shown in Figure 5.25. A commercial 30 hp motor drive is utilized. Customized controller is implemented to generate single-phase output voltage waveform as shown in Figure 5.24.

Following the design steps in the previous sections, an interphase inductor is designed as shown in Figure 5.26. Cooling case has been designed and potting material has been added for the interphase inductor as shown in Figure 5.27. The inductor in Figure 5.28 has been mounted on the cold plate.

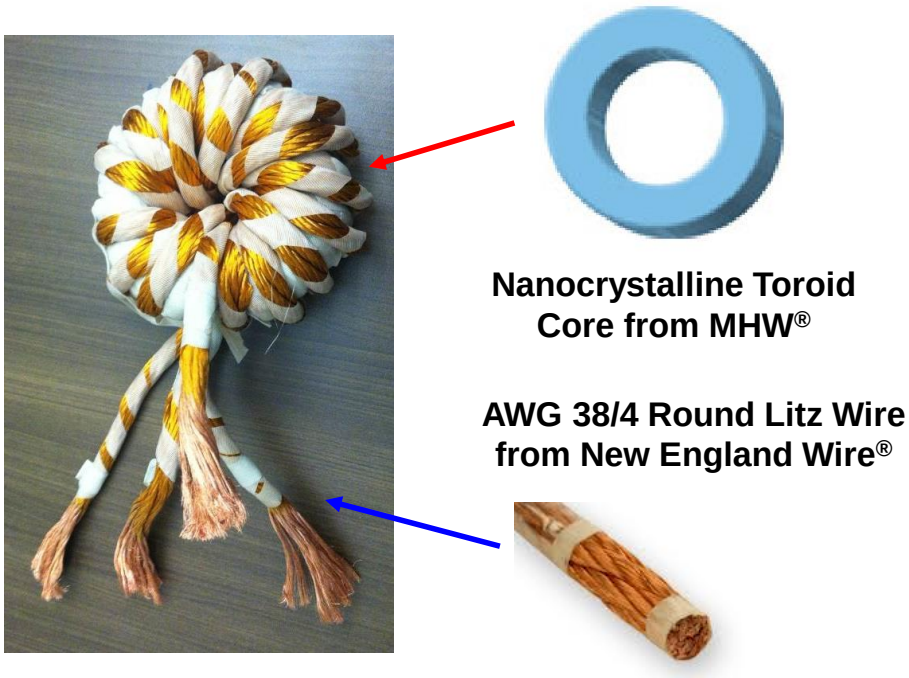

Figure 5.26. Interphase inductor design details

Figure 5.27. Interphase inductor in cooling case with potting

Figure 5.28. Interphase inductor thermal test setup

Volt-second excitation can be applied on the inductor to emulate the core loss, as shown in Figure 5.29. The yellow wave is the voltage applied to the inductor, and the red one is the current going through the windings. As can be seen in Figure 5.29, the current peak-to-peak value is

smaller than 1 A, which means the winding loss is negligible. As a result, the temperature rise is mainly caused by the core loss.

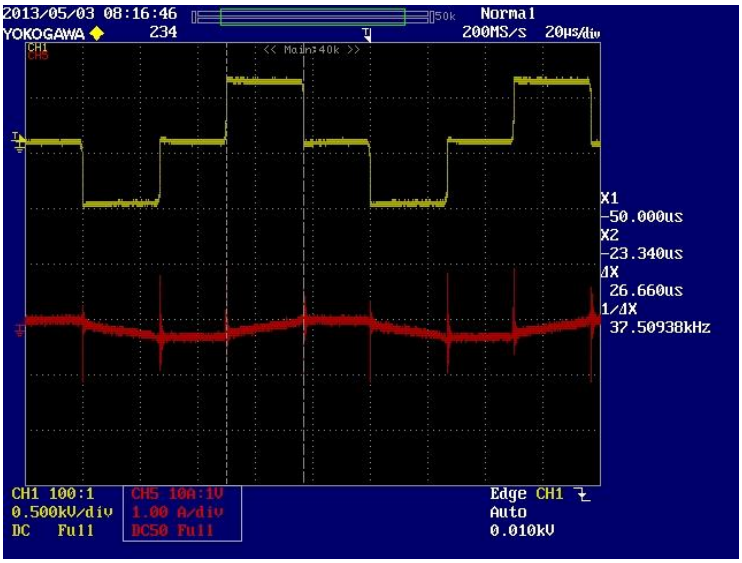

Figure 5.29. Interphase inductor core loss emulation test

For winding loss emulation, high AC currents are needed. To reach high current value with a small power rating motor drive, three single-phase transformers are designed as shown in Figure 5.30.

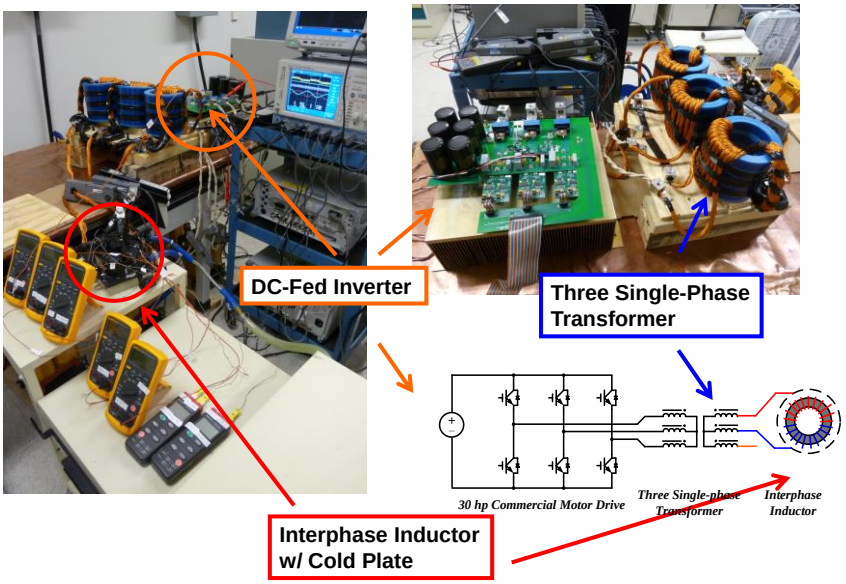

Figure 5.30. High current emulation testbed

With these 10:1 transformers, the motor drive testbed can generate 100 Arms / 400 Hz current to the interphase inductor, as shown in Figure 5.31.

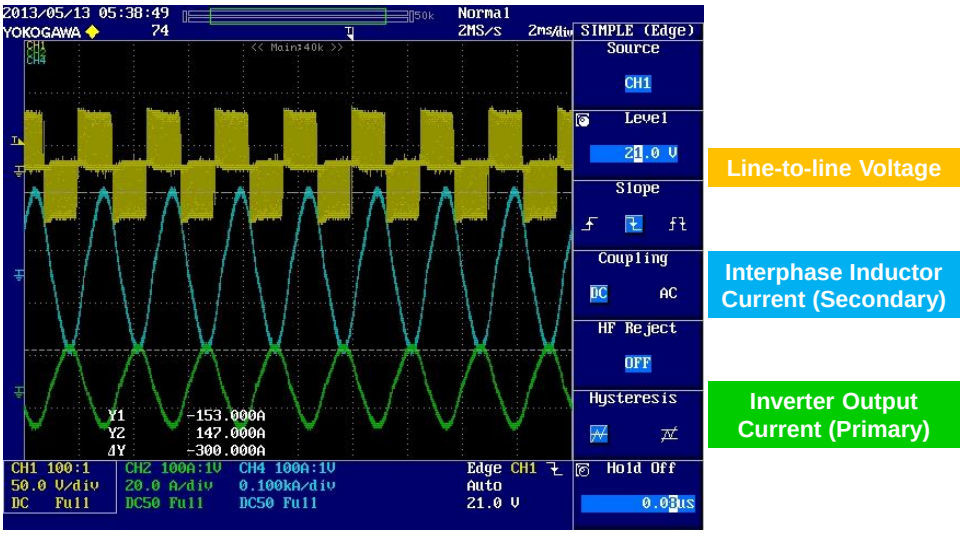

Figure 5.31. Interphase inductor high current test waveform

Considering the small leakage inductance of the interphase inductor, the temperature rise of the inductor is mainly due to the winding loss.

Assuming the heat source as a whole, the final temperature rise of the interphase inductor can be the sum of the two tests as 37°C. In the final power stage system, the test result is around 40°C. The emulation testbed is proved to be effective in estimating the thermal performance of the final conditions.

5.6 Summary of Liquid Cooling Design Procedure

Considering all the aspects of liquid-cooling design of the inductors, a practical procedure can be summarized as shown in Figure 5.32.

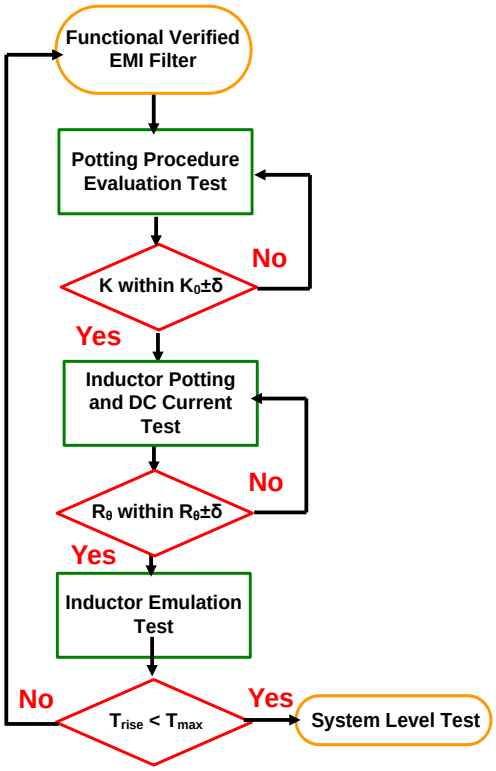

Figure 5.32. Practical liquid cooling design method for high current rating inductors

With the simplified thermal model of the cooling setup, initial design of the inductor can be carried out. The potting process would be evaluated as the second step, making sure the potting material is acting with expected thermal conductivity, before potting the real inductor. If the test results is not satisfactory, the potting process needs to be double checked and carried out again until the thermal conductivity meet the tolerance range. Afterwards, dc current tests can be conducted to characterize the thermal model of the cooling setup. To ensure the inductor is ready for final system-level test, the setup is recommended to be put in the emulation testbed and test both core and winding loss based on the thermal model in the previous step. If the result is not within the expectation, either the emulation test needs to be redesigned, or the loss model of the inductor requires further improvement. After the emulation test, this inductor with cooling setup can be implemented into the final system for further system-level tests.

5.7 Conclusion

In this chapter, the author summarizes a practical procedure for the liquid-cooling design of the magnetic components in high power motor drive systems. Based on literature study and practical experience, the procedure avoids time-consuming FEA simulation. It can be directly used by magnetic designers. The effectiveness of the procedure has been verified by experimental results.

Chapter 6 Parasitic Analysis on Liquid-Cooled EMI Filter in DC-Fed Motor Drives

6.1 Introduction

Parasitic components in EMI filters often play an important role in the noise suppressing performance. For the parasitic impedance analysis, works are mainly focusing on two aspects. One is the characterization of the parasitic components on the filter component itself. For example, the equivalent-paralleling capacitance (EPC) and leakage inductance [26, 54, 102-105] of single- and three-phase common-mode chokes have been modeled according to the physical structure of the cores and windings. Similarly, the influence of the lead length of the DM capacitors on the equivalent-series-inductance (ESL) has been discussed in [67]. The impedance change caused by parasitic components can lead to change on the practical noise attenuation. The other aspect of parasitic study is focusing on the mutual coupling between different filter components. Simplified models and design rules have been summarized for either capacitive coupling [106] or magnetic coupling [66, 107].

These works introduce the concept of high frequency (10s kHz to 10s MHz) impedance characterization into the power electronics design. However, mainly based on functional verification of either single or three-phase EMI filters, most of these studies do not consider the influence of the cooling design on the EMI filter performance, especially liquid-cooling.

In the application of high power motor drives in transportation systems, liquid-cooling is usually one key method of thermal management for the inductors in EMI filters [86]. As discussed in [86] and [95], to get efficient cooling of the inductors, usually case and potting are needed to encapsulate the inductor before mounting it on the cold plate. Besides the winding and core, two more components are added into the CM or DM inductor structures as the metal case and the potting material.

In this chapter, the influence of cooling encapsulation on CM and DM inductors and their related attenuation is analyzed. In section 1, the cooling setups for EMI inductors in high power motor drives are introduced. The relative permittivity of the potting material is characterized through experiments. In Section 2, the CM impedance characterization of the CM choke is reviewed. Based on previous analysis, the case and potting impacts have been taken into consideration. The analyzing result has been verified with measurement on prototype single and three-phase CM chokes. In Section 3, the leakage inductance of the CM choke with cooling encapsulation has been characterized. The influence of the case and potting has been validated through leakage inductance measurement. In Section 4, the encapsulation influence on DM inductors is summarized and verified. The general influence of the cooling setup is discussed in the conclusion section.

6.2 Inductor Liquid-Cooling Setup Introduction

Comparing with liquid cooling of semiconductor devices, the cooling setup of inductor is different in two aspects. Firstly, the heat source of the inductor is three-dimensional. Secondly, the surface of the inductor is not as neat as devices, considering the wire and core shape and structures. Air gaps are inevitable between wires and between wire and core. As a result,

encapsulation technology is usually utilized for the liquid-cooling design of the inductor. In this chapter, the case / potting / inductor structure of liquid-cooling is selected as a benchmark. A simplified cross-sectional view of the setup can be shown in Figure 6.1.

In the practice of CM choke and DM inductor design, 1/16" aluminum is selected. Duralco® 128 is chosen as the potting material. For high density design, the case diameter is selected to be as close to the size of the inductor as possible. Figure 6.2 shows the original DC CM choke before being put in the case and potted. Figure 6.3 demonstrate the condition when the choke is put in the case without potting. Figure 6.4 shows the scene of the DC CM choke after potting.

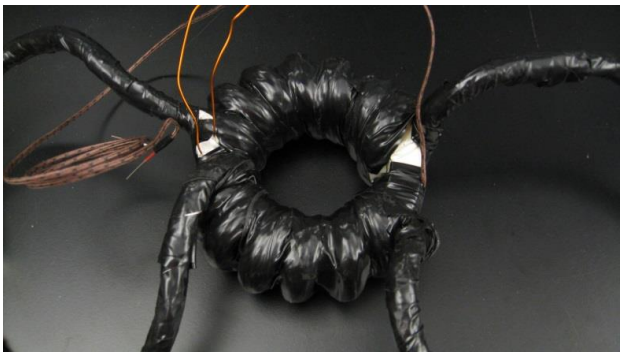

Figure 6.1. DC CM choke without being put in cooling case

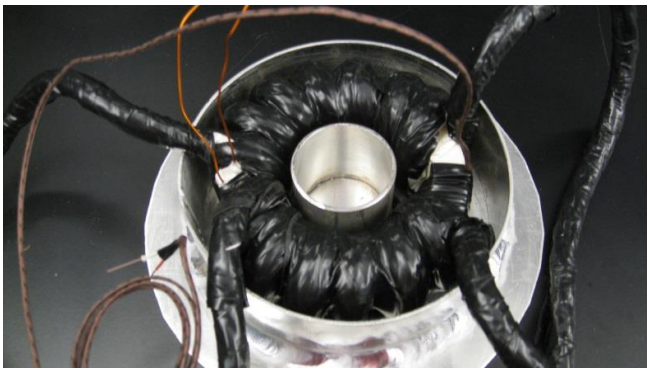

Figure 6.2. DC CM choke in cooling case

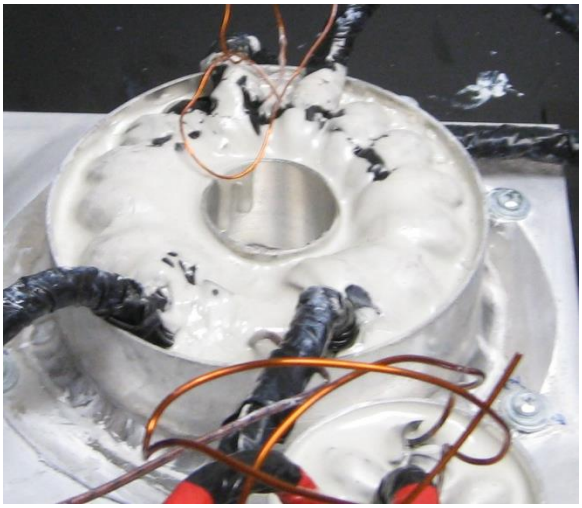

Figure 6.3. DC CM choke in cooling case with potting

Similarly, Figure 6.4, Figure 6.5, and Figure 6.6 show the images of the DM inductor in the three conditions of no case, with case, and with case and potting.

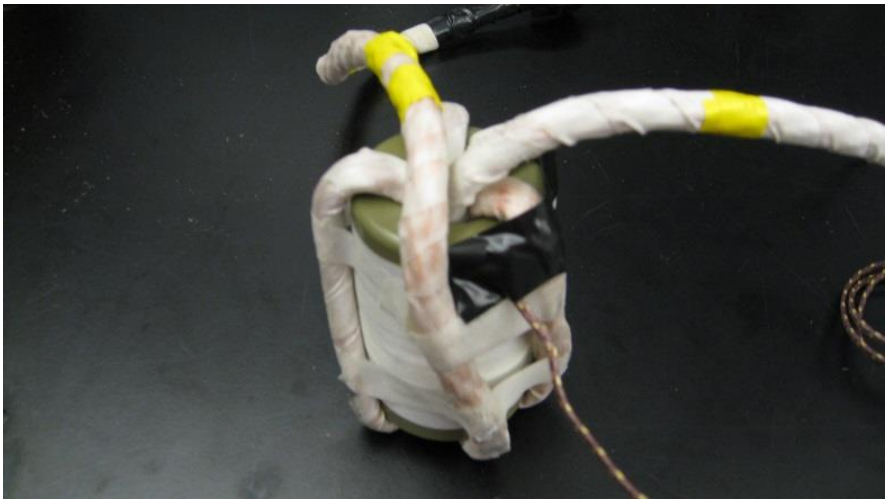

Figure 6.4. DM inductor before being put in cooling case

Figure 6.5. DM inductor in cooling case

Figure 6.6. DM inductor in cooling case with potting

The potting material is designed aiming at high thermal conductivity. The relative permittivity of the material cannot be found in the datasheet. As a result, one test is carried out to characterize the permittivity of the material as shown in Figure 6.7.

Figure 6.7. Example capacitor built by potting material vs. air capacitor

Two example capacitors have been built with same plate area and distance. One is filled with air and the other is with cured Duralco® 128. The impedance measurement result is shown in Figure 6.8.

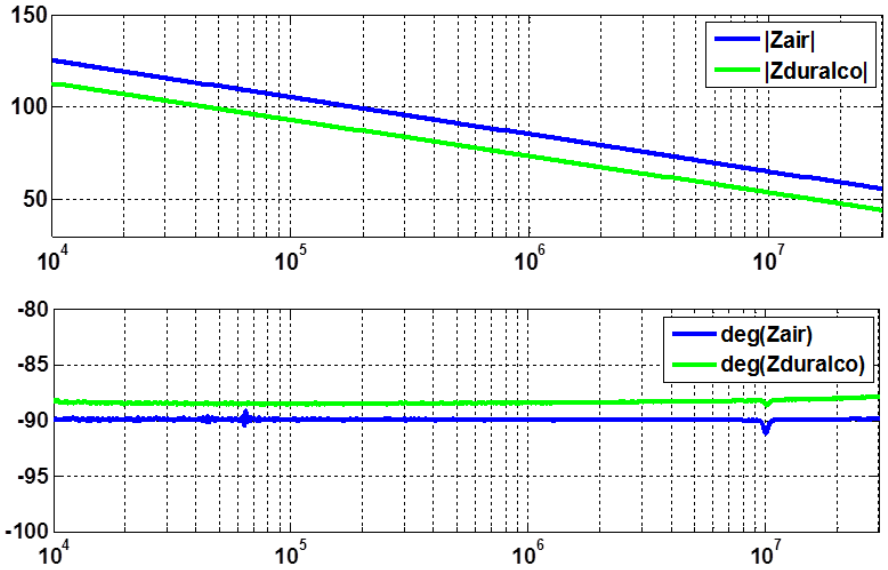

Figure 6.8. Capacitance comparison for relative permittivity characterization

From the measurement, it can be estimated that the relative permittivity of the potting material is around 4.

6.3 Case and Potting Influence on CM Impedance of CM Choke

According to [108] and [102], the equivalent paralleling capacitance of the CM choke is mainly dominated by the turn-to-turn parasitic capacitance. Based on the analysis of capacitance on a conductive core in [108], a simplified equivalent circuit can be derived in Figure 6.9.

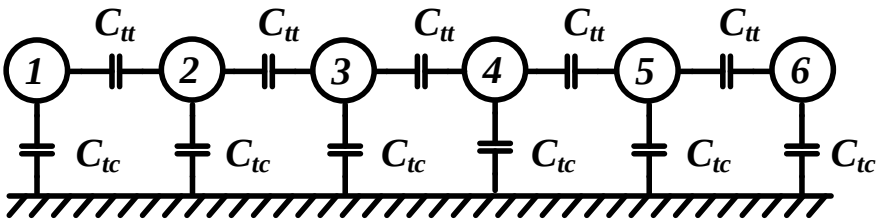

Figure 6.9. Equivalent parasitic capacitance circuit for CM choke

As shown in Figure 6.10, Ctt stands for the equivalent turn-to-turn capacitance. Ctc represents the turn-to-case capacitance. As discussed in [108], Ctc = 2Ctt. Assuming single layer of winding, as is the case in the EMI CM choke and DM inductor, the equivalent capacitance follows (6.1):

$$EPC(n) = \frac{C_{tt}}{2 + \frac{C_{tt}}{EPC(n-2)}} + C_{tt} \tag{6.1}$$

In the equation, EPC(n) stands for the equivalent paralleling capacitance with n turns. As can be found, the capacitance value is related to the EPC with (n-2) turns. As a result, for 6-turn condition of the DC CM choke, the EPC can be calculated as (6.2):

$$EPC(6) = \frac{26}{19} C_{tt} \tag{6.2}$$

According to (6.2), if adding the case without potting, and assuming the CM inductance value does not change, the resonance frequency of the CM impedance will be reduced as (6.3):

$$f_{C\_Case} = \sqrt{\frac{19}{26}} f_C \approx 0.855 f_C \tag{6.3}$$

Considering the relative permittivity of the potting material, the corner frequency will be further reduced by half as (6.4):

$$f_{C\_Potting} = \sqrt{\frac{1}{4}} f_{C\_Case} = 0.5 f_{C\_Case} \tag{6.4}$$

As verification, the CM impedance of the DC CM choke has been measured under all three conditions, as shown in Figure 6.10. As shown, the zero-crossing points on the phase diagram validate the analysis on the three corner frequencies.

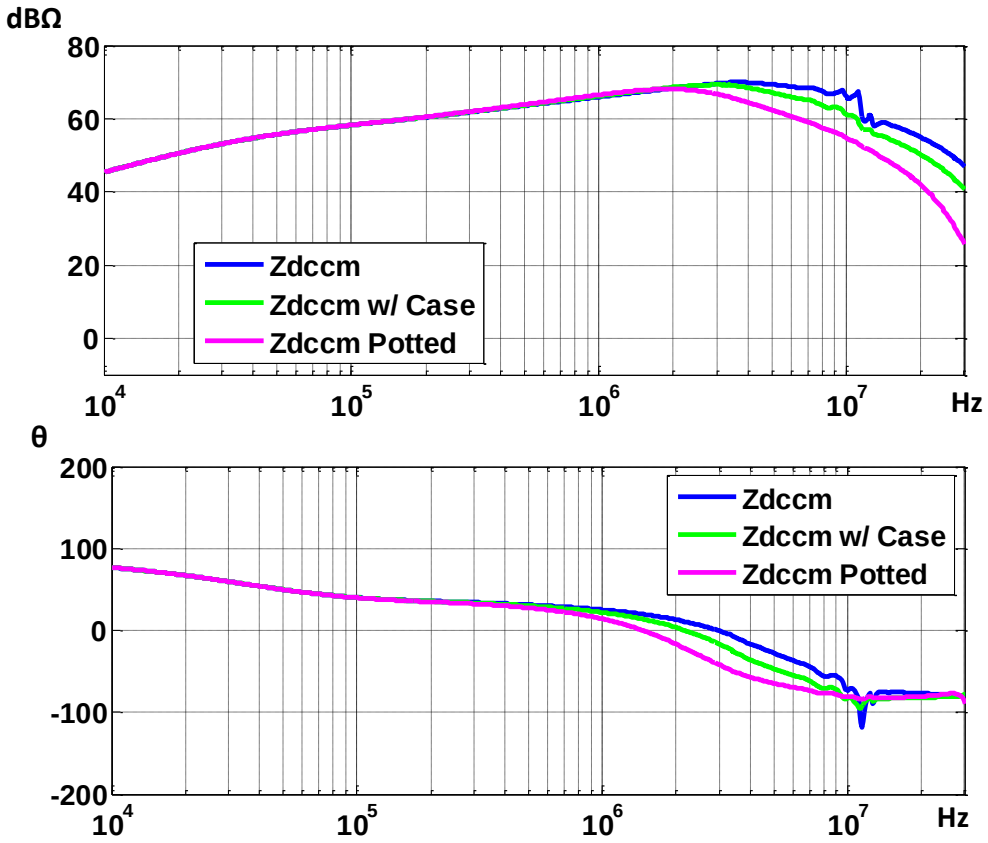

Figure 6.10. Verification of EPC model

6.4 Case and Potting Influence on DM Impedance of CM Choke

The leakage inductance of the CM choke can be utilized as part of the DM filter. According to [26] and [54], the single and three-phase CM choke leakage inductance can be characterized with Figure 6.11 and Figure 6.12:

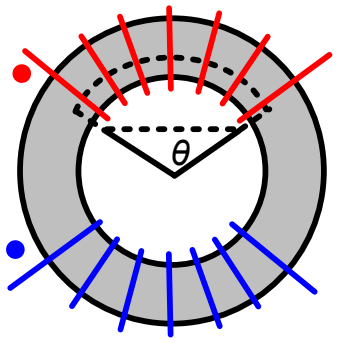

Figure 6.11. Conventional DC CM choke leakage flux path

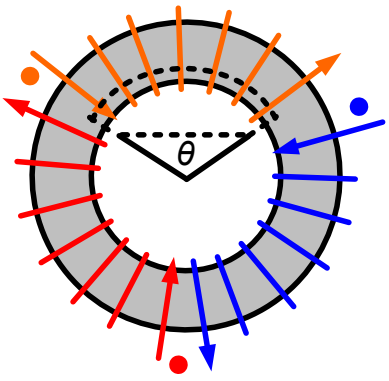

Figure 6.12. Conventional AC CM choke leakage flux path

The leakage inductance can be derived as (6.5):

$$L_{\sigma} = \mu_0 N^2 \frac{A_e}{l_{eff}} \tag{6.5}$$

In (6.5), N stands for the winding turns number. Ae is the cross-sectional area of the core. l_{eff} represents the length of the flux. Literatures have discussed several practical methods to estimate

this length. Assuming the core is of high permeability, like in this example CM choke of nanocrystalline material, leff can be empirically treated as the length of the path in the air.

However, when cooling case has been added in the setup, the leakage flux path has been changed. According Maxwell's Equations, the flux path with the case can be shown in Figure 6.13.

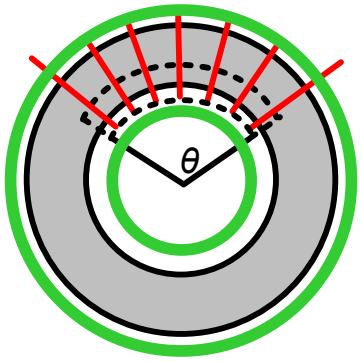

Figure 6.13. Leakage flux path with conductive case

Because of the existence of the case, the flux path is in the arc shape instead of as a string. As a result, the l_{eff} will become longer, as shown in (6.6):

$$l_{eff\_case} = \frac{2\pi r \times \frac{\theta}{360}}{2r \times \sin\left(\frac{\theta}{2}\right)} l_{eff} = \frac{\pi \frac{\theta}{360}}{\sin\left(\frac{\theta}{2}\right)} l_{eff} \tag{6.6}$$

According to (6.5), the new leakage inductance can be characterized as (6.7):

$$L_{\sigma\_case} = \frac{\sin\left(\frac{\theta}{2}\right)}{\pi \frac{\theta}{360}} L_{\sigma} \tag{6.7}$$

As verification, the leakge impedance of the DC CM choke has been measured under all three conditions, as shown in Figure 6.14. As shown, the zero-crossing points on the phase diagram validate the analysis on the three corner frequencies.

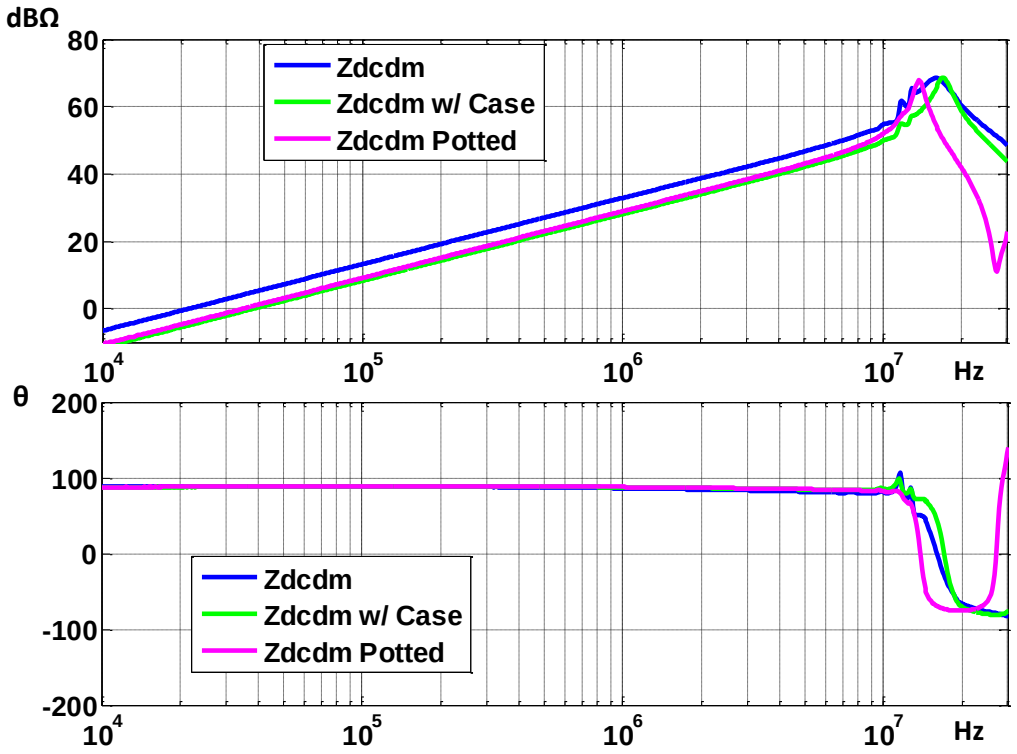

Figure 6.14. Leakage impedance modeling verification

6.5 Case and Potting Influence on DM Impedance of DM Inductor

As shown in Section 2, the influence of the cooling setup on DM impedance of DM inductor is similar with the CM impedance. The case and potting material will increase the EPC of the inductor following (6.1). In the design of DM inductor, the turns number is 5. As a result, the EPC with the case has been increased to (6.8):

$$EPC(5) = \frac{11}{8} C_{tt} \tag{6.8}$$

According to (6.2), if adding the case without potting, and assuming the DM inductance value does not change, the resonance frequency of the DM impedance will be reduced as (6.9):

$$f_{C\_Case} = \sqrt{\frac{8}{11}} f_C \approx 0.853 f_C \tag{6.9}$$

As verification, the DM impedance of the DM inductor has been measured under all three conditions, as shown in Figure 6.15. As shown, the zero-crossing points on the phase diagram validate the analysis on the three corner frequencies.

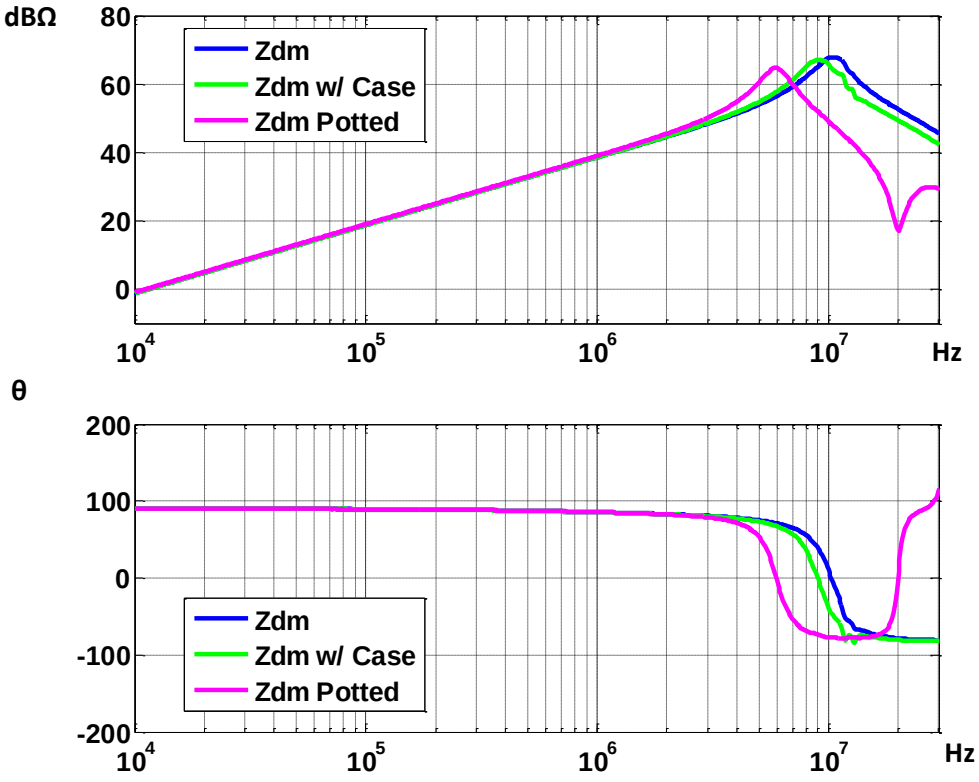

Figure 6.15. DM impedance modeling verification

6.6 Conclusion

In this chapter, the self-parasitic impedance of CM and DM inductors in the case and potting material has been characterized. Based on previous study of the EPC and leakage inductance model, simplified calculation methods have been summarized for the new EPC and leakage inductance. The calculated impedance has been verified with prototype inductor measurement.

Chapter 7 A Comprehensive Design Procedure for High Density EMI Filter in High Power Motor Drives

7.1 Introduction

The design of EMI filter is a systematic task. For a comprehensive design, different aspects of knowledge need to be combined. At the EMI filter component level, impedance modeling of inductors and capacitors are required [26, 54, 55], while improvement on core or capacitor materials are monitored [44]. Different EMI filter topologies have been considered and compared [27, 40, 48]. To avoid unnecessary overdesign, the system noise source [23, 52] and propagation paths [57, 77] need to be characterized. As a reliable product, cooling design [86, 95] and packaging impact [66, 67] on the EMI filter should also be concerned.

[25, 52] have proposed methods of EMI filter design considering the high frequency modeling of the EMI filter. [49, 50, 72] discuss the optimal design of EMI filters in certain topologies. [107, 109] give some rule of thumbs in laying the inductors and capacitors considering the parasitic influence. However, it is hard to find a method containing all the practical aspects of the EMI filter design mentioned above. A comprehensive design guide is needed.

On the other hand, as discussed in [11, 18, 58, 65], mixed-mode (MM) noise and noise-mode transformation usually exist in real power converter systems and can easily mislead designers to

design CM filter to suppress DM noise or vice versa. However, only limited works consider these phenomena in the design process. [63] take the single-phase SMPS MM noise into account when measuring the bare noise. But the NMT is not concerned. [52] has built a computer-based optimization tool for selecting the high density EMI filter design from all possible options of inductors and capacitors. Theoretically this will finally find out the optimal design by trying every possible combination of design variables. But it will be very time-consuming and complicated to use considering the size of the database and all the nonlinear equations. As a summary, a design procedure concerning the NMT and MM noise shall be developed so that unnecessary iteration and overdesign can be avoided.

In this chapter, a comprehensive design procedure for high density EMI filter in high power motor drives is proposed. It features as concerning all the practical aspects in the design, including high frequency impedance of the filter components, selection of EMI filter topology, noise source and load impedance characterization, cooling design and its impact on EMI filter performance. Meanwhile, the method contains the procedure of evaluation tests, considering the influence of MM noise and NMT. In Section 7.2, the conventional design procedure of EMI filter is reviewed. The proposed design method is introduced with a flow chart. In Section 7.3, the first part of the method, EMI bare noise acquisition, is explained with a 100 kW design task example. The impedance characterization of filter components and system source and load has also been reviewed and discussed. Afterwards, the optimal selection of EMI filter topology and component value is analyzed in Section 7.4. In Section 7.5, the decision making procedure is discussed during the evaluation of the EMI filter performance, considering the MM noise and NMT. The cooling design and realization for the EMI filter are also discussed. Section 7.6 shows

the experimental verification of the design method with a 100 kW motor drive system. Conclusion is summarized in Section 7.7.

7.2 High Power EMI Filter Design Procedure

Figure 7.1 shows the flow chart of a conventional design procedure.

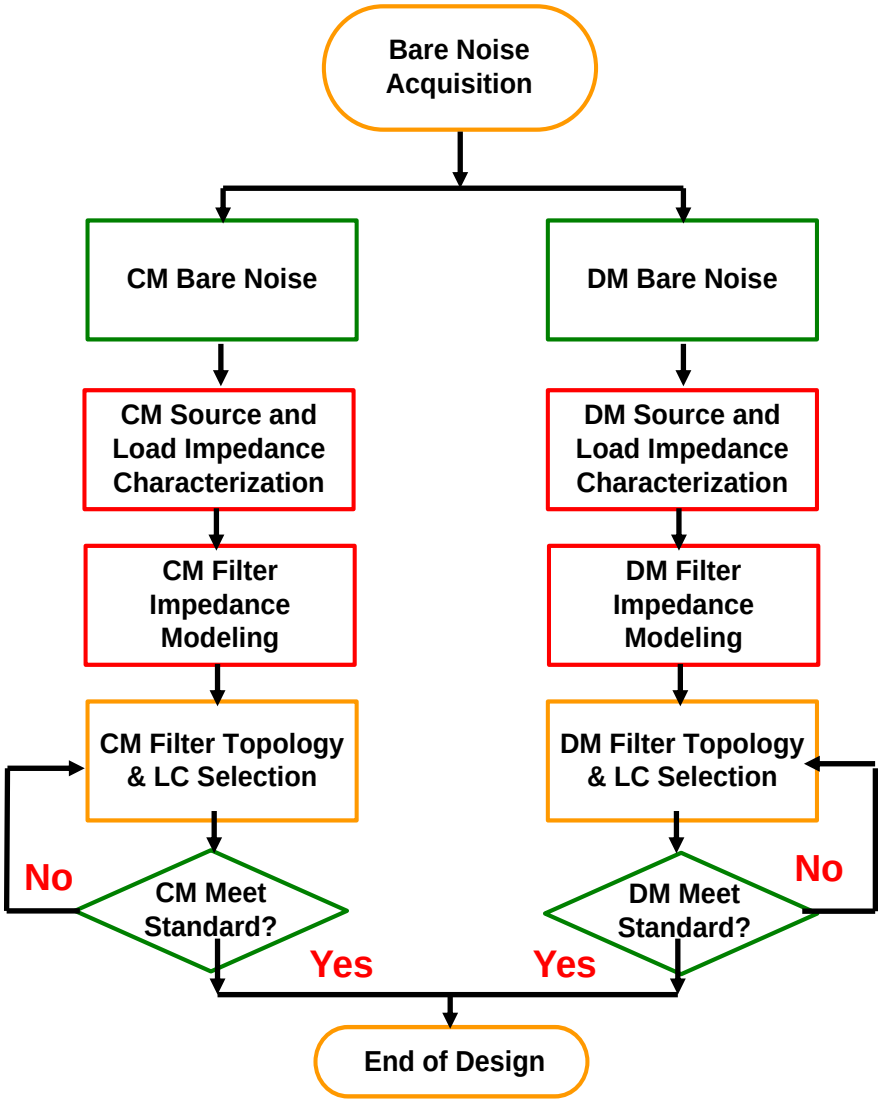

Figure 7.1. Conventional EMI filter design procedure

As the start of the design, the system EMI noise without adding any EMI filter is acquired in the form of CM and DM noise. Since this is a general design method, no special application is applied. As a result, no dc or ac side noise is specified in the acquisition step. Afterwards, the design of CM and DM filter is carried out separately. CM or DM filter components are selected and optimized through either CM or DM iteration loop, including measurement of the system impedance, evaluation of the filter performance and select the best combination of filter components. If both CM noise with CM filter and DM noise with DM filter meet the standard, the design is finished.

Based on the discussion and conclusion in previous chapters, the conventional design method has two aspects not considered for the high power three-phase motor drive system. The first one is the interaction between CM and DM noise, which has been discussed in Chapter 2 and 3. The second one is the cooling design of the filter and its impact on filter performance. Without concerning these two parts, the design procedure can easily introduce unnecessary filter weight or extra iteration design steps.

According to the knowledge of MM noise in Chapter 2 and NMT in Chapter 3, together with the cooling design and analysis in Chapter 5 and Chapter 6, a new design procedure is proposed, as shown in Figure 7.2.

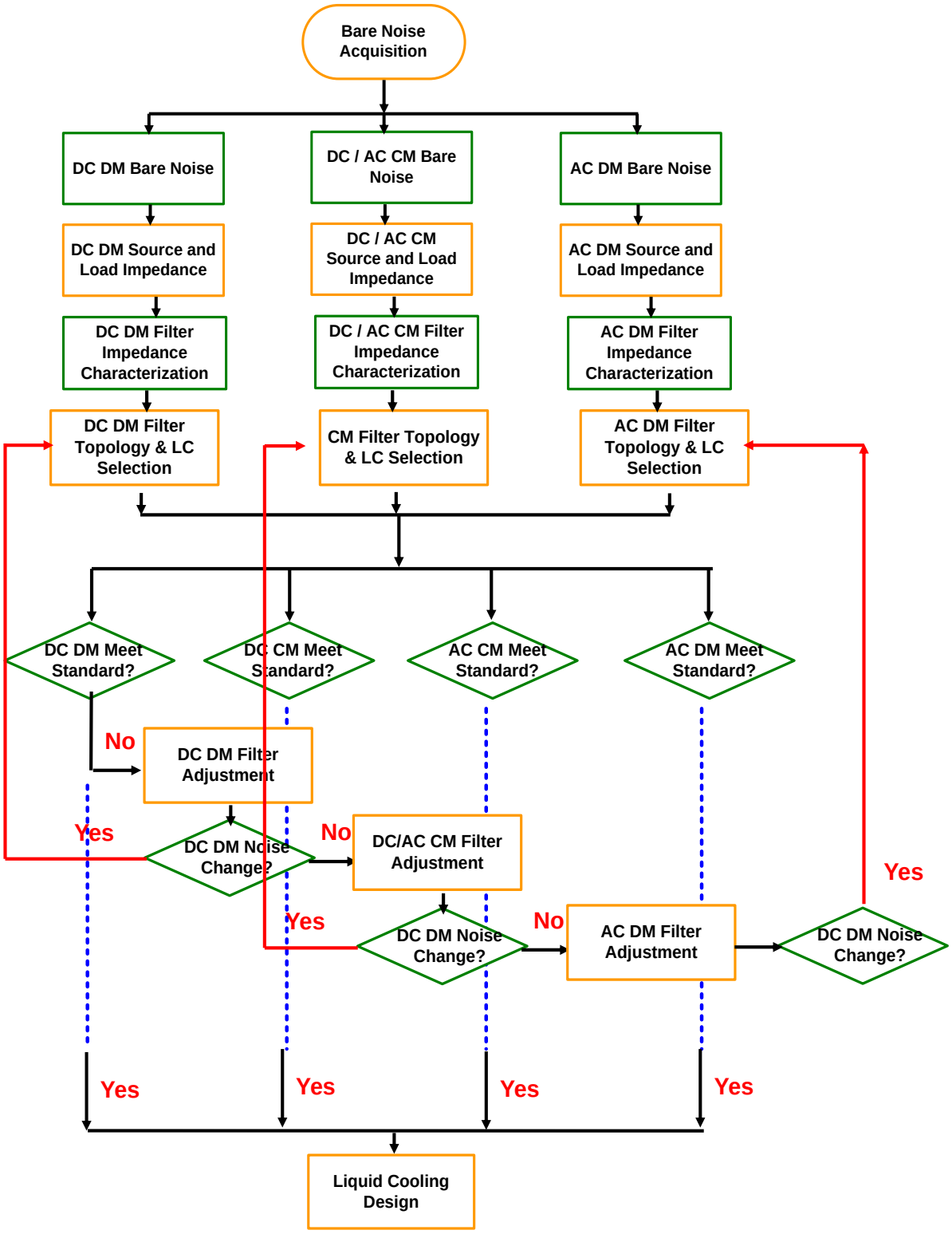

Figure 7.2. Proposed EMI filter design procedure for high power motor drive system

Based on the features of the motor drive circuit topology discussed in [27], the proposed method firstly divides the design task into three parts, including the CM filter, DC DM filter and AC DM filter. Impedance measurement would then be carried out for each bare noise acquisition and system modeling. Filter components are selected afterwards, aiming at high power density and low weight. Concerns of the weight and impact of cooling is also taken in this step. Being different from the conventional procedure, the proposed method has a systematic evaluation procedure for the performance of the designed filter, considering both MM noise and NMT. After the designed filter is verified with the standard, cooling design can be carried out as the final step of the design procedure.

7.3 System EMI Bare Noise Acquisition and System Impedance Modeling

The coupling between dc and ac side EMI noise in motor drives has been discussed in [27] and [43]. As a result, the dc and ac EMI noise of dc-fed three-phase motor drive can be divided into three parts: CM noise, DC DM noise and AC DM noise, as shown in Figure 7.3.

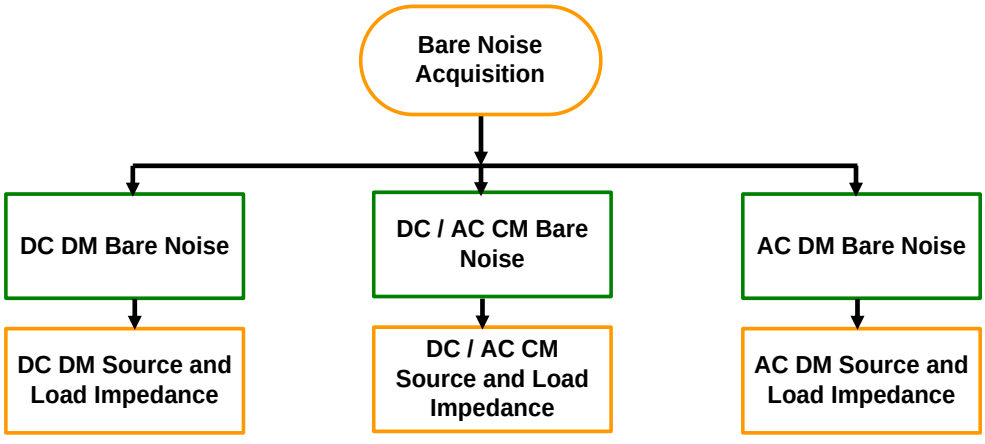

Figure 7.3. Bare noise acquisition and impedance characterization

7.3.1 CM Noise Acquisition and Impedance Characterization

Figure 7.4 shows the equivalent circuit of the CM noise propagation path. It combines both dc and ac side circuit by the parasitic grounding capacitance of the power stage.

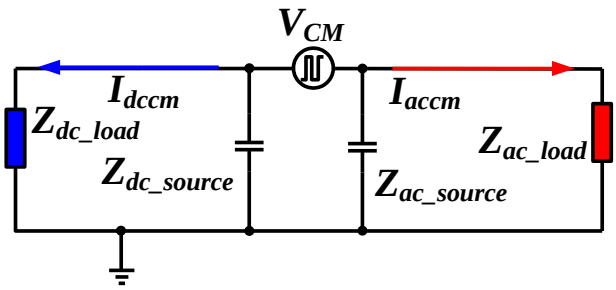

Figure 7.4. Equivalent CM circuit

As discussed in Chapter 2, the measurement of DC CM and AC CM noise is shown in Figure 7.5 and Figure 7.6.

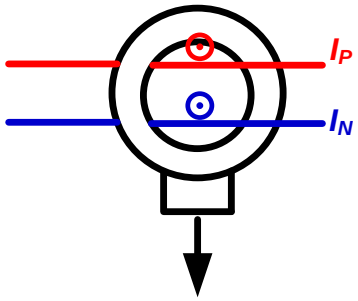

Figure 7.5. DC CM noise measurement

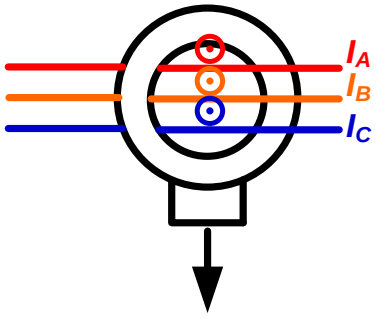

Figure 7.6. AC CM noise measurement

Figure 7.7 shows how the impedance measurement is carried out for the Z_{dc_load}, with the two output terminals of the LISNs shorted.

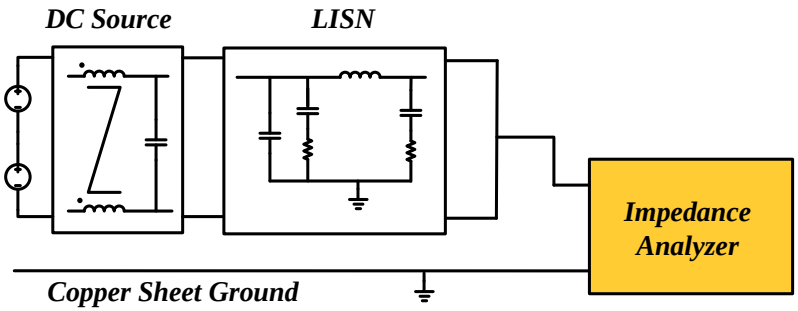

Figure 7.7. DC CM load impedance measurement

Figure 7.8 demonstrates the way of measuring the Z_{ac_load}. The three input terminals of the cable are shorted together.

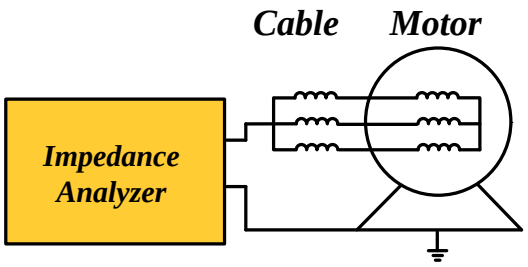

Figure 7.8. AC CM load impedance measurement

A 100 kW motor in Figure 7.9 with 90 feet cable in Figure 7.10 is measured as an example. Figure 7.11 shows the example CM impedance of the motor and cable.

Figure 7.9. Example 100 kW induction machine

Figure 7.10. Example 90 feet three-conductor motor cable

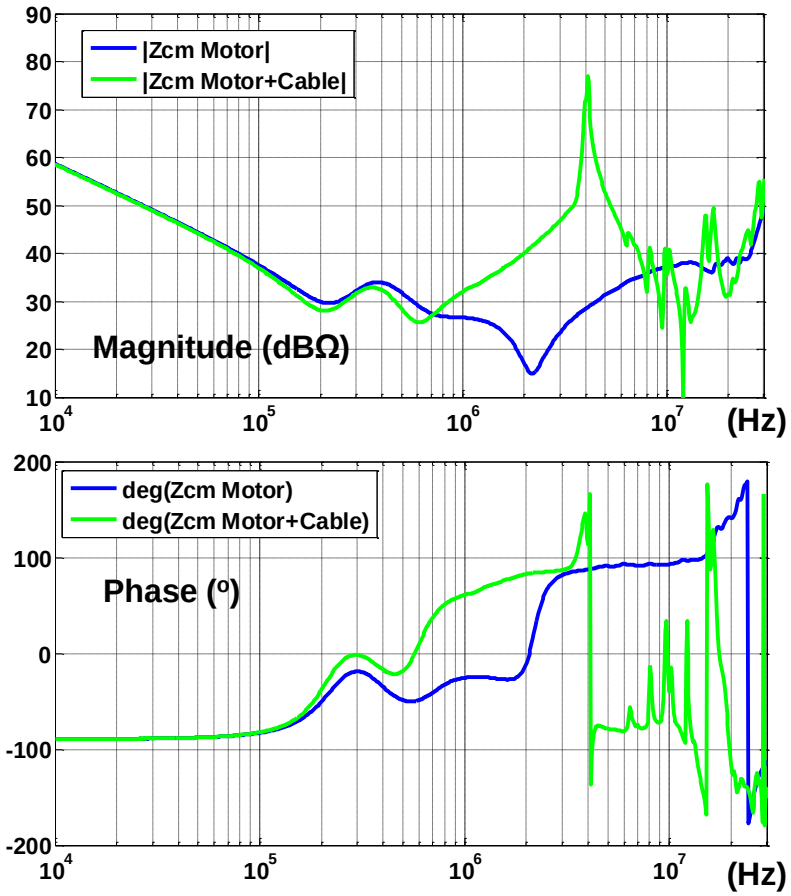

Figure 7.11. Example CM load impedance of 100 kW motor and 90 feet cable

According to the measurement of the impedance, as well as the modulation scheme and topology of the motor drive, the CM bare noise of both dc and ac side can be identified. As an example, a neutral point clamped three-level voltage source inverter is selected with SPWM scheme. The simulated voltage bare noise and calculated current bare noise of both dc and ac sides are shown in Figure 7.12 and Figure 7.13.

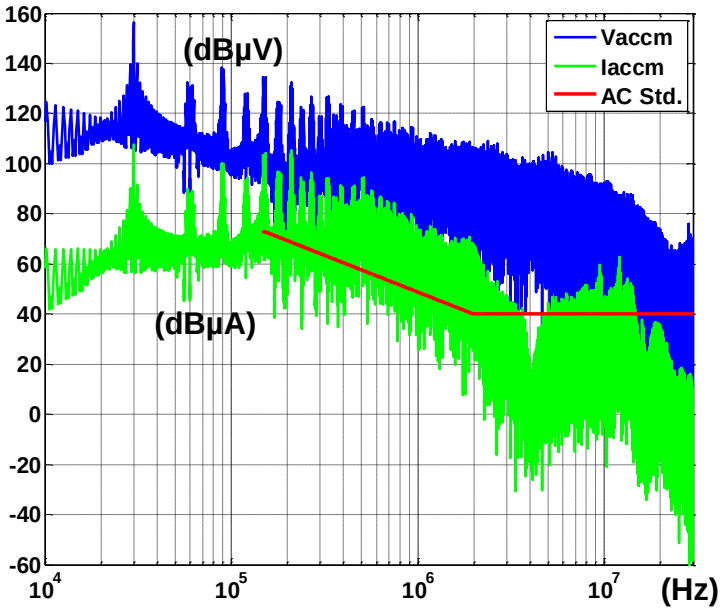

Figure 7.12. Example AC CM voltage and current noise

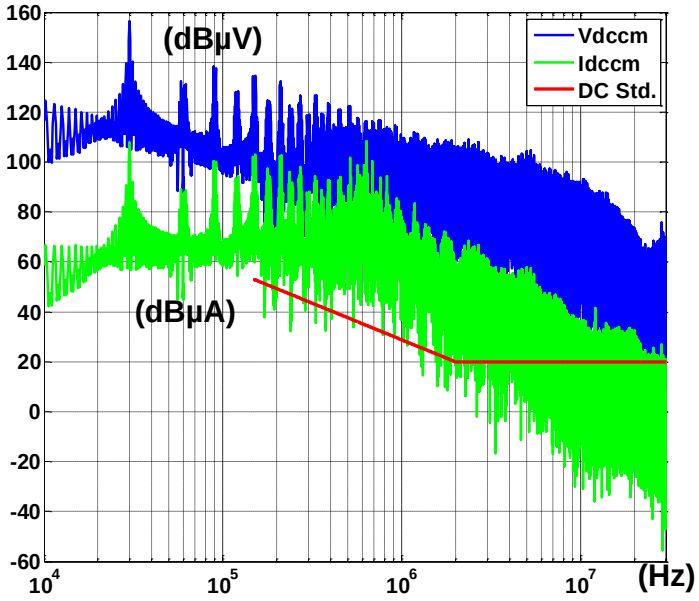

Figure 7.13. Example DC CM voltage and current noise

7.3.2 AC DM Noise Acquisition and Impedance Characterization

Figure 7.14 shows the equivalent circuit of AC DM noise propagation path.

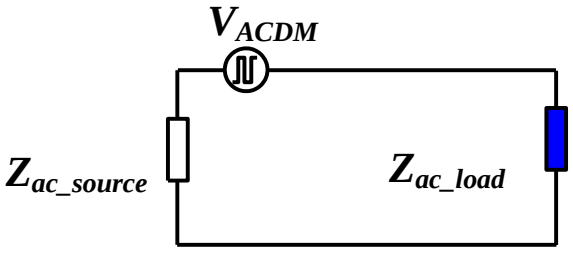

Figure 7.14. AC DM equivalent circuit

The measurement of the AC DM noise is shown in Figure 7.15.

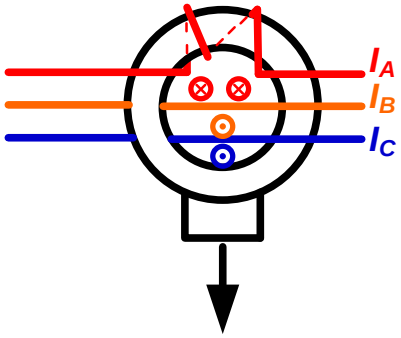

Figure 7.15. AC DM noise measurement

The load impedance is defined as the input impedance of the cable and the motor. The DM measurement is shown in Figure 7.16. The impedance analyzer tests the impedance between Phase A and shorted Phase B and C.

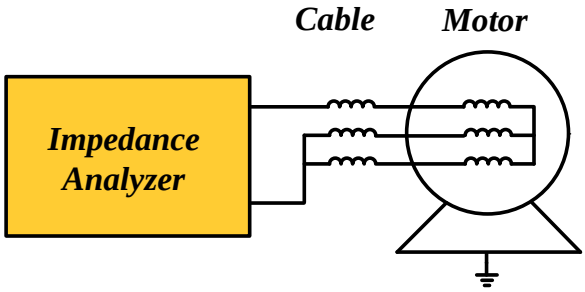

Figure 7.16. DM load impedance measurement

Figure 7.17 shows the AC DM impedance of the example 100 kW motor and 90 feet cable.

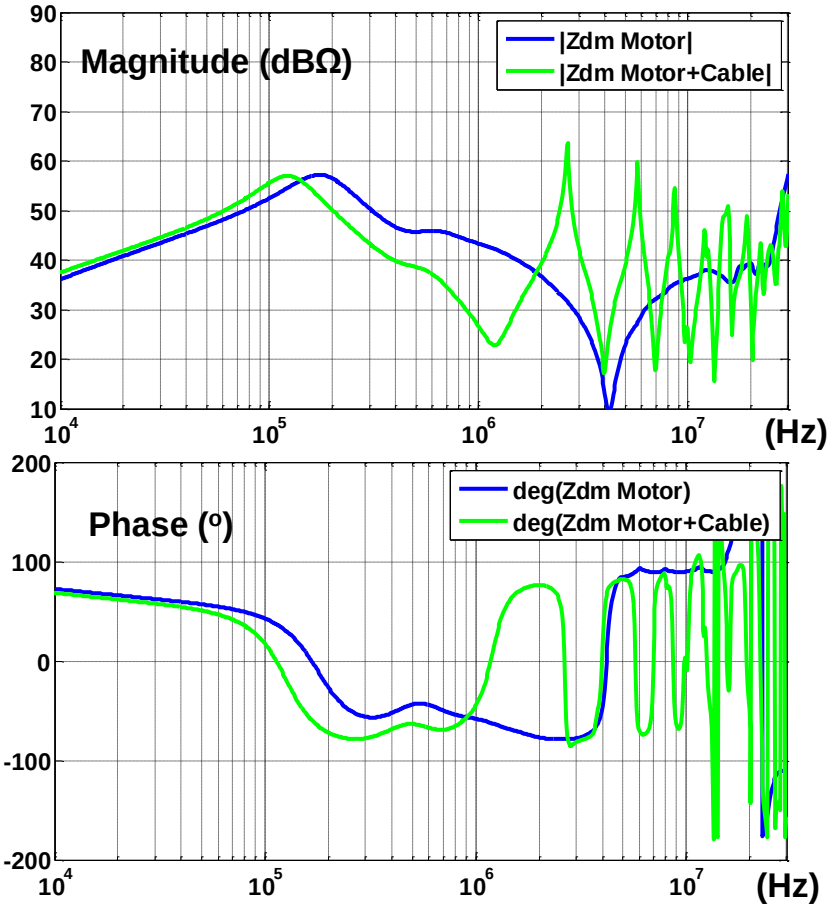

Figure 7.17. AC DM impedance of example motor and cable

Similar with the study in CM noise, the bare AC DM voltage and current noise can be calculated as shown in Figure 7.18:

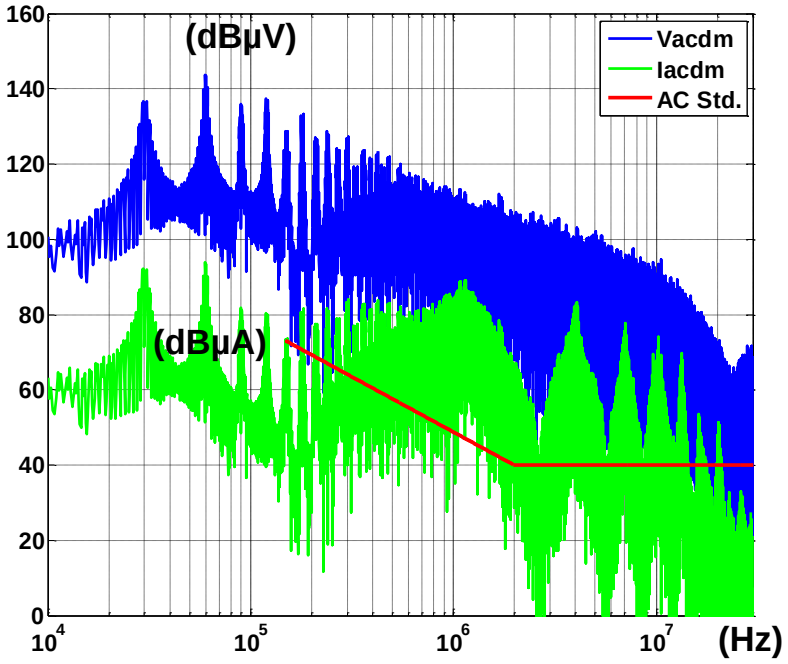

Figure 7.18. Example AC DM voltage and current noise

7.3.3 DC DM Noise Acquisition

Figure 7.19 shows the equivalent circuit of the DC DM noise propagation path.

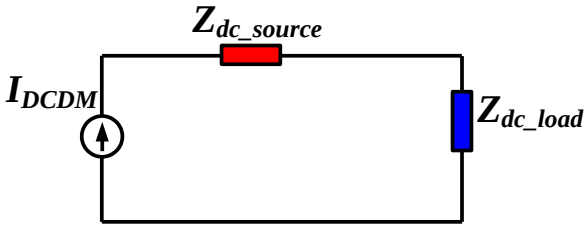

Figure 7.19. DC DM equivalent circuit

The measurement method for DC DM noise is shown in Figure 7.20.

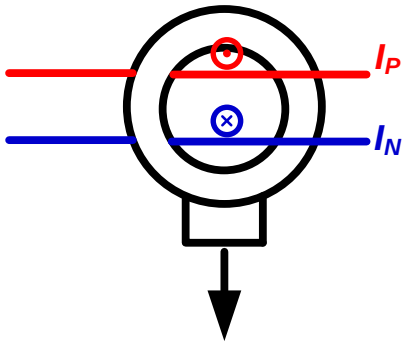

Figure 7.20. DC DM noise measurement

As a result, the example DC DM noise is shown in Figure 7.21.

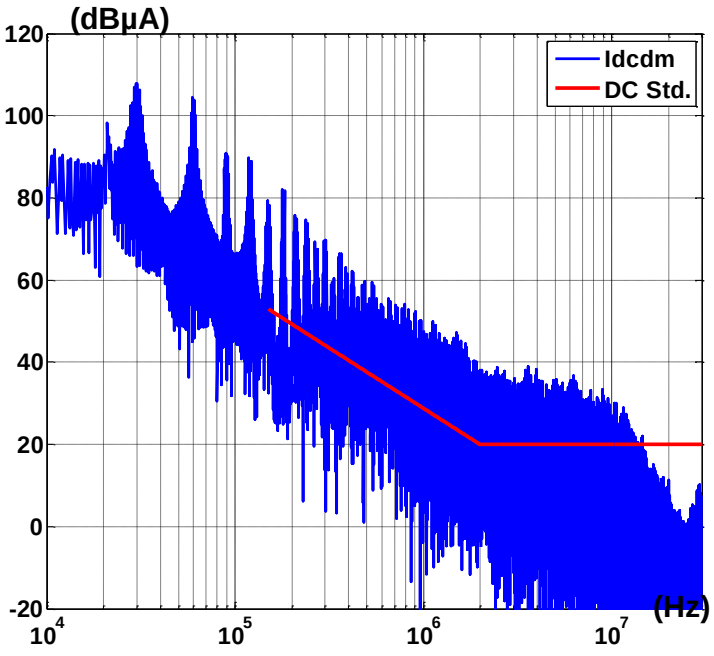

Figure 7.21. Example DC DM noise

7.4 EMI Filter Topology Selection

As shown in Figure 7.22, after getting the system EMI bare noise and impedance, the optimal selection of filter topology and components can be carried out.

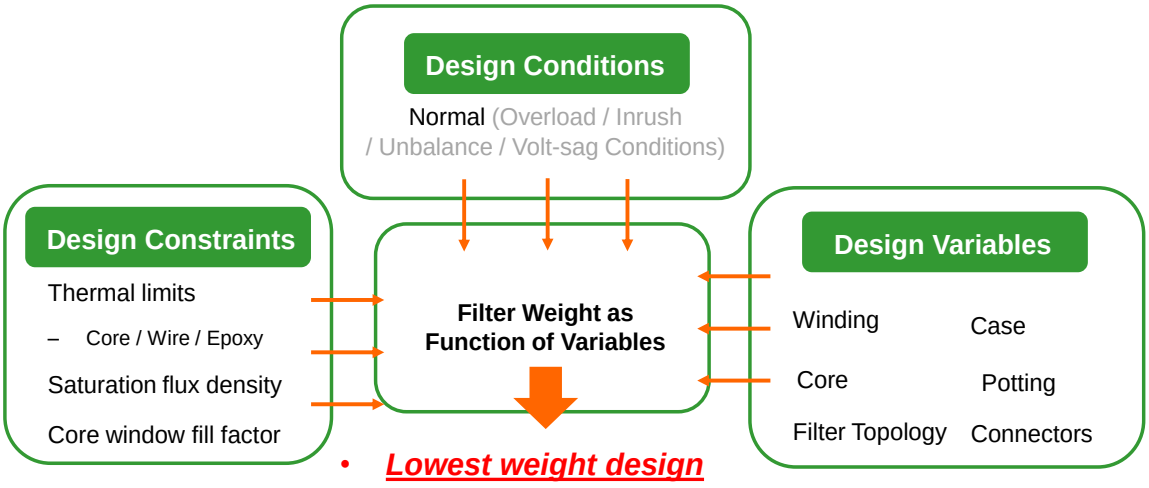

Figure 7.22. Filter optimal design for minimum weight

According to the characterization of the system source and load impedance, the insertion gain of the EMI filter in the practical system can be characterized. For example, as shown in Figure 7.23, Figure 7.24 and Figure 7.25, different CM filter topologies are listed.

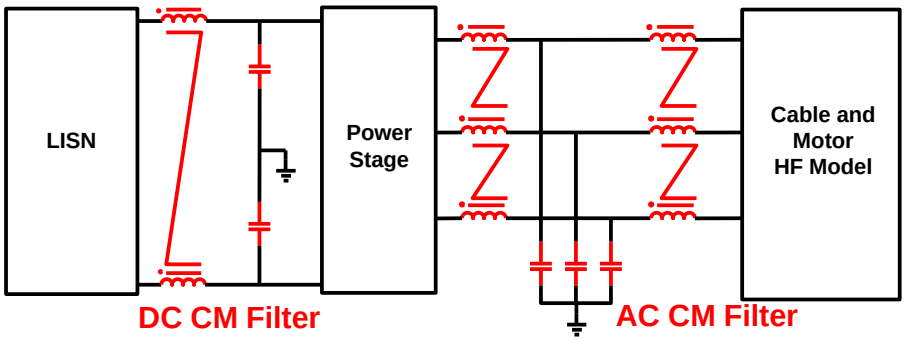

Figure 7.23. DC CM CL and AC CM LCL filter circuit

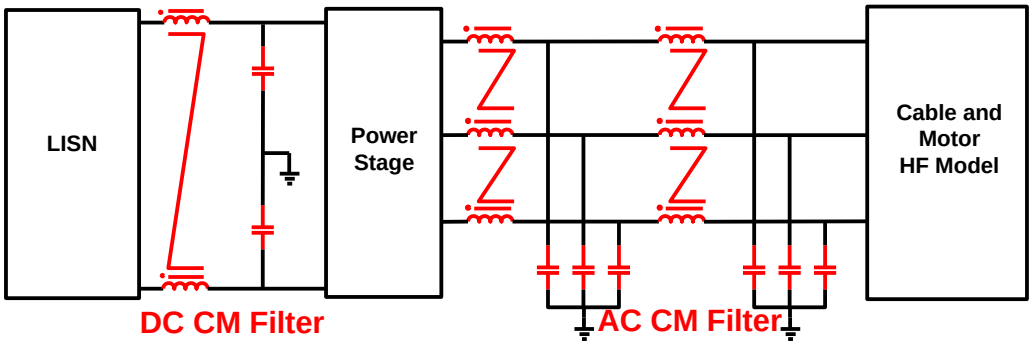

Figure 7.24. DC CM CL and AC CM LCLC filter circuit

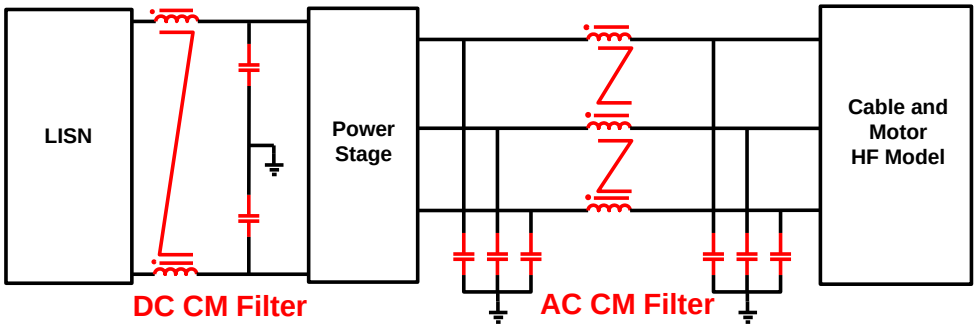

Figure 7.25. DC CM CL and AC CM CLC filter

In Figure 7.26, the insertion gains of the different topologies can be compared. Comparing with the required attenuation of the bare noise, the minimum weight combination of inductors and capacitors can then be selected.

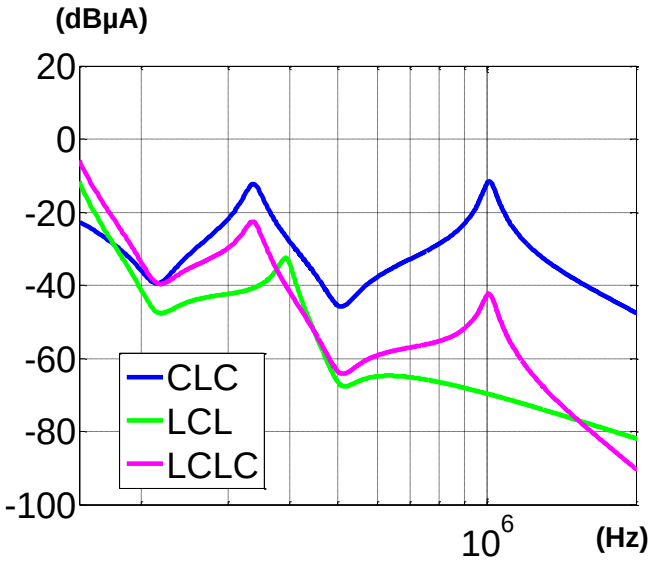

Figure 7.26. Insertion gain comparison of different CM filter topology

7.5 Performance Evaluation of Designed EMI Filter and Cooling Design

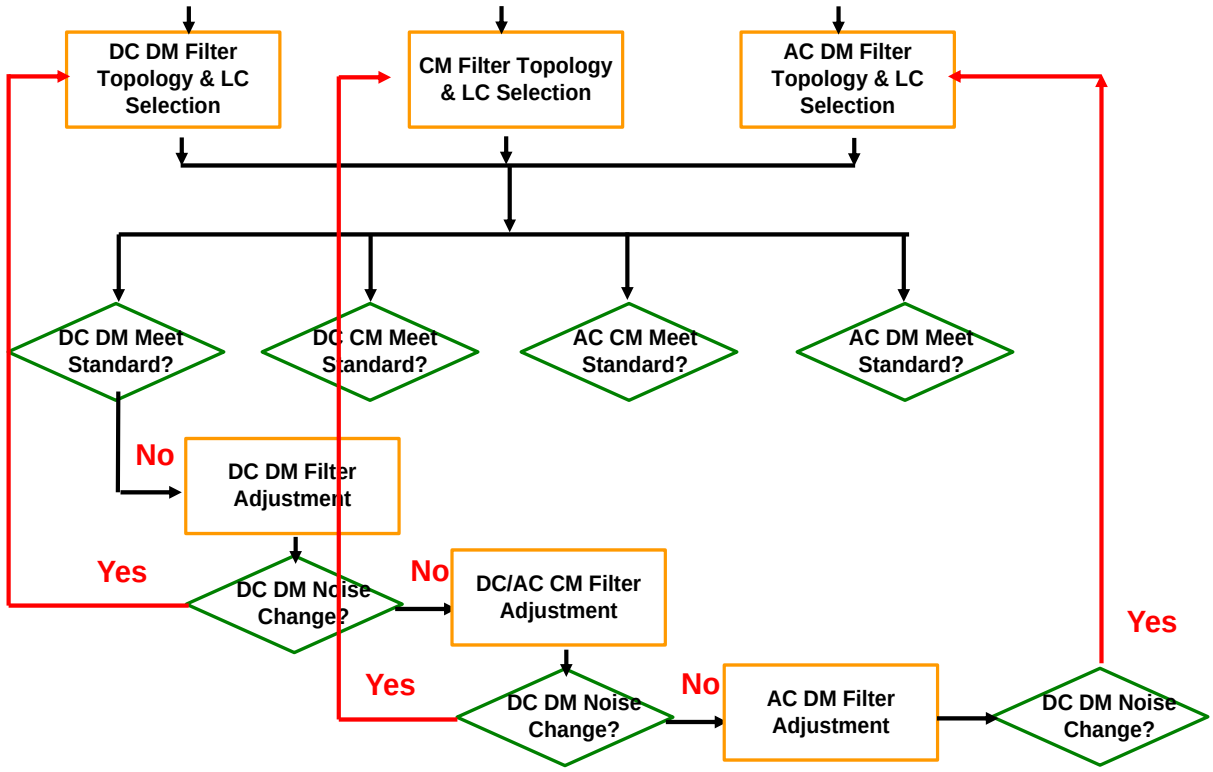

Figure 7.27. DC DM noise evaluation

Figure 7.27 shows an example of the DC DM EMI filter performance evaluation. After selecting the topology of the DC DM filter as well as the inductor and capacitor values, the filter should be put into the motor drive system and test its attenuation on DC DM noise. Because of the existence of the MM noise and NMT phenomena, the measurement of the DC DM noise might include other mode of noise, for example DC CM noise if dc side grounding impedance is not well balanced. As a result, the proposed procedure suggests implementing all designed filters, instead of just installing the testing filter in the conventional method. If the DC DM noise with all filters meets the standard, the designer can continue to test other modes of noise.

However, if the result does not meet the standard, a careful study should be carried out before making the decision of tuning only DC DM filter.

Considering the MM noise and NMT phenomena, failure of DC DM noise meeting the standard does not indicate directly that DC DM filter is not designed well. Instead, all modes of noise should be checked. A practical way is to adjust each type of filter slightly, like increasing 50% of the capacitance of the filter capacitor, and verify that if the change of the filter introduces any change on the DC DM noise. For example, if the DC CM noise changes according to the change of DC CM filter, then MM noise due to system unbalance is causing the DC DM noise not meeting the standard. The most effective way is then to improve the design of the CM filter instead of the DC DM filter, which is usually the choice from the conventional method.

Figure 7.27 only shows the evaluation of DC DM noise. In practice, all four types of noises should be evaluated. If all four types of noise meet the standard, the line noise of dc and ac side can then meet the standard.

According to Chapter 5 and 6, the liquid-cooling case can be designed for the CM and DM inductors. Potting materials can be selected. Following the procedure of Figure 5.32, the cooling of the evaluated EMI filter can be designed.

As an example, Figure 7.28 shows the evaluated 100 kW EMI filter before being put into cases with potting materials. Figure 7.29 and Figure 7.30 show the EMI filter implemented with cooling design and mounted on the cold plate. In Figure 7.29, the DC CM choke and AC DM inductors are mounted on one cold plate. The opposite side of the cold plate is designed for the cooling of the IGBT devices in the power stage of the motor drive. AC CM chokes are mounted on the other cold plate in Figure 7.30.

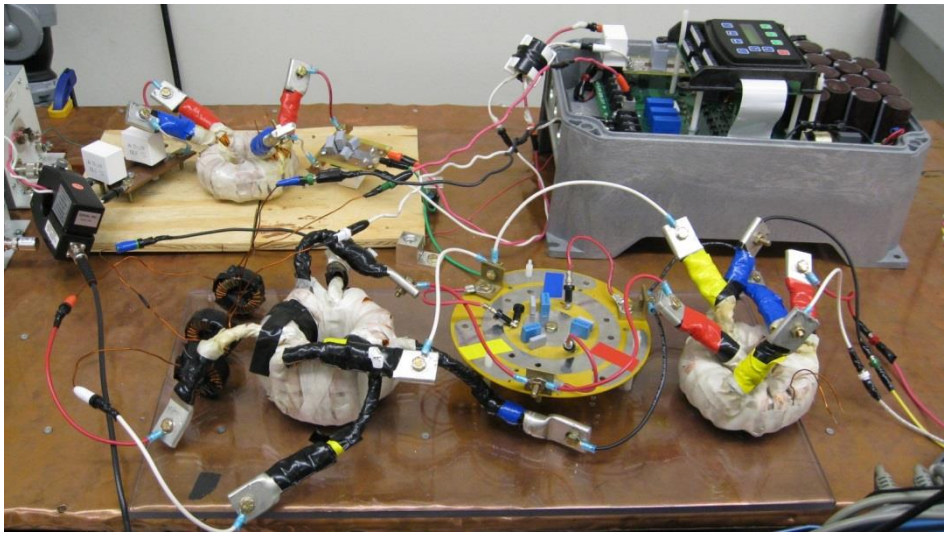

Figure 7.28. Example EMI filter without cooling

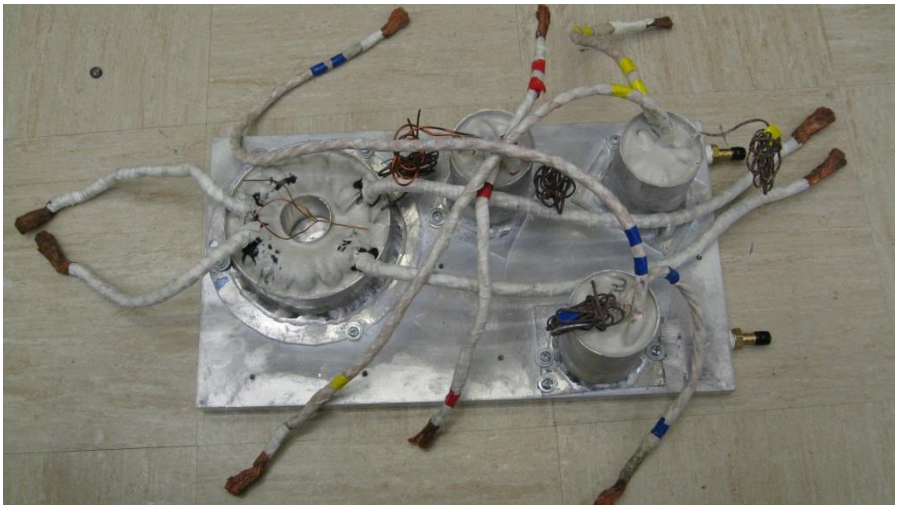

Figure 7.29. Example EMI filter with cooling design: Part 1

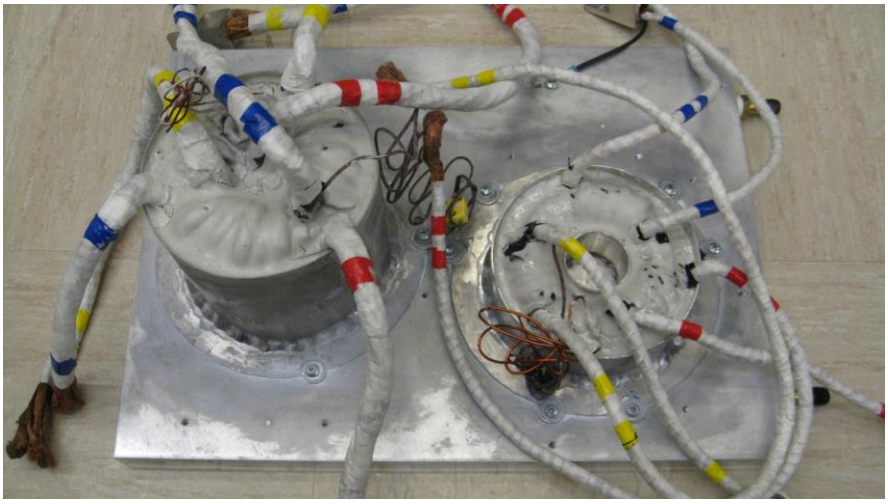

Figure 7.30. Example EMI filter with cooling design: Part 2

7.6 100 kW Motor Drive System Experimental Verification

Figure 7.31 shows the whole system of the interleaved three-level motor drive. The whole system is liquid-cooled. In Figure 7.31, the system with the EMI filter is connecting with a resistive load for thermal tests.

Figure 7.31. 100 kW motor drive system test setup

As shown in Figure 7.32 and Figure 7.33, both the DC and AC side EMI noise have met the DO160 standard after adding the EMI filter.

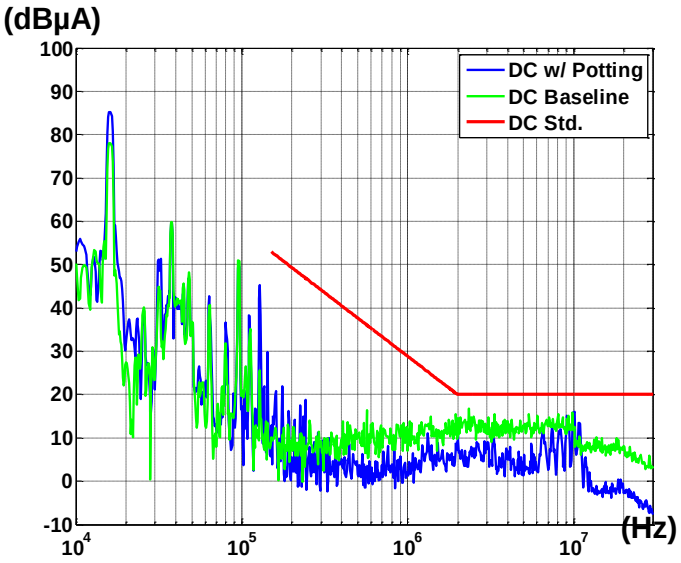

Figure 7.32. Dc side EMI noise after adding the EMI filter: with and without cooling design

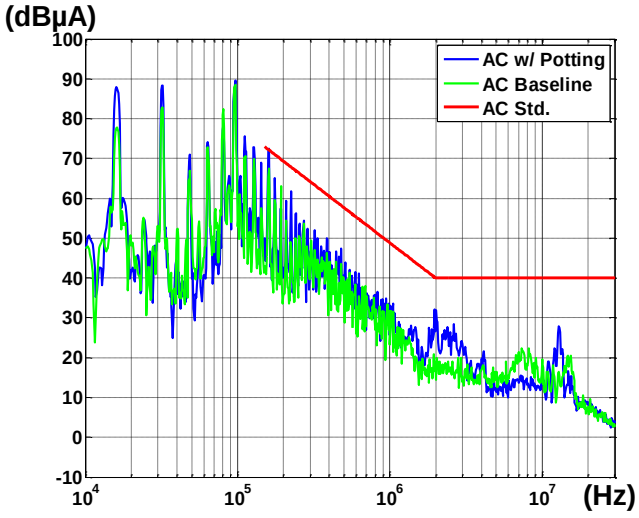

Figure 7.33. Ac side EMI noise after adding the EMI filter: with and without cooling design

A paper design of the EMI filter using conventional method has been carried out. Assuming similar cooling design method, if not considering the MM noise and NMT phenomena, the total weight of the EMI filter will be much higher than this high density design result, as shown in Figure 7.34.

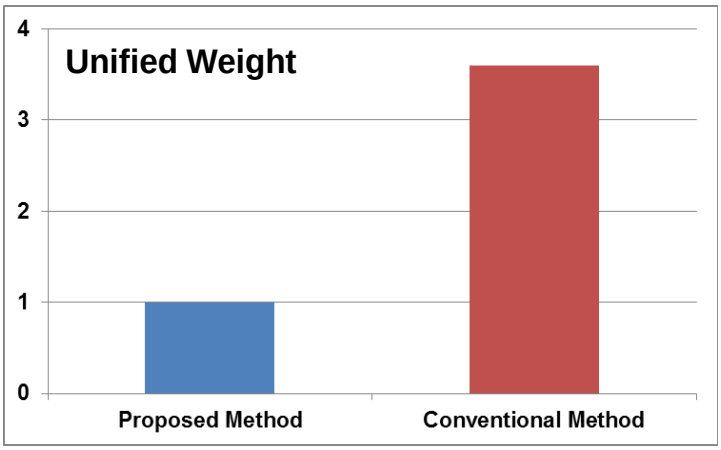

Figure 7.34. Per unit EMI filter weight comparison: conventional method vs. proposed method

7.7 Conclusion

In this chapter, a comprehensive design procedure has been proposed for high density EMI filter design in high power motor drives. Combining all the technologies discussed in the previous chapters, the design method considers the mm noise, the noise-mode transformation, the cooling design and its parasitic impact. As verification, a filter has been designed, fabricated and tested for a 100 kW motor drive for the aircraft application. The designed filter can help suppress the EMI noise below the required standard. It has also been validated as thermal and

functional correct when implemented into the final system. Comparing with traditional design method, the proposed design procedure produces a design of three times the power density.

Chapter 8 Conclusion and Future Work

8.1 Conclusion

In this dissertation, a comprehensive design method has been proposed towards a high density EMI filter in high power three-phase motor drive systems. Specific conclusions can be drawn in details as below:

Firstly, the mixed-mode noise exists in the output of three-phase motor drives, and largely impacts the power density of the designed EMI filter. The charging and discharging of the parasitic grounding capacitance of the motor under three-phase PWM schemes will introduce MM noise on the output side of the system. Amplitude of the MM noise is related to the three-phase voltage vector of the inverter. As the verification of the existence of the MM noise, an effective way is to compare the DM noise of the system, when implementing DM filter only and when implementing both CM and DM filter. Without considering the MM noise in the filter design process, unnecessary DM filter weight will be introduced to attenuate this MM nosie. Since the MM noise is part of the CM noise, if the CM filter is well designed and CM noise is well attenuated, the MM noise can be effectively suppressed. The combination of CM and DM filter in evaluating the DM noise is needed in a comprehensive design method.

Secondly, there are noise mode transformations in three-phase motor drive systems and they will also influence the power density of the designed EMI filter. The noise mode transformation is due to the unbalance of the impedance of the noise propagation path. DC CM noise can be found in the DC DM noise measurement, because of the grounding unbalance of the LISNs. AC

DM noise can be transformed into AC CM spectrum by the unbalance of the leakage inductance and DM capacitors. These transformations mislead designers to overdesign CM filter to attenuate DM noise, and vice versa. However, since no new noise is brought in, if both CM and DM filters have been installed, the influence of the transformation of the noise can be reduced. The transformation of the noise should also be considered in a comprehensive design method for high density EMI filter.

Thirdly, EMI filters at the motor-end can also effectively suppress CM noise of the motor drive. Comparing with conventional EMI filter added at the inverter-end, these motor-end filters have the benefit of avoiding carrying high currents and being able to be implemented during the motor manufacturing process. However, the performance of these filters can be influenced by the grounding parasitic capacitance. At higher frequency than several mega Herts, the attenuation is not as much as equivalent inverter-end filters. Meanwhile, safety issues should be considered when applying the chassis-end CM filter on the motor side.

Fourthly, this dissertation provides a practical design procedure for the liquid-cooling of EMI filter components, especially CM and DM inductors. To get an effective cooling design, the designer should consider the potting process and how to evaluate the thermal model. Before implementing the filter into the system for final full power tests, emulation tests are also important. Testbed can be designed to emulate the voltage and current condition of the final tests.

Fifthly, the conventional liquid-cooling design with the case and potting material will influence the impedance of CM and DM inductors. Because of the existence of the conductive case around the winding of the inductor, the leakage inductance of both single and three-phase CM chokes will be reduced. Meanwhile, the equivalent paralleling capacitance (EPC) will

increase because of the case. Furthermore, the potting material may have higher permittivity than the air. This will introduce higher EPC into the inductors.

Considering the MM noise, the NMT, and the cooling design as well as its influence on filter impedance, a comprehensive design procedure for high density EMI filter in three-phase high power motor drives can be summarized. The weight of the cooling design as well as its impact on the impedance can be considered during the paper design stage. When evaluating the filter design, a comprehensive decision making procedure is proposed considering the existence of the MM noise and the NMT. This method is verified in a 100 kW motor drive system and proved to be effective in weight saving and noise attenuation.

8.2 Future Work

For the study of the MM noise, a mathematic relationship between the MM noise and different PWM schemes can be developed. Since the MM noise can be quantified for each switching status, the general MM noise in one fundamental period can be summarized according to the dwelling time of each switching status.

Considering the analysis on the system impedance unbalance, further study can be carried out on filter component parasitic improvement. In this dissertation, the work is focusing on the analysis of noise mode transformation, instead of solving the impedance unbalance problem. With different methods of adjusting the layout design of the filter components, the system impedance caused by filter components can be improved.

The aim of the motor-end EMI filter study is not to build a real filter that makes the motor chassis floating. The major concern is whether the motor can be designed according to the

impedance required from the EMI point of view. Future work can be applied on the design of special motor towards an EMI-free impedance.

The cooling testbed described in Chapter 5 is effective in identifying the loss of passive components. In future work, inductor loss under PWM excitation can be analyzed based on the testbed.

The parasitic influence study in Chapter 6 is mainly focusing on the self-parasitic components of the inductors after adding the cooling packages. Future work can be carried out on the mutual coupling study of inductors and capacitors with the liquid-cooling setup.

The saturation of the CM choke is influencing the performance of the EMI filter. A detailed model under different operation conditions of the motor drive can be developed for the volt-second excitation on the CM choke. Based on the model, the saturation of the CM choke will be effectively avoided from the design stage.

8.3 Publication List

This list includes papers directly related to the main topic of doctoral research.

1. F. Luo, X. Zhang, D. Boroyevich, P. Mattavelli, J. Xue, F. Wang, N. Gazel, "*On discussion of AC and DC side EMI filters design for conducted noise suppression in DC-fed three phase motor drive system,*" in Proc. of IEEE Applied Power Electronics Conference and Exposition (APEC), pp. 667 – 672, Mar., 2011.
2. D. Jiang, F. Wang, and J. Xue, "*PWM impact on CM noise and AC CM choke for variable-speed motor drives*," in Proc. of IEEE Energy Conversion Congress and Exposition (ECCE), pp. 1881 – 1888, Sept., 2011.

3. J. Xue, F. Wang, X. Zhang, D. Boroyevich, and P. Mattavelli, "*Design of output passive EMI filter in DC-fed motor drive*," in Proc. of IEEE Applied Power Electronics Conference and Exposition (APEC), pp. 634 – 640, Feb, 2012.

4. J. Xue, and F. Wang, "*Modeling and design of common-mode inductor for conductive EMI noise suppression in DC-fed motor drive system*," in Proc. of IEEE Energy Conversion Congress and Exposition (ECCE), pp. 645 – 651, 2012.

5. J. Xue, F. Wang, and W. Chen, "*A study of motor-end EMI filter on output common-mode noise suppression in DC-fed motor drive system*," in Proc. of IEEE Applied Power Electronics Conference and Exposition (APEC), pp. 1556 – 1561, 2013.

6. X. Zhang, D. Boroyevich, P. Mattavelli, J. Xue, and F. Wang, "*EMI filter design and optimization for both AC and DC side in a DC-fed motor drive system*," in Proc. of IEEE Applied Power Electronics Conference and Exposition (APEC), pp. 1556 – 1561, 2013.

7. J. Xue, and F. Wang, "*Mixed-mode EMI noise in three-phase DC-fed PWM motor drive system*," in Proc. of IEEE Energy Conversion Congress and Exposition (ECCE), pp. 4312 – 4317, 2013.

Reference

[1] R. I. Jones, "The More Electric Aircraft: the past and the future?," in *Electrical Machines and Systems for the More Electric Aircraft (Ref. No. 1999/180), IEE Colloquium on*, 1999, pp. 1/1-1/4.

[2] R. Quigley, "More electric aircraft," in *Applied Power Electronics Conference and Exposition, 1993. APEC'93. Conference Proceedings 1993., Eighth Annual*, 1993, pp. 906-911.

[3] J. Rosero, J. Ortega, E. Aldabas, and L. Romeral, "Moving towards a more electric aircraft," *Aerospace and Electronic Systems Magazine, IEEE,* vol. 22, pp. 3-9, 2007.

[4] J. A. Weimer, "Electrical power technology for the more electric aircraft," in *Digital Avionics Systems Conference, 1993. 12th DASC., AIAA/IEEE*, 1993, pp. 445-450.

[5] G. Gong, M. L. Heldwein, U. Drofenik, J. Minibock, K. Mino, and J. W. Kolar, "Comparative evaluation of three-phase high-power-factor AC-DC converter concepts for application in future more electric aircraft," *Industrial Electronics, IEEE Transactions on*, vol. 52, pp. 727-737, 2005.

[6] J. A. Weimer, "The role of electric machines and drives in the more electric aircraft," in *Electric Machines and Drives Conference, 2003. IEMDC'03. IEEE International*, 2003, pp. 11-15.

[7] W. Cao, B. C. Mecrow, G. J. Atkinson, J. W. Bennett, and D. J. Atkinson, "Overview of electric motor technologies used for more electric aircraft (MEA)," *Industrial Electronics, IEEE Transactions on,* vol. 59, pp. 3523-3531, 2012.

[8] A. Boglietti, A. Cavagnino, A. Tenconi, and S. Vaschetto, "The safety critical electric machines and drives in the more electric aircraft: A survey," in *Industrial Electronics, 2009. IECON'09. 35th Annual Conference of IEEE*, 2009, pp. 2587-2594.

[9] C. Avery, S. Burrow, and P. Mellor, "Electrical generation and distribution for the more electric aircraft," in *Universities Power Engineering Conference, 2007. UPEC 2007. 42nd International*, 2007, pp. 1007-1012.

[10] D. Izquierdo, R. Azcona, F. Del Cerro, C. Fernandez, and B. Delicado, "Electrical power distribution system (HV270DC), for application in more electric aircraft," in *Applied Power Electronics Conference and Exposition (APEC), 2010 Twenty-Fifth Annual IEEE*, 2010, pp. 1300-1305.

[11] Q. Song and C. Dan, "Mixed-mode EMI noise and its implications to filter design in offline switching power supplies," *Power Electronics, IEEE Transactions on*, vol. 17, pp. 502-507, 2002.

[12] D. Liu and J. Jiang, "High frequency characteristic analysis of EMI filter in switch mode power supply (SMPS)," in *Power Electronics Specialists Conference, 2002. pesc 02. 2002 IEEE 33rd Annual*, 2002, pp. 2039-2043.

[13] R. Chen, "Integrated EMI filters for switch mode power supplies," Ph. D. dissertation, Virginia Polytechnic Institute and State University, 2004.

[14] R. Chen, J. van Wyk, S. Wang, and W. Odendaal, "Technologies and characteristics of integrated EMI filters for switch mode power supplies," in *Power Electronics Specialists Conference, 2004. PESC 04. 2004 IEEE 35th Annual*, 2004, pp. 4873-4880.

[15] K. Mainali and R. Oruganti, "Conducted EMI mitigation techniques for switch-mode power converters: A survey," *Power Electronics, IEEE Transactions on*, vol. 25, pp. 2344-2356, 2010.

[16] L. Rossetto, S. Buso, and G. Spiazzi, "Conducted EMI issues in a 600-W single-phase boost PFC design," *Industry Applications, IEEE Transactions on,* vol. 36, pp. 578-585, 2000.

[17] M. Jin, M. Weiming, P. Qijun, K. Jun, Z. Lei, and Z. Zhihua, "Identification of essential coupling path models for conducted EMI prediction in switching power converters," *Power Electronics, IEEE Transactions on,* vol. 21, pp. 1795-1803, 2006.

[18] P. Kong, Y. Jiang, and F. C. Lee, "Common mode EMI noise characteristics of low-power AC–DC converters," *Power Electronics, IEEE Transactions on,* vol. 27, pp. 731-738, 2012.

[19] X. Wu, D. Xu, Z. Wen, Y. Okuma, and K. Mino, "Design, modeling, and improvement of integrated EMI filter with flexible multilayer foils," *Power Electronics, IEEE Transactions on,* vol. 26, pp. 1344-1354, 2011.

[20] M. L. Heldwein and J. W. Kolar, "Impact of EMC Filters on the Power Density of Modern Three-Phase PWM Converters," *Power Electronics, IEEE Transactions on,* vol. 24, pp. 1577-1588, 2009.

[21] M. Hartmann, H. Ertl, and J. W. Kolar, "EMI filter design for a 1 MHz, 10 kW three-phase/level PWM rectifier," *Power Electronics, IEEE Transactions on,* vol. 26, pp. 1192-1204, 2011.

[22] K. Raggl, T. Nussbaumer, and J. W. Kolar, "Guideline for a simplified differential-mode EMI filter design," *Industrial Electronics, IEEE Transactions on,* vol. 57, pp. 1031-1040, 2010.

[23] T. Nussbaumer, M. L. Heldwein, and J. W. Kolar, "Differential mode input filter design for a three-phase buck-type PWM rectifier based on modeling of the EMC test receiver," *Industrial Electronics, IEEE Transactions on,* vol. 53, pp. 1649-1661, 2006.

[24] M. Hartmann, H. Ertl, and J. W. Kolar, "EMI filter design for high switching frequency three-phase/level PWM rectifier systems," in *Applied Power Electronics Conference and Exposition (APEC), 2010 Twenty-Fifth Annual IEEE*, 2010, pp. 986-993.

[25] Y. Sheng, W. Eberle, and L. Yan-Fei, "A novel EMI filter design method for switching power supplies," *Power Electronics, IEEE Transactions on,* vol. 19, pp. 1668-1678, 2004.

[26] M. J. Nave, "On modeling the common mode inductor," in *Electromagnetic Compatibility, 1991. Symposium Record., IEEE 1991 International Symposium on*, 1991, pp. 452-457.

[27] H. Akagi and T. Doumoto, "A passive EMI filter for preventing high-frequency leakage current from flowing through the grounded inverter heat sink of an adjustable-speed motor drive system," *Industry Applications, IEEE Transactions on,* vol. 41, pp. 1215-1223, 2005.

[28] H. Akagi and S. Tamura, "A Passive EMI Filter for Eliminating Both Bearing Current and Ground Leakage Current From an Inverter-Driven Motor," *Power Electronics, IEEE Transactions on,* vol. 21, pp. 1459-1469, 2006.

[29] H. Akagi and T. Shimizu, "Attenuation of Conducted EMI Emissions From an Inverter-Driven Motor," *Power Electronics, IEEE Transactions on,* vol. 23, pp. 282-290, 2008.

[30] H. Akagi and T. Oe, "A specific filter for eliminating high-frequency leakage current from the grounded heat sink in a motor drive with an active front end," *Power Electronics, IEEE Transactions on,* vol. 23, pp. 763-770, 2008.

[31] U. T. Shami and H. Akagi, "Identification and discussion of the origin of a shaft end-to-end voltage in an inverter-driven motor," *Power Electronics, IEEE Transactions on,* vol. 25, pp. 1615-1625, 2010.

[32] U. T. Shami and H. Akagi, "Experimental discussions on a shaft end-to-end voltage appearing in an inverter-driven motor," *Power Electronics, IEEE Transactions on,* vol. 24, pp. 1532-1540, 2009.

[33] H. Akagi and T. Doumoto, "An approach to eliminating high-frequency shaft voltage and ground leakage current from an inverter-driven motor," *Industry Applications, IEEE Transactions on,* vol. 40, pp. 1162-1169, 2004.

[34] S. Ogasawara and H. Akagi, "Circuit configurations and performance of the active common-noise canceler for reduction of common-mode voltage generated by voltage-source PWM inverters," in *Industry Applications Conference, 2000. Conference Record of the 2000 IEEE,* 2000, pp. 1482-1488.

[35] H. Akagi, S. Srianthumrong, and Y. Tamai, "Comparisons in circuit configuration and filtering performance between hybrid and pure shunt active filters," in *Industry Applications Conference, 2003. 38th IAS Annual Meeting. Conference Record of the*, 2003, pp. 1195-1202.

[36] J.-S. Lai, X. Huang, E. Pepa, S. Chen, and T. W. Nehl, "Inverter EMI modeling and simulation methodologies," *Industrial Electronics, IEEE Transactions on,* vol. 53, pp. 736-744, 2006.

[37] H. Zhu, J.-S. Lai, A. R. Hefner, Y. Tang, and C. Chen, "Modeling-based examination of conducted EMI emissions from hard and soft-switching PWM inverters," *Industry Applications, IEEE Transactions on,* vol. 37, pp. 1383-1393, 2001.

[38] J.-S. Lai, X. Huang, S. Chen, and T. W. Nehl, "EMI characterization and simulation with parasitic models for a low-voltage high-current AC motor drive," *Industry Applications, IEEE Transactions on,* vol. 40, pp. 178-185, 2004.

[39] X. Huang, E. Pepa, J.-S. Lai, S. Chen, and T. W. Nehl, "Three-phase inverter differential mode EMI modeling and prediction in frequency domain," in *Industry Applications Conference, 2003. 38th IAS Annual Meeting. Conference Record of the*, 2003, pp. 2048-2055.

[40] N. Hanigovszki, J. Landkildehus, G. Spiazzi, and F. Blaabjerg, "An EMC evaluation of the use of unshielded motor cables in AC adjustable speed drive applications," *Power Electronics, IEEE Transactions on,* vol. 21, pp. 273-281, 2006.

[41] N. Hanigovszki, "EMC output filters for adjustable speed drives," Ph. D. dissertation, Videnbasen for Aalborg UniversitetVBN, Aalborg UniversitetAalborg University, Det Teknisk-Naturvidenskabelige FakultetThe Faculty of Engineering and Science, Institut for EnergiteknikDepartment of Energy Technology, 2005.

[42] N. Hanigovszki, J. Landkildehus, and F. Blaabjerg, "Output filters for AC adjustable speed drives," in *Applied Power Electronics Conference, APEC 2007-Twenty Second Annual IEEE,* 2007, pp. 236-242.

[43] Y. Y. Maillet, "High-Density Discrete Passive EMI Filter Design for Dc-Fed Motor Drives," Master thesis, Virginia Polytechnic Institute and State University, 2008.

[44] Y. Maillet, L. Rixin, W. Shuo, W. Fei, R. Burgos, and D. Boroyevich, "High-Density EMI Filter Design for DC-Fed Motor Drives," *Power Electronics, IEEE Transactions on,* vol. 25, pp. 1163-1172, 2010.

[45] R. Lai, Y. Maillet, F. Wang, S. Wang, R. Burgos, and D. Boroyevich, "An integrated EMI choke for differential-mode and common-mode noise suppression," *Power Electronics, IEEE Transactions on,* vol. 25, pp. 539-544, 2010.

[46] X. Lei, F. Feng, and S. Jian, "Behavioral modeling methods for motor drive system EMI design optimization," in *Energy Conversion Congress and Exposition (ECCE), 2010 IEEE,* 2010, pp. 947-954.

[47] L. Xing, "EMI Filter Design and Optimization for Three-Phase Motor Drive Systems," Ph. D. dissertation, RENSSELAER POLYTECHNIC INSTITUTE, 2011.

[48] X. Lei and S. Jian, "Conducted Common-Mode EMI Reduction by Impedance Balancing," *Power Electronics, IEEE Transactions on,* vol. 27, pp. 1084-1089, 2012.

[49] L. Xing, F. Feng, and J. Sun, "Optimal damping of EMI filter input impedance," *Industry Applications, IEEE Transactions on,* vol. 47, pp. 1432-1440, 2011.

[50] L. Xing and J. Sun, "Optimal damping of multistage EMI filters," *Power Electronics, IEEE Transactions on,* vol. 27, pp. 1220-1227, 2012.

[51] L. Xing and J. Sun, "Motor drive system EMI reduction by asymmetric interleaving," in *Control and Modeling for Power Electronics (COMPEL), 2010 IEEE 12th Workshop on*, 2010, pp. 1-7.

[52] W. Shen, F. Wang, D. Boroyevich, and Y. Liu, "Definition and acquisition of CM and DM EMI noise for general-purpose adjustable speed motor drives," in *Power Electronics Specialists Conference, 2004. PESC 04. 2004 IEEE 35th Annual*, 2004, pp. 1028-1033.

[53] M. Heldwein, T. Nussbaumer, F. Beck, and J. Kolar, "Novel three-phase CM/DM conducted emissions separator," in *Applied Power Electronics Conference and Exposition, 2005. APEC 2005. Twentieth Annual IEEE*, 2005, pp. 797-802.

[54] M. L. Heldwein, L. Dalessandro, and J. W. Kolar, "The three-phase common-mode inductor: Modeling and design issues," *Industrial Electronics, IEEE Transactions on*, vol. 58, pp. 3264-3274, 2011.

[55] J. Xue and F. Wang, "Modeling and design of common-mode inductor for conductive EMI noise suppression in DC-fed motor drive system," in *Energy Conversion Congress and Exposition (ECCE), 2012 IEEE*, 2012, pp. 645-651.

[56] N. Aoki, K. Satoh, and A. Nabae, "Damping circuit to suppress motor terminal overvoltage and ringing in PWM inverter-fed AC motor drive systems with long motor leads," *Industry Applications, IEEE Transactions on*, vol. 35, pp. 1014-1020, 1999.

[57] J. Xue, F. Wang, X. Zhang, D. Boroyevich, and P. Mattavelli, "Design of output passive EMI filter in DC-fed motor drive," in *Applied Power Electronics Conference and Exposition (APEC), 2012 Twenty-Seventh Annual IEEE*, 2012, pp. 634-640.

[58] M. Jin and M. Weiming, "A new technique for modeling and analysis of mixed-mode conducted EMI noise," *Power Electronics, IEEE Transactions on*, vol. 19, pp. 1679-1687, 2004.

[59] H.-I. Hsieh, J.-S. Li, and D. Chen, "Effects of X capacitors on EMI filter effectiveness," *Industrial Electronics, IEEE Transactions on*, vol. 55, pp. 949-955, 2008.

[60] M. M. Jha, K. B. Naik, and S. P. Das, "Types of electro magnetic interferences in SMPS and using Y-capacitor for mitigation of Mixed Mode noise," in *Power, Control and Embedded Systems (ICPCES), 2010 International Conference on*, 2010, pp. 1-6.

[61] H. I. Hsieh, D. Chen, and S. Q. A. F. D. Procedure, "Incorporating Mixed—Mode EMI Noise for Off-Line Switching Power Supplies," *IEEE IPEMC,* pp. 147-152, 2004.

[62] H.-I. Hsieh, "A procedure including mix-mode noise for designing EMI filters for off-line applications," in *Vehicle Power and Propulsion Conference, 2008. VPPC'08. IEEE*, 2008, pp. 1-6.

[63] H.-I. Hsieh, "Effects of mix-mode noise emissions on the design method of power factor correction boost rectifier EMI filters," in *Power Electronics Conference (IPEC), 2010 International*, 2010, pp. 2438-2443.

[64] F.-Y. Shih, D. Y. Chen, Y.-P. Wu, and Y.-T. Chen, "A Procedure for Designing EMI Filters for AC Line Applications," *IEEE Transactions on Power Electronics,* vol. 11, 1996.

[65] S. Wang and F. C. Lee, "Investigation of the transformation between differential-mode and common-mode noises in an EMI filter due to unbalance," *IEEE transactions on electromagnetic compatibility,* vol. 52, pp. 578-587, 2010.

[66] S. Wang, F. C. Lee, D. Y. Chen, and W. G. Odendaal, "Effects of parasitic parameters on EMI filter performance," *Power Electronics, IEEE Transactions on,* vol. 19, pp. 869-877, 2004.

[67] S. Wang, F. C. Lee, and W. G. Odendaal, "Characterization and parasitic extraction of EMI filters using scattering parameters," *Power Electronics, IEEE Transactions on,* vol. 20, pp. 502-510, 2005.

[68] S. Wang, F. C. Lee, and J. D. Van Wyk, "Design of inductor winding capacitance cancellation for EMI suppression," *Power Electronics, IEEE Transactions on,* vol. 21, pp. 1825-1832, 2006.

[69] S. Wang, J. D. van Wyk, and F. C. Lee, "Effects of interactions between filter parasitics and power interconnects on EMI filter performance," *Industrial Electronics, IEEE Transactions on,* vol. 54, pp. 3344-3352, 2007.

[70] S. Wang, Y. Y. Maillet, F. Wang, R. Lai, F. Luo, and D. Boroyevich, "Parasitic Effects of Grounding Paths on Common-Mode EMI Filter's Performance in Power Electronics Systems," *Industrial Electronics, IEEE Transactions on,* vol. 57, pp. 3050-3059, 2010.

[71] D. Fu, P. Kong, S. Wang, F. C. Lee, and M. Xu, "Analysis and suppression of conducted EMI emissions for front-end LLC resonant DC/DC converters," in *Power Electronics Specialists Conference, 2008. PESC 2008. IEEE*, 2008, pp. 1144-1150.

[72] P. Kong, S. Wang, and F. C. Lee, "Common mode EMI noise suppression for bridgeless PFC converters," *Power Electronics, IEEE Transactions on,* vol. 23, pp. 291-297, 2008.

[73] R. Chen, J. D. Van Wyk, S. Wang, and W. G. Odendaal, "Improving the characteristics of integrated EMI filters by embedded conductive layers," *Power Electronics, IEEE Transactions on,* vol. 20, pp. 611-619, 2005.

[74] H. Chen and Z. Qian, "Modeling and characterization of parasitic inductive coupling effects on differential-mode EMI performance of a boost converter," *Electromagnetic Compatibility, IEEE Transactions on,* vol. 53, pp. 1072-1080, 2011.

[75] P.-S. Chen and Y.-S. Lai, "Effective EMI filter design method for three-phase inverter based upon software noise separation," *Power Electronics, IEEE Transactions on,* vol. 25, pp. 2797-2806, 2010.

[76] P. Kong, S. Wang, F. C. Lee, and Z. Wang, "Reducing common-mode noise in two-switch forward converter," *Power Electronics, IEEE Transactions on,* vol. 26, pp. 1522-1533, 2011.

[77] C. Jettanasen, F. Costa, and C. Vollaire, "Common-mode emissions measurements and simulation in variable-speed drive systems," *Power Electronics, IEEE Transactions on,* vol. 24, pp. 2456-2464, 2009.

[78] G. Skibinski, "Design methodology of a cable terminator to reduce reflected voltage on AC motors," in *Industry Applications Conference, 1996. Thirty-First IAS Annual Meeting, IAS'96., Conference Record of the 1996 IEEE*, 1996, pp. 153-161.

[79] B. Bolsens, K. De Brabandere, J. Van den Keybus, J. Driesen, and R. Belmans, "Transmission line effects on motor feed cables: terminator design and analysis in the Laplace-domain," in *Electric Machines and Drives Conference, 2003. IEMDC'03. IEEE International*, 2003, pp. 1866-1872.

[80] N. Mutoh and M. Kanesaki, "A suitable method for ecovehicles to control surge voltage occurring at motor terminals connected to PWM inverters and to control induced EMI noise," *Vehicular Technology, IEEE Transactions on,* vol. 57, pp. 2089-2098, 2008.

[81] A. von Jouanne and P. N. Enjeti, "Design considerations for an inverter output filter to mitigate the effects of long motor leads in ASD applications," *Industry Applications, IEEE Transactions on*, vol. 33, pp. 1138-1145, 1997.

[82] M. Earley and J. Sargent, "National Electrical Code 2011 Handbook," ed: National Fire Protection Associations, Quincy, MA, 2010.

[83] M. A. Maldonado, N. M. Shah, K. J. Cleek, P. S. Walia, and G. J. Korba, "Power management and distribution system for a more-electric aircraft (MADMEL)-program status," in *Energy Conversion Engineering Conference, 1997. IECEC-97., Proceedings of the 32nd Intersociety*, 1997, pp. 274-279.

[84] W. Homeyer, E. Bowles, S. Lupan, P. Walia, and M. Maldonado, "Advanced power converters for more electric aircraft applications," in *Energy Conversion Engineering Conference, 1997. IECEC-97., Proceedings of the 32nd Intersociety*, 1997, pp. 591-596.

[85] I. Moir and A. Seabridge, *Aircraft systems: mechanical, electrical and avionics subsystems integration* vol. 21: John Wiley & Sons, 2008.

[86] R. Wrobel and P. Mellor, "Thermal design of high-energy-density wound components," *Industrial Electronics, IEEE Transactions on*, vol. 58, pp. 4096-4104, 2011.

[87] F. Z. Feng, J. Horowy, D. Pal, S. Schwitters, and C. G. Thiel, "Light-weight, conduction-cooled inductor," ed: Google Patents, 2012.

[88] D. Driessen, F. Feng, D. Pal, and C. G. Thiel, "High current, multiple air gap, conduction cooled, stacked lamination inductor," ed: Google Patents, 2009.

[89] R. S. Downing, "Immersion cooled inductor apparatus," ed: Google Patents, 2014.

[90] P. F. Wernicki, "Cooled high power vehicle inductor and method," ed: Google Patents, 2009.

[91] A. M. Ritter, R. G. Wagoner, J. H. Parslow, and A. Amer, "Cast-coil inductor," ed: Google Patents, 2012.

[92] A. B. Eriksson and J. Forslin, "Induction device," ed: Google Patents, 2012.

[93] A. Leclercq and L. Vedda, "Liquid cooled electromagnetic continuous casting mold," ed: Google Patents, 1976.

[94] R. J. Hoppe and M. W. Metzler, "Inductor transformer cooling apparatus," ed: Google Patents, 1990.

[95] R. Wrobel, N. McNeill, and P. H. Mellor, "Performance analysis and thermal modeling of a high-energy-density prebiased inductor," *Industrial Electronics, IEEE Transactions on*, vol. 57, pp. 201-208, 2010.

[96] J. Li, T. Abdallah, and C. R. Sullivan, "Improved calculation of core loss with nonsinusoidal waveforms," in *Industry Applications Conference, 2001. Thirty-Sixth IAS Annual Meeting. Conference Record of the 2001 IEEE*, 2001, pp. 2203-2210.

[97] W. Shen, F. Wang, D. Boroyevich, and C. Tipton, "Loss characterization and calculation of nanocrystalline cores for high-frequency magnetics applications," *Power Electronics, IEEE Transactions on*, vol. 23, pp. 475-484, 2008.

[98] J. Muhlethaler, J. Biela, J. W. Kolar, and A. Ecklebe, "Core losses under the DC bias condition based on Steinmetz parameters," *Power Electronics, IEEE Transactions on*, vol. 27, pp. 953-963, 2012.

[99] J. Muhlethaler, J. Biela, J. W. Kolar, and A. Ecklebe, "Improved core-loss calculation for magnetic components employed in power electronic systems," *Power Electronics, IEEE Transactions on*, vol. 27, pp. 964-973, 2012.

[100] X. Nan and C. R. Sullivan, "An improved calculation of proximity-effect loss in high-frequency windings of round conductors," in *Power Electronics Specialist Conference, 2003. PESC'03. 2003 IEEE 34th Annual*, 2003, pp. 853-860.

[101] H. Rossmanith, M. Doebroenti, M. Albach, and D. Exner, "Measurement and characterization of high frequency losses in nonideal litz wires," *Power Electronics, IEEE Transactions on*, vol. 26, pp. 3386-3394, 2011.

[102] G. Grandi, M. K. Kazimierczuk, A. Massarini, and U. Reggiani, "Stray capacitances of single-layer solenoid air-core inductors," *Industry Applications, IEEE Transactions on,* vol. 35, pp. 1162-1168, 1999.

[103] T. C. Neugebauer and D. J. Perreault, "Parasitic capacitance cancellation in filter inductors," *Power Electronics, IEEE Transactions on,* vol. 21, pp. 282-288, 2006.

[104] H. Y. Lu, J. G. Zhu, and S. R. Hui, "Experimental determination of stray capacitances in high frequency transformers," *Power Electronics, IEEE Transactions on,* vol. 18, pp. 1105-1112, 2003.

[105] L. Dalessandro, F. da Silveira Cavalcante, and J. W. Kolar, "Self-capacitance of high-voltage transformers," *Power Electronics, IEEE Transactions on,* vol. 22, pp. 2081-2092, 2007.

[106] M. Shallal and J. Harrison, "Electric field, potential and capacitance of a sphere-plane electrode system," in *Proceedings of the Institution of Electrical Engineers*, 1969, pp. 1115-1118.

[107] S. Wang, F. Lee, and W. Odendaal, "Controlling the parasitic parameters to improve EMI filter performance," in *Applied Power Electronics Conference and Exposition, 2004. APEC'04. Nineteenth Annual IEEE*, 2004, pp. 503-509.

[108] A. Massarini and M. K. Kazimierczuk, "Self-capacitance of inductors," *Power Electronics, IEEE Transactions on,* vol. 12, pp. 671-676, 1997.

[109] S. Wang, P. Kong, and F. C. Lee, "Common mode noise reduction for boost converters using general balance technique," *IEEE transactions on power electronics*, vol. 22, pp. 1410-1416, 2007.

VITA

Jing Xue was born on August 3rd, 1986, in Xiangfan, Hubei Province, China. He received his Bachelor of Science Degree from Tsinghua University, Beijing in August, 2008, in the major of electrical engineering. In August 2010, he received his Master of Science Degree from Virginia Polytechnic Institute & State University, in the major of electrical engineering. He began his Doctor of Philosophy study from August 2010, in the University of Tennessee, Knoxville.